ANTI-INFLAMMATORY PROPERTIES AND IDENTIFICATION OF PUTATIVE PROTEIN TARGETS OF PHYTOCHEMICALS PRESENT IN MASHUA (*TROPAEOLUM TUBEROSUM*) TUBER AND ACEROLA (*MALPIGHIA EMARGINATA*) LEAF BY DARTS METHODOLOGY

A Dissertation

by

MARIA ELISA SCHRECKINGER MINOLI

Submitted to the Office of Graduate and Professional Studies of
Texas A&M University
in partial fulfillment of the requirements for the degree of

DOCTOR OF PHILOSOPHY

Chair of Committee,	Luis Cisneros-Zevallos
Committee Members,	Joseph Awika
	Nancy Turner
	Chaodong Wu
Head of Department,	Boon Chew

August 2016

Major Subject: Food Science and Technology

ABSTRACT

Cellular targets for the majority of dietary phytochemicals remain unknown, presenting a challenge for the understanding of how these dietary components provide health benefits. Recently a new methodology, drug affinity responsive target stability (DARTS), was developed for this purpose. The objective of this study was to evaluate the anti-inflammatory properties of mashua (*Tropaeolum tuberosum*) tuber and acerola leaf (*Malpighia emarginata*) extracts and to identify the protein targets of its phytochemicals by using DARTS methodology.

The first aim was to investigate the anti-inflammatory properties of mashua extracts and to identify the cellular targets of its phytochemicals. Mashua 203040 and 203081 extracts exerted anti-inflammatory properties in LPS-stimulated macrophages. Through DARTS methodology we identified pyruvate kinase M (PKM) as a potential target of the phytochemicals present in both extracts. Additionally, mashua extracts reduced reactive oxygen species (ROS) levels and consequently affected the expression of ROS dependent LPS-induced pro-inflammatory genes. LC-MS profiling revealed that both mashua extracts contained mainly phenolics and isothiocyantes. In this study, we demonstrated that phytochemicals from mashua reduce LPS-induced inflammation in RAW264.7 macrophages by targeting PKM and reducing ROS.

The second aim was to identify the bioactive compounds acting as COX-2 inhibitors in acerola leaf by using bioassay-guided fractionation and DARTS methodology. The leaf extract (F4) was fractionated into three fractions (F1, F2, and F3)

and results indicated that F4, F2, and F3 inhibited COX-2 activity. F2 showed the highest COX-2 inhibitory effect among the fractions, and also showed binding to COX-2 by DARTS. Thus, its subfractions (F2A, F2B, and F2C) were further tested for their ability to bind and inhibit COX-2 activity. All subfractions inhibited COX-2 activity but only F2A and F2C showed binding by DARTS. F2C was further fractionated and only fraction F2C4, containing terpenes, inhibited COX-2 activity. In this study, we identify the group of compounds from acerola leaf, which are responsible for the inhibition of COX-2 activity.

In conclusion we were able to characterize many of the phytochemicals present in mashua tuber and acerola leaf and to identify the putative targets responsible for their anti-inflammatory effect *in vitro.*

DEDICATION

To my mom, for her unconditional love and support

ACKNOWLEDGEMENTS

First, I would like to express my sincere gratitude to my advisor Dr. Luis Cisneros-Zevallos for his continuous support and guidance throughout my Ph.D. I would also like to thank my committee members, Dr. Joseph Awika, Dr. Nancy Turner, and Dr. Chaodong Wu, for their support.

I would like to give my sincere thanks to Dr. Vimal Nair for his support in the chemistry work and to Dr. Woo Young Bang for his assistance in the molecular biology work. Also, I would like to thank my labmates Prerna Bhargava, Shareena Sreedharan, Fang Mian Chang, and Facundo Ibañez for laboratory assistance and their friendship.

Finally, thanks to my family and friends for their love and encouragement.

TABLE OF CONTENTS

Page

Page

LIST OF FIGURES

Page

Page

Page

LIST OF TABLES

Page

Page

CHAPTER I

INTRODUCTION AND LITERATURE REVIEW

Chronic Inflammation and Metabolic Disorders

Inflammation is an innate or adaptive response of the immune system that is triggered by different stimuli or conditions, including infection, tissue injury, (*1*) and dietary stress (*2*). Upon the induction of an inflammatory response, there is usually a sequential release of inflammatory mediators and recruitment of leukocytes to the inflammation site. Once these cells reach the inflammation site, they become activated and release more mediators, creating a vast communication network between the metabolic tissue and immune system cells (*3*). The inflammatory mediators include antimicrobial mediators such as reactive oxygen and nitrogen species, which directly target the pathogens (*4*); chemokines like monocyte chemotactic protein-1(MCP-1/CCL2), which recruit leukocytes to the inflammation site (*5*); and cytokines such as tumor necrosis factor-α (TNFα), which serve as signaling molecules that coordinate and regulate the inflammation response (*6*, *7*).

In a successful acute inflammatory response, the infectious agent is eliminated, the inflammatory response is resolved, and the tissue is repaired (*1*). The inadequate resolution of inflammation or an uncontrolled inflammatory response can lead to a chronic inflammation state. Chronic inflammation is usually defined as a pathological condition characterized by continuously active inflammatory response, which predisposes the host to different metabolic diseases, including diabetes (*8*),

atherosclerosis (*9*), neurodegenerative diseases, (*10*) and some types of cancers (*11*). For instance, in an obese host, the excess of nutrients can cause dietary stress in the adipose tissue, which induces the production of TNF-α by adipocytes. Consequently, resident macrophages become activated and produce more inflammatory mediators, resulting in a low-grade chronic inflammatory state. Many studies have shown that this chronic inflammation state promotes insulin resistance and metabolic deterioration in obesity (*12*). Furthermore, chronic inflammation plays a role in the development and progression of certain cancers such us colon cancer (*13*). As mentioned previously, in a chronic inflammation state there is a constant production of cytokines and other mediators such as ROS. These chemical mediators can directly damage cell components (i.e. DNA) and also alter the intracellular signaling of the cells. In this scenario, chronic inflammation can contribute to tumor initiation by inducing DNA damage and chromosomal instability. Also, through the alteration of signaling pathways, it can enhance cell proliferation, resistance to apoptosis, stimulated angiogenesis, among other factors that contribute to cancer progression, cell invasion, and metastasis (*14*).

Macrophage Polarization and Chronic Inflammation

Macrophages play a central role in many different immune pathological phenomena that lead to chronic inflammation and associated diseases. These include the over-production of pro-inflammatory cytokines such as TNF-α and interleukin 1-beta (IL-1β) and other inflammatory mediators like NO and ROS *(15)*. Due to the critical role of cytokines and other inflammatory mediators in the development and pathogenesis

of chronic inflammation and associated conditions, they have become an important target for the intervention of these diseases *(7)*.

To understand the regulation of inflammatory mediators by macrophages, it is crucial to define the mechanisms that regulate macrophage metabolic activity *(16)*. In response to different environmental signals, macrophages can reprogram into many different phenotypes with diverse functions. Despite the various phenotypes of macrophages, there are two mainly recognized, the classically activated macrophages or M1 and the alternative activated macrophages or M2 *(17)*. Macrophages polarize into M1 phenotype upon the stimulation with interferon-γ (IFNγ) or certain Toll-like receptor (TLR) ligands such as lipopolysaccharide (LPS). This phenotype has a strong microbicidal activity and is characterized by the production of pro-inflammatory cytokines such as TNF-α and other inflammatory mediators such as ROS and NO. Instead, exposure to cytokines IL-4 and IL-3 polarizes macrophages to M2 phenotype. This phenotype helps clear extracellular parasites, resolve the inflammatory response, and promotes tissue remodeling, among other functions *(17, 18)*.

Each macrophage phenotype metabolizes glucose differently according to their function and their needs (Biswas and Mantovani 2012). Normally, resting cells produce ATP through a combination of glycolysis and mitochondrial respiration. During glycolysis, glucose is converted to pyruvate, which enters the tricarboxylic acid (TCA) cycle in the mitochondria and becomes oxidized to generate ATP. However, M1 macrophages, similarly to cancer cells, exhibit a different metabolism. These cells, besides energy, have a high demand for biosynthetic precursors used for the synthesis of

pro-inflammatory proteins *(19)*. To meet these new needs, the cells switch their metabolism from a low rate of glycolysis followed by the oxidation of pyruvate in the mitochondria, to a high rate of glycolysis and a much lower rate of oxidative phosphorylation. Pyruvate is converted into lactate by lactate dehydrogenase (LDH) in the cytosol, instead of entering the TCA cycle. This change in the metabolic profile involves a switch in the expression of many genes such as glucose transporter 1 (GLUT1), lactate dehydrogenase A (LDHA), and pyruvate dehydrogenase 1 (PDK1). This phenomenon occurs under aerobic conditions and is known as the "Warburg effect" after Otto Warburg, who first defined it *(6, 19, 20)*. Instead, M2 macrophages continue to obtain most of their energy through oxidative phosphorylation which helps them accomplish their function in tissue remodeling and repair *(16)* (Figure 1).

Targeting the Warburg effect has become an interesting intervention approach for inflammatory related diseases, due to its critical role in M1 polarization and consecutive over production of pro-inflammatory mediators. Some of the possible targets of the Warburg effect include hexokinase, pyruvate dehydrogenase kinase (PDK), and pyruvate kinase M2 (PKM2), among others *(19)*.

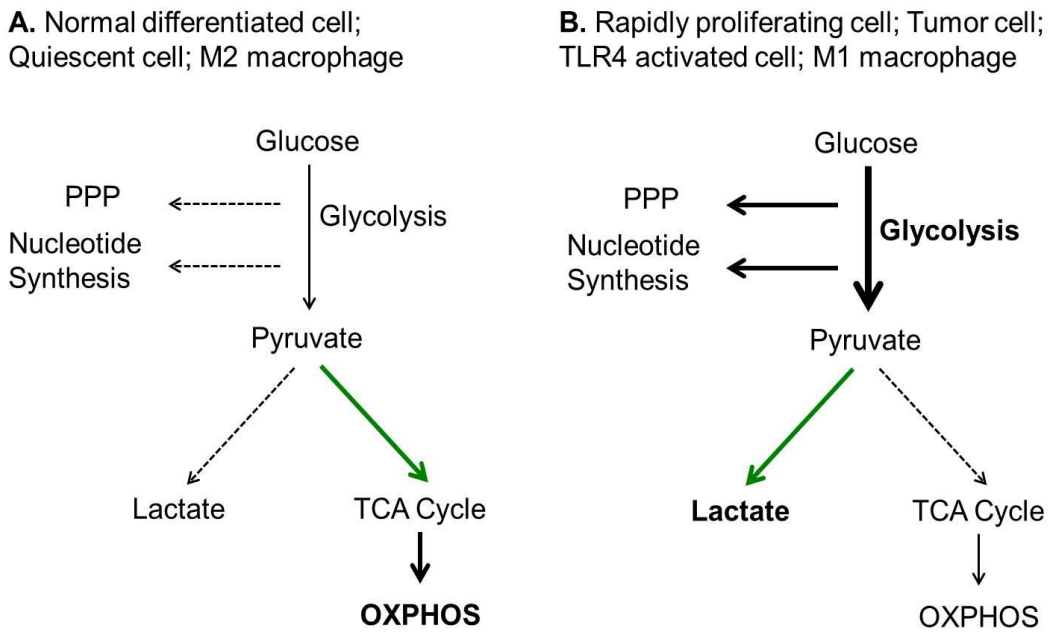

Figure 1 Schematic illustration of metabolic pathways of normal resting cells (A) compared to activated immune cells or cancer cells (B). Adapted from B. Kelly and L. O'Neill, 2015 (*6*).

Inflammatory Pathways with a Special Focus on NF-κB

Three inflammatory pathways have been mainly implicated in the pathogenesis of inflammatory diseases: IKK–nuclear factor-κB (NF-κB), Jak-Stat and mitogen-activated protein kinase (MAPK) pathways. Moreover, these pathways interact with one another and with other pathways in a highly regulated manner creating a vast signaling network between immune cells and cells from different tissues (*21*-*23*). One of the most studied pathways is the NF-*κ*B pathway. Initially, it was believed that this pathway was mainly activated in immune cells, but now it is recognized that it can be activated in most cells including adipose tissue, liver, and central nervous system (*24*). NF-*κ*B is a

transcription factor that regulates the expression of various genes, mainly those with pro-inflammatory and anti-apoptotic functions (*25*). The activation of the NF-κB pathway in macrophages and tissue cells plays a central role in the initiation and promotion of the inflammatory response. The signaling cascade that promotes the activation of NF-κB starts when cytokines or pathogen-associated molecular patterns (PAMPs) stimulate receptors located in the surface of the cell, including toll-like receptors (TLRs) (*24*). NF-κB dimers are normally sequestered in the cytosol of resting cells by inhibitory proteins known as the inhibitor of κB (IκB), which prevent its nuclear translocation. Once cytokines or PAMPs initiate the signaling cascades, the inhibitor of kB kinase (IKK) complex is activated. The activated IKK phosphorylates IκB, promoting its degradation and release of the NF-κB (*24, 25*). Free NF-κB translocates to the nucleus and promotes the expression of pro-inflammatory genes such as *COX-2*, *IFN-β* (*17*), and eventually *iNOS* (*26, 27*).

Role of Reactive Oxygen Species in Inflammation

ROS are molecules with strong oxidizing capabilities that are normally produced as byproducts of oxygen metabolism. The major ROS produced by cells are superoxide anion ($O_2^{-\bullet}$), hydroxyl radical ($OH^{\bullet}$), and hydrogen peroxide (H_2O_2). ROS are mainly generated as byproducts of mitochondrial metabolism through the electron transport chain (*28, 29*). However, another important source of ROS, especially in macrophages and endothelial cells, is the enzymatic reaction catalyzed by NADPH oxidases (NOX). Production of ROS by NOX is triggered by LPS and pro-inflammatory cytokines such as TNFα, and this is crucial in the inflammatory response (*28*). At high concentrations,

ROS can have harmful effects on cells because they can oxidize and damage cellular constituents such as proteins, lipids, and DNA. However in normal conditions, ROS play a crucial role in different cellular functions, such as cell proliferation, chemotaxis, and apoptosis (*28, 29*). In normal conditions, the presence of antioxidants balances the damaging effects of ROS. Some of these antioxidants are enzymes such as catalase and glutathione peroxidase or other molecules, such as glutathione and carotenoids (*30*). In an inflammation state, ROS, besides serving as a microbicidal agent, regulates different signaling pathways implicated in an inflammation response. For instance, ROS plays a major role in the activation of NF-κB (*31, 32*) and hypoxia-inducible factor 1α (HIF1α), which is a central regulator of the Warburg effect (*33*). In this scenario, ROS is an important mediator in the initiation and progression of inflammation related metabolic diseases (*28*).

Dietary Phytochemicals and Inflammation

It is now recognized by the scientific community that food, besides providing us with nutrients, can also help us prevent certain diseases. Many groups of foods have been shown to be beneficial for the prevention of different diseases. For instance, studies suggest that the high consumption of cereal fiber, whole grains, fruits, and vegetables is associated with a lower risk of colorectal cancer (*34, 35*); also, the consumption of fish, fruits and vegetables reduce the risk of stroke and coronary heart disease (*36-39*). In addition, the use of medicinal plants for the treatment of different diseases is a common practice in many cultures around the world (*40*). For example, Mashua tuber (*Tropaeolum tuberosum)* has been traditionally and extensively used as a medicinal plant

in the Andean region, for health improvements related to kidney and liver pain, skin eczemas, and prostate disorders (*41*).

Fruits, vegetables, and other edible plants such as herbs and spices or plant products such as tea and wine are rich in phytochemicals. Many of these chemicals found in plants have been shown to have bioactive properties, and are known to be responsible for many of the health beneficial properties attributed to plants (*42*). Most of these phytochemicals are secondary metabolites, which do not appear to be involved in the plant's photosynthesis, respiration, growth, and development, but possess other functions. Some of the functions that secondary metabolites have in plants are protection of plants from herbivores and microbial infection, attraction of pollinators, allelopathic agents, and protection against UV (*43*). Phytochemicals can be classified based on their biochemical origin as carotenoids, phenolics, alkaloids, nitrogen-containing compounds, and organosulfur compounds (*44*). Many of these chemicals have shown to reduce inflammation and related diseases through different mechanisms, by interfering at several points of cellular inflammatory pathways (*45*). Some of the mechanisms through which phytochemicals modulate inflammation are exerting antioxidant properties (*46-48*) and scavenging reactive oxygen species (*49-51*), modulating the activity of pro-inflammatory enzymes such as iNOS (*52*) and COX-2 (*53-55*), and modulating different inflammatory pathways such as NF-κB (*56-58*), STATs (*59, 60*), and MAPKs pathways (*61-63*). The modulation of inflammation by phytochemicals through any of the above-mentioned mechanisms usually results in a reduction of pro-inflammatory mediators which positively impacts inflammation and related diseases (*45*). Moreover, many

phytochemicals have more than one target (*64*), and when several of those phytochemicals are consumed concurrently the effect is superior, which makes it very attractive for therapeutic use (*65*).

Target Identification of Bioactive Compounds

Cellular targets for the majority of dietary phytochemicals remain unknown, presenting a challenge for understanding how these dietary components provide health benefits. The lack of knowledge about the molecular targets responsible for the beneficial and/or adverse side effects of most dietary compounds limits their potential use as medicinal foods, supplements or drugs, and their regulation (*64, 66*). Despite the great effort in the past decades to establish methods for the identification of the cellular targets of small molecules, this step, in many cases, continues to be the most challenging and the most limiting in chemical biology research. The reasons behind this deficit include the different chemical nature of bioactive molecules and their varying affinity for targets, the different nature of the target proteins and their varying abundance, and analytical methods not being sufficiently developed (*66*).

There are different methods and technologies that have been reported to identify proteins targets. These approaches can fundamentally be classified into direct (target-based) or indirect (phenotype-based) approaches (*67, 68*). The target-based approaches provide the most direct route to find the target protein. Affinity chromatography is a direct approach and remains the most widely used method for this purpose (*69, 70*). In affinity chromatography, the small molecule is usually attached to a solid support (e.g., Affi-Gel agarose beads) or labeled with an affinity tag (e.g., biotin). Then, proteins

bound to the small molecule are purified and identified using mass spectrometry analysis. Once the potential targets are identified, further studies need to be done to confirm the direct binding and its biological relevance (*67, 69, 71*). Although affinity-based target identification techniques directly detect the target, these are limited due to the necessity to derivatize the small molecule without losing bioactivity. In addition, these studies are time-consuming and require high expertise in medicinal chemistry; and most of the time the small molecule cannot be modified without losing its activity (*72*).

On the other hand, the indirect or phenotype-base approach identifies possible protein targets by profiling the biological effects of the small molecules. In this approach, when the compound of interest interferes with a cellular event whose regulatory pathways have been reported, protein targets can be narrowed down as possible candidates. Proteomics and genomics analyses have helped gather information about the biological activity of small molecules and target profiling. The disadvantage of this approach is that it depends on the drug's ability to induce specific cellular or biochemical responses (*67-69, 73*).

Drug Affinity Responsive Target Stability (DARTS)

Drug affinity responsive target stability (DARTS) is a simple and universally applicable target identification approach recently developed, that overcomes many of the limitations of other target identification methodologies. This approach relies on the drug-protein interaction but does not require modification of small molecules. The strategy of DARTS is based on the principle that binding of small molecules will stabilize target proteins, making them less susceptible towards proteolysis (*74*). Proteins,

under physiological conditions, are in a dynamic equilibrium, at which they can acquire alternative conformations and exhibit local reversible unfolding. When a ligand binds to a protein, the equilibrium shifts to a thermodynamically more stable state in which the target proteins experience less conformational fluctuations and unfolding. Under these conditions, the resistance to denaturation and proteolysis is markedly increased (*72, 75-77*). Lomenick et al (*74*), took advantage of this principle and proposed to use it to identify potential protein targets without derivatizing or immobilizing the small molecules. They also suggested methodologies that can be used together with DARTS to identify the protease-protected proteins. A schematic illustration of DARTS is shown in Figure 2.

The overall procedure of DARTS is relatively standardized, but there are several steps that must be modified for each experiment, which include the source of protein, selection of small molecule and protease, and their concentration ranges. For the source of protein, generally, any cell type that is sensitive to the biological effects of the small molecule can be used. The small molecule believed to bind proteins should meet certain criteria to be suitable for DARTS. This includes mainly small molecules that are not susceptible to proteolysis. There are many different proteases available that could be used with DARTS, but the ones that have primarily been used are thermolysin and Pronase. Briefly, in DARTS the cell lysates (or pure protein) are prepared and quantified, the compound of interest and a negative control are added, and the proteolysis is preformed (*78, 79*).

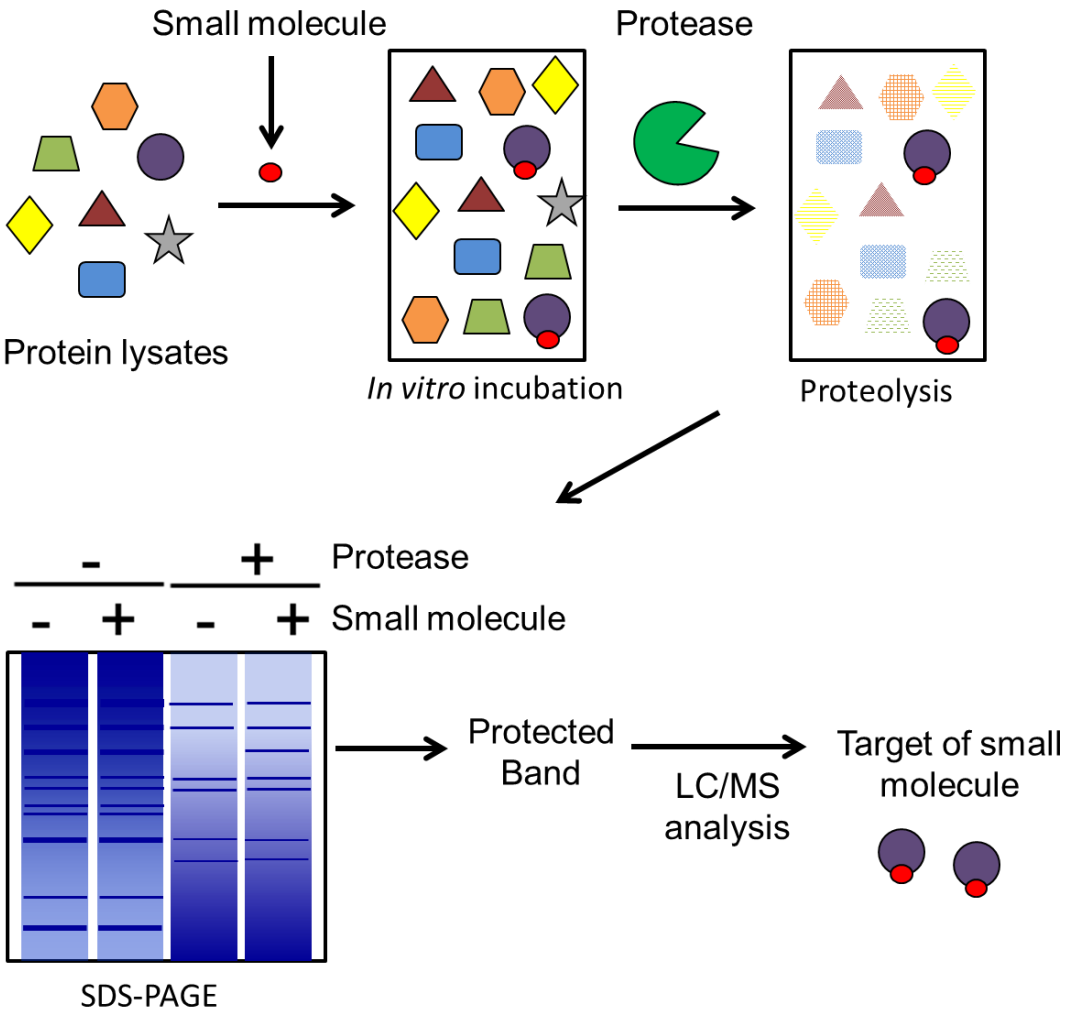

Figure 2 Flowchart of DARTS strategy used to identify protein targets of small molecules. Adapted from E. Tashiro and M. Imoto, 2012 (*67*). Mammalian or yeast cell lysates are incubated with the small molecule of interest, followed by the digestion of the mixture by the selected protease (usually pronase or thermolysin). The protein samples are separated by SDS-PAGE electrophoresis and the gel is stained with coomassie blue or silver staining. The lanes of the stained gel are analyzed for bands that are more intense in treated samples over the control. Once band differences are found, each band can be cut out, digested with trypsin, and analyzed with mass spectrometry to identify the potential target of the small molecule (*74*).

In order to identify targets of the compound of interest, one or more proteomics techniques must be used after the proteolysis. These techniques include but are not limited to Western blotting, SDS-PAGE, and gel-free MS-based proteomics. The simplest procedure for DARTS involves separation of the digested drug-treated and control protein samples by SDS–PAGE, staining the gel with Coomassie Blue, or silver stain, and analyzing the lanes of the gel for bands that are more intense in treated samples over the control. Once band differences are found, each band can be cut out, digested with trypsin, and analyzed by mass spectrometry (MS/MS) (*72, 78, 79*). Further studies need to be done to confirm the direct binding to the target protein and its biological relevance. The key advantage of DARTS is that it uses native small molecules; therefore it can potentially be used to identify binding targets for any small molecule even without knowing the chemical identity or purity of the compound. Thus, DARTS is suitable for target identification of bioactive natural product extracts. The main limitation of DARTS resides primarily in its low sensitivity especially for proteins of lower abundance. There is the need to use additional methods that will assist in finding more subtle differences in protein abundance. Another limitation of DARTS is that some proteins may not be stabilized sufficiently by ligand binding leading to false negatives (*72, 74*). DARTS has been used in different studies to identify the cellular targets of different compounds. For instance, eIF4A was identified as the target of resveratrol through the use of DARTS (*74*). Also, this approach was used to reveal that grape seed extract (GSE) targets endoplasmic reticulum (ER) stress response proteins in human colon cancer cells (*80*) and the dietary compound isoliquiritigenin targets GRP78

in breast cancer stem cells (*81*). In addition, DARTS was used in the development of a C-terminal Hsp90 inhibitor, KU174, which demonstrates anti-cancer activity in prostate (*82*).

Objective and Hypotheses

Overall Objective and Central Hypothesis

Overall Objective: To evaluate the anti-inflammatory properties of mashua tuber and acerola leaf extracts and to identify the protein targets of its phytochemicals by using DARTS methodology.

Central Hypothesis: The phytochemicals present in mashua tuber and acerola leaves will suppress inflammatory markers and DARTS will allow the identification the associated-protein targets.

Specific Aims

Aim 1 (Chapter II): To investigate the anti-inflammatory properties of mashua extracts in RAW 264.7 macrophages and to identify the protein targets of its phytochemicals by using DARTS methodology.

***Hypothesis*:** Mashua extracts will suppress inflammation in RAW 264.7 macrophages and the use of DARTS will allow the identification the associated-protein targets.

Objectives

1.1 To determine the anti-inflammatory properties of mashua extracts in RAW264.7 macrophages.

1.2 To characterize the phytochemicals from mashua.

1.3 To use DARTS methodology to determine the protein targets of mashua phytochemicals in RAW264.7 macrophages.

1.4 To determine the mechanism of action by which mashua phytochemicals exert their anti-inflammatory properties in RAW264.7 macrophages.

1.5 To describe the Warburg effect in LPS stimulated RAW264.7 macrophages.

Aim 2 (Chapter III): To identify the bioactive compounds acting as COX-2 inhibitors in acerola leaf extract by using bioassay-guided fractionation and DARTS methodology.

***Hypothesis*:** Bioassay-guided fractionation and DARTS will allow the identification of phytochemicals acting as COX-2 inhibitors in acerola leaf extract.

Objectives

2.1 To evaluate the effect of acerola leaf extract and its components on COX-2 activity.

2.2 To characterize the phytochemicals from acerola leaves.

2.3 To use bioassay-guided fractionation and DARTS methodology to identify the bioactive compounds acting as COX-2 inhibitors in acerola leaf extract.

2.4 To evaluate DARTS as a screening technique.

CHAPTER II

TARGET IDENTIFICATION USING DARTS: MASHUA (*TROPAEOLUM TUBEROSUM*) EXTRACTS EXERT ANTI-INFLAMMATORY PROPERTIES AND ATTENUATE THE LPS-INDUCED WARBURG-LIKE EFFECT IN RAW264.7 MACROPHAGES BY INHIBITING PYRUVATE KINASE M AND REDUCING ROS

Overview

Cellular targets for the majority of dietary phytochemicals remain unknown, presenting a challenge for understanding how these dietary components provide health benefits. The Andean tuber mashua (*Tropaeolum tuberosum*) has sparkled interest because of its history in traditional medicinal use. The objective of this study was to investigate the anti-inflammatory properties of mashua extracts and to identify the cellular targets of its phytochemicals. The extracts of six genotypes of mashua (203081, 203070, 203040, 203109, 203003 and 203021) were screened for their anti-inflammatory properties using RAW 264.7 macrophages. Results indicated that all mashua extracts reduced ($P \leq 0.05$) nitric oxide (NO) levels and all, except for 203076, reduced ($P \leq 0.05$) reactive oxygen species (ROS) after 19 h of LPS stimulation. Extracts 203040 and 203081 were the most active to reduce both NO and ROS production, and thus were selected to further study the cellular targets of its phytochemicals. Through DARTS methodology we identified pyruvate kinase M (PKM) as a potential target of the phytochemicals present in both extracts. The biological relevance of the binding of

mashua phytochemicals to PKM was validated by showing that both extracts inhibit pyruvate kinase (PK) activity. Furthermore, mashua extracts reduced LPS- induced PK activity, lactate levels, mitochondrial dehydrogenase activity and *GLUT1* gene expression, indicating the effect of mashua on the LPS-induced Warburg effect. Additional results showed that mashua extracts reduced early (6 h) and late (19 h) ROS levels and consequently affected the expression of ROS dependent LPS-induced pro-inflammatory genes such as *IL-1β, TNFα, iNOS*, *COX-2* and *IFN-β.* LC-MS profiling revealed that both mashua extracts contained mainly phenolics and isothiocyanates. In order to understand the identity of the mashua phytochemicals that possess the anti-inflammatory properties, mashua 202040 and 203081 fractions (F1, F2, F3, F4, F4MeOH and F4H_2O) were evaluated for their effects on LPS-induced ROS and NO, and their ability to bind to PKM2. Results showed that both, phenolics and isothiocyantes in both mashua extracts have anti-inflammatory properties. In this study, we demonstrate that phytochemicals from two genotypes of mashua reduce LPS-induced inflammation in RAW264.7 macrophages by targeting PKM and reducing ROS.

Introduction

Cellular targets for the majority of dietary phytochemicals remain unknown, presenting a challenge for understanding how these dietary components provide health benefits. Despite the great effort in the past decades to establish methods for the identification of the cellular targets of small molecules, this step, in many cases, continues to be the most challenging and the most limiting in chemical biology research (*66, 67*). The reasons behind this deficit include the different chemical nature of

bioactive molecules and their varying affinity for targets, the different nature of the target proteins and their varying abundance, and analytical methods not being sufficiently developed (*66*). Recently a new methodology, drug affinity responsive target stability (DARTS), was developed for this purpose. DARTS is simple and universally applicable target identification approach that overcomes some of the limitations of traditional methods. This approach is based on the lower susceptibility to proteolysis after the drug is bound to the protein target. The key advantage of DARTS over other target identification is that the small molecules are used without the need for chemical modification. Because DARTS is not limited by the chemical structure of the drug, it can be used to identify molecular targets for any small molecule, even without knowing its chemical identity or purity (*72, 74*).

Chronic inflammation is a pathological condition characterized by continued active inflammation response and has been implicated in the development of a variety of diseases, including obesity, diabetes (*8*), atherosclerosis (*9*), neurodegenerative diseases (*10*) and some types of cancers (*11*). Macrophages play a central role in many different immune pathological phenomena that lead to chronic inflammation and associated diseases. These include the over-production of pro-inflammatory cytokines such as tumor necrosis factor-alpha (TNF-α) and interleukin 1-beta (IL-1β) and other inflammatory mediators like reactive oxygen species (ROS) and nitric oxide (NO) (*15*). Recently, there have been new insights on the importance of metabolic changes in macrophages on its activation and the resultant inflammatory response. Similar to tumor cells, LPS-activated macrophages have the ability to switch from oxidative

phosphorylation to aerobic glycolysis, a phenomenon known as the "Warburg Effect"(*19*). Pyruvate kinase M2 (PKM2), a protein kinase and transcriptional coactivator, plays an essential role in the Warburg Effect and the in the activation of macrophages. Thus, PKM2 has emerged as a novel target for inflammation and related diseases (*83, 84*).

Natural food products have gained interest in the past decades as new sources of health beneficial agents due to their usually low toxicity in humans. Mashua (*Tropaeolum tuberosum)* is an Andean tuber crop that belongs to the Tropaeolaceae family. Mashua has been cultivated since the time of the Incas and is mainly found in the high Andes from Colombia to northwest Argentina. Mashua tubers are usually 5–15 cm long and 3–6 cm broad in their distal part and can vary considerably in shape and color. The tuber skin can display white, yellow, purple or red tones and some of them present mottled or striped patterns. Mashua has been traditionally and extensively used as a medicinal plant for health improvements related to kidney and liver pain, skin eczemas and prostate disorders (*41*). Studies on the phytochemical composition of mashua have indicated the presence of glucosinolates and its hydrolysis product, isothiocyanates (*85-87*) and phenolic compounds (*88, 89*). The glucosinlates that have been reported in mashua include *p*-methoxybenzyl, 2–propyl, 2–butyl, 4-hydroxybenzyl and benzyl glucosinolates (*85-87*). Among the phenolic compounds that have been reported in mashua are gallic acid, gallocatechin, epigallocatechin, procyanidin B2 and epigallocatechin derivatives, different hydroxycinnamic and hydroxybenzoic acid derivatives and rutin and/or myricetin derivatives (*90*). For purple colored tubers the

major anthocyanins found were delphinidin di- and tri-glycosides acylated with acetic acid (*89*). Mashua has been shown to possess anti-microbial and nematocidal properties attributed to the presence of isothiocyanates (*91*). Also, mashua has been shown to protect against LDL oxidation and oxidative hemolysis of erythrocytes (*92*). The antioxidant properties of mashua have been mostly attributed to the phenolic compounds present in this tuber (*93*).

The objective of this study was to investigate the anti-inflammatory properties of mashua extracts and to identify the cellular targets of its phytochemicals. Moreover, LPS stimulated RAW 264.7 macrophage cell line was investigated as a model of the Warburg effect.

Materials and Methods

Freeze dried tubers of six genotypes of mashua (*Tropaeolum tuberosum*) were supplied by the International Potato Center (CIP, Lima, Peru). Upon arrival at Texas A&M University, the samples were frozen and kept at −80 °C until use. The following chemicals were used in the experiments: Lipopolysaccharide (LPS), Diphenyleneiodonium (DPI), 2′,7′-Dichlorofluorescin diacetate (DCFA), Griess reagent, Sodium nitrite solution, Dulbecco's Modified Eagle's Medium (DMEM)/low glucose, phenol red-free DMEM/low glucose, penicillin/streptomicyn mixture, DMSO and Fetal Bovine Serum (FBS) were purchased from Sigma (St. Louis, MO). Glucose and sodium bicarbonate were purchased from Acros Organics (Fair Lawn, NJ) and sodium bicarbonate from Mallinckrodt Chemicals (Phillipsburg, NJ). Pronase and Protease Inhibitor Mixture EDTA-free were purchased from Roche Applied Science

(Indianapolis, IN). Disuccinimidyl suberate was purchased from Thermo Scientific Pierce (Waltham, MA). The CellTiter 96® AQ_{ueous} non-radioactive cell proliferation assay kit was purchased from Promega (Madison, WI) and the Nuclear Extract Kit from Active Motif (Carlsbad, CA). Antibodies against PKM2, PKM1 and ACTIN were purchased from Cell Signaling Technology (Danvers, MA). Macrophages RAW 264.7 (cell line TIB-71™) was acquired from the American Type Culture Collection (ATCC) (Manassas, VA).

Extraction and Fractionation

The sample preparation and fractionation procedure is illustrated in Figure 3. A 4 g portion of lyophilized powder of mashua was dissolved in a mixture of MeOH/acetone/H_2O (5:4:1) and placed in a shaker for 12 hours at 4°C. The extract was removed and new extraction solvent was added. This procedure was repeated two additional times. The extract was then filtered through Whatman #1 filter paper and evaporated at 45 °C using a rotavapor (Büchi, Switzerland). The remaining aqueous extracts (5 ml) were loaded into a SEP Pack C18 cartridge (55−105 μm, Waters Corp., Milford, MA) previously conditioned to pH 7.0. The cartridge was first washed with 150 mL of water (pH 7.0). After, compounds were eluted with 50 ml of ethyl acetate, 50 ml of acetone and 50 ml of methanol, respectively. The water from the wash was adjusted to pH 2.0. This mixture of compounds was loaded into a second cartridge previously conditioned at pH 2.0.

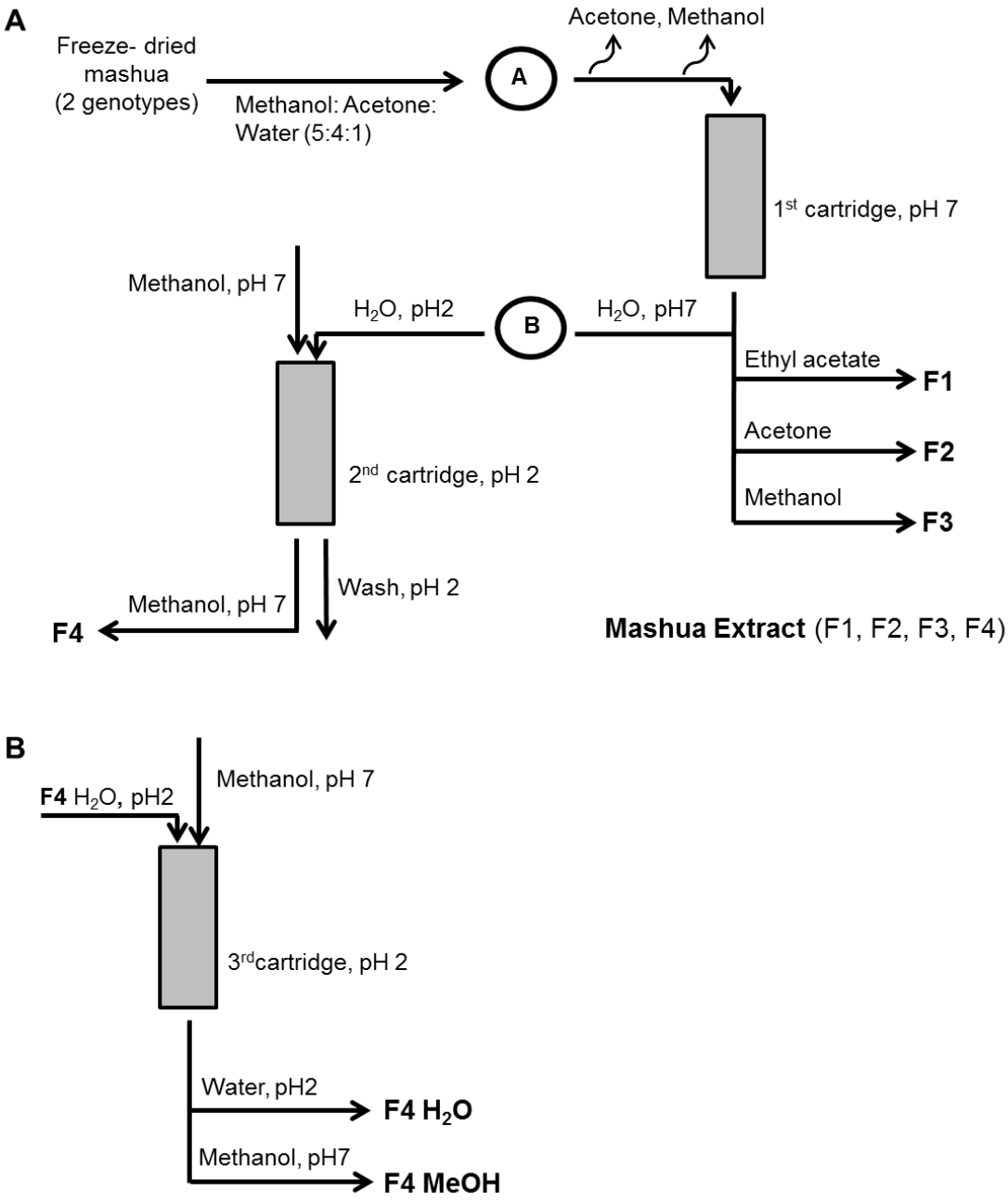

Figure 3 Extraction and fractionation scheme used for mashua to obtain fractions F1, F2, F3, and F4 (A) and F4 H_2O and F4 MeOH (B).

The compounds bound to the matrix of the second cartridge were later eluted with 50 mL of methanol. The four fractions obtained were mixed (mashua extract) or left as individual fractions (F1, F2, F3, F4) (Figure 3A). Fraction F4 was further cleaned to remove remaining sugars. For this, the sample was loaded into a SEP Pack C18 cartridge previously conditioned to pH 2.0. The cartridge was first washed with 150 mL of water (pH 2.0) and then the compounds were eluted with 50 ml of methanol to obtain fractions F4H_2O and F4MeOH respectively (Figure 3B). Extracts and fractions were evaporated at 45 °C using a Centrivap (Labcono) and stored at −20 °C.

During the extraction process a yield of ~ 82, ~ 94, ~ 85, ~ 88, ~ 149, and ~ 58 mg of a MeOH/acetone/H_2O solvent crude extract powder was obtained from each 4 g of freeze-dried 203003, 203021, 203040, 203076, 203109 and 203081 mashua powder, respectively. For mashua 203081, during the fractionation process, a yield of ~ 36, ~ 17, ~ 12 and ~ 67 mg of fraction powders were obtained for F1, F2, F3 and F4 fractions respectively, per each 4 g of the freeze-dried mashua powder. For mashua 203040, during the fractionation process, a yield of ~ 36, ~ 32, ~ 31.4 and ~ 62 mg of fraction powders were obtained for F1, F2, F3 and F4 fractions respectively, per each 4 g of the freeze-dried mashua powder. Additionally, F4 was further fractionated with yields of ~ 24.5 and ~ 6.1 mg of F4H_2O and F4MeOH respectively for mashua 203081 and of ~ 22.9 and ~ 4.4 mg of F4H_2O and F4MeOH respectively for mashua 203040, per each 0.3 g of the dried F4 mashua powder.

LC-MS Analysis and Conditions

Samples were dissolved in MeOH and 10 µl at a concentration of 5 mg/ml was injected into the LC-MS instrument for analysis. The system used was a Surveyor (Thermo Scientific, USA) coupled to Surveyor DAD. The eluents were acetonitrile/methanol (1:1), formic acid (0.5:99.5, v/v) (phase A) and formic acid–water (0.5:99.5, v/v) (phase B). The applied elution conditions were: 0-2 min, 2% A, 98% B; 3-5 min, 5%A, 95% B, 5-30 min, 20% A, 80% B; 30-72min, 35% A, 65% B; 72-83 min, 100% A, 0% B; 83-85 min was held isocratic, 100% A; 87-90min 2% A, 98% to the starting condition. The chromatograms were monitored at 330, 280, 210 nm; and complete spectral data were recorded in the range 200–600 nm. A reversed-phase Phenomenex (Torrance, USA) Luna C_{18} column (150mm×4.6mm i.d. and particle size 3_m) with a Waters Nova-Pack C_{18} guard column (10mm×3.9mm i.d, 4_m) was used and a flow of 200 µL/min from the DAD eluent was directed to the ESI interface using a flow-splitter. Nitrogen was used as desolvation gas, at 275°C and a flow rate of 60 L/h, and no cone gas was used. Mass spectra were obtained on a MS Finnigan LCQ Deca XP Max, ion trap mass spectrometer coupled at the exit of the diode array detector and equipped with a *Z*-spray ESI source, and run by Xcalibur version 1.3 software (Thermofinnigan-Surveyor, San José, USA). A potential of 1.5 kV was used on the capillary for positive ion mode. The source block temperature was held at 120°C.

Analysis of Total Phenolics (TP)

Total phenolics were determined using the method described by Swain and Hillis (*94*). The extract was dissolved in methanol (30 mg of powder extract/ml of methanol).

Methanolic extracts (13 μL) were diluted with nanopure water (208 μL) in a 96-well microplate well, followed by the addition of 0.25 N Folin–Ciocalteu reagent (15 μL). The mixture was incubated for 3 min, and then, 1 N Na_2CO_3 (26 μL) was added. The final mixture was incubated for 2 h at room temperature in the dark. Spectrophotometric readings at 725 nm were collected using a plate reader (Synergy HT, Bio-Tek Instruments, Inc., Winooski, VT). Total phenolics were expressed as mg chlorogenic acid equivalents (CAE)/mg of crude extract.

Cell Culture and Treatment of Mashua Extracts and Fractions

Raw 264.7 macrophages were grown in the DMEM-low glucose (pH 7.2 – 7.4) including 4 g/l glucose, 3.7 g/l sodium bicarbonate, 10% fetal bovine serum (FBS) and antibiotics (100 units/ml penicillin and 100 μg/ml streptomycin) in a humidified atmosphere with 5% CO_2 at 37°C. Cells were used at a passage of 3 to 8 in this study. For treatments of cells with mashua extracts and its fractions (F1, F2, F3, F4, F4H_2O, and F4MeOH), the cells were plated at 0.5×10^5 cells/well in a 96-well black or clear bottom plates (Costar, Cambridge, MA) for MTS test, NO/ROS and lactate measurements, and at 0.5×10^6 cells/well in 6-well plate (BD Biosciences, Franklin Lakes, NJ) for gene expression, protein expression, crosslinking and pyruvate kinase activity analysis, and then cultured overnight. The cells were treated with the growth medium containing 1 μg/ml LPS either with or without 5 h-pre-treatment of mashua extracts and its fractions. Cells were stimulated with LPS for either 6 h or 19 h and treated with mashua extracts and its fractions for either 11 h or 24 h (including pre-treatment), depending on the experiment. Mashua extracts and its fractions were

dissolved in the growth medium including 0.5 % DMSO, which was used as a control in all experiments. Finally, cells and medium at the time points indicated were used for various measurements in this study.

Cell Viability and LPS-Induced Mitochondrial Dehydrogenase Activity

Macrophages were plated at 0.5×10^5 cells/well in 96-well clear bottom plates (Costar) and cultured overnight. For the cell viability test, cells were treated with mashua extracts and its fractions for 24 h. For the measurement of mitochondrial dehydrogenase, cells were stimulated with LPS for 19 h either with or without 5 h-pre-treatment of mashua extracts and its fractions. Cell viability and mitochondrial dehydrogenase activity were evaluated using the MTS assay kit (Promega, Madison, WI), according to the manufacturer's instructions. The quantity of formazan product was measured at 490 nm and is directly proportional to the mitochondrial dehydrogenase activity (*95*).

Detection of Extracellular Nitric Oxide and Intracellular Reactive Oxygen Species Production

Macrophages were plated at 0.5×10^5 cells/well in a 96-well black and clear bottom plates (Costar) and cultured overnight. The cells were stimulated with LPS for times indicated in this study either with or without 5 h-pre-treatment of mashua extracts and its fractions as described above. Finally, cells and medium were used for the ROS and NO assays, respectively.

First, the nitric oxide (NO) production was assessed as the accumulation of nitrite (NO_2^-) in the medium using a colorimetric reaction with Griess reagent. Briefly, 50 µl of cell culture supernatants were obtained at 19 h after LPS treatment and 100 mM sodium

nitrite solution was diluted with nanopure water for the preparation of standards from 10 to 100 μM. Subsequently, the cell supernatants and standards were mixed with an equal (1:1) volume of Griess reagent and finally absorbance was measured at 540 nm using a 96-well microplate reader (Synergy HT, Bio-Tek Instruments, Inc., Winooski, VT). Second, intracellular ROS production was measured by 2′,7′-Dichlorofluorescin diacetate (DCFA). Briefly, the cell culture medium was removed by aspiration at times indicated in this study after the LPS challenge, and subsequently cells were exposed to 10 μM DCFA in phenol red/FBS-free DMEM for 30 min, then washed twice with the phenol red/FBS-free DMEM. Finally, fluorescence was read immediately at wavelengths of 485 nm for excitation and 528 nm for emission on a 96-well microplate reader (Synergy HT, Bio-Tek Instruments, Inc., Winooski, VT).

DARTS

The target identification using drug affinity responsive target stability (DARTS) methodology used was based on the protocol by Lomenick et al. (*78*). Macrophages were plated at 1 $\times 10^6$ cells/well in 150 x 25 mm clear plates and cultured overnight. The cells then were stimulated with LPS for 19 h. Subsequently, cells were washed twice with DPBS and lysed with M-PER (Pierce) supplemented with protease and phosphatase inhibitors. Protein concentrations were determined by the Pierce BCA protein assay kit (Thermo Fisher Scientific, Rockford, IL). Lysates were incubated with 400 μg/ml of mashua extracts, 400 μg/ml of mashua fractions or DMSO (control) for 3 h at room temperature. Each sample was then divided into two to six aliquots, each of which underwent proteolysis with pronase or mock proteolysis, for 25 min at room

temperature. A 1:250, 1:500, 1:1000, 1:2500 and/or 1:5000 ratios of Pronase versus cell lysates protein concentration were used for proteolysis. Proteolysis was stopped by addition of loading buffer or protease inhibitor, and this was followed by coomassie blue staining, silver staining or western blot analysis. Commassie blue and silver staining were used to visualize the in gel band protection by mashua extracts. The target protein was cut out of the gel, digested and identified by MALDI-TOF analysis (*78*).

PKM1 and PKM2 Protein Expression and Western Blot Analysis

Cells were washed twice with DPBS and lysed with M-PER (Pierce) supplemented with protease and phosphatase inhibitors. Protein concentrations were determined by the Pierce BCA protein assay kit (Thermo Fisher Scientific, Rockford, IL). Prepared protein samples were loaded on a gel with a pre-stained, broad-range, molecular weight protein marker (Bio-Rad). Proteins were fractionated by electrophoresis using 10 % polyacrylamide gels. The gels were transferred by wet blotting onto PVDF membranes (Millipore, Bedford, MA). The membranes were blocked with 5 % skim milk in Tris-buffered saline with 1% Tween-20 (TBS-T) for 1 h with gentle shaking. Membranes were then incubated overnight with a specific primary antibody against PKM2 (1:1000), PKM1 (1:1000) and Actin (1:5000) at 4 °C. The membranes were washed four times with TBS-T and incubated for 1 h at room temperature with the secondary antibody conjugated with horseradish peroxidase (HRP) at 1:5000 dilution. Specific bands were developed using a SuperSignal West Femto enhanced chemiluminescence (ECL) Western blotting detection kit (Pierce, Thermo Fisher Scientific, Inc., Rockford, IL) and the signals were captured by Chemi Doc XRS

(Bio-Rad Laboratories, Hercules, CA). Bands were quantified using densitometry with ImageJ software (NIH, Bethesda, MD).

Nuclear Fractionation

Nuclear extracts were obtained using a Nuclear Extract Kit (Active Motif 40010) according to manufacturer's recommendations. Briefly, cells were washed twice with ice-cold DPBS and collected by scraping in DPBS. Cells were then pelleted and resuspended in hypotonic buffer. Next, detergent was added to the samples, and then these were centrifuged for 30 s at 14,000×*g*. The supernatant (cytoplasmic fraction) was removed and saved. The nuclear pellet was resuspended in complete lysis buffer and the nuclear protein fraction was collected after centrifugation for 10 s at 14,000×*g*. PKM2 nuclear protein expression was analyzed by Western blot as described previously.

PKM2 Crosslinking Analysis

Cells were washed twice with ice-cold DPBS and collected by scraping in DPBS with 1× Complete Protease Inhibitor Mixture, EDTA-free (Roche Applied Science). Samples were incubated with 1 mM disuccinimidyl suberate (Thermo Scientific Pierce) for 30 min at room temperature. The reaction was quenched with the addition of 1 M Tris, pH 7.5, to 30 mM final concentration and incubated for 10 min at room temperature. After quenching, cross-linked samples were lysed and protein concentrations were determined by the Pierce BCA protein assay kit (Thermo Fisher Scientific, Rockford, IL). Western blot analysis was used to analyze PKM2 crosslinked samples as described previously.

Pyruvate Kinase Activity Assay

Pyruvate kinase activity was measured after cell lysates were directly exposed to mashua treatments and also in cells lysates that had been previously treated with mashua during their growth. For the first procedure, macrophages were plated at 1×10^5 cells/well in 150 x 25 mm clear plates and cultured overnight. The cells were then stimulated by LPS for 19 h. Cell lysates where exposed to mashua treatments and pyruvate kinase activity was measured. For the second procedure, macrophages were plated at 0.5×10^6 cells/well in 6-well plates (Costar) and cultured overnight. The cells were stimulated by LPS for 19 h either with or without 5 h-pre-treatment of mashua extracts. Pyruvate kinase activity in cell lysates was measured using the pyruvate kinase activity assay kit (BioVision, Mountain View, CA) according to the manufacturer's instructions. Briefly, in this assay, phosphoenolpyruvate and ADP are converted into pyruvate and ATP by the reaction catalyzed by PK. Then, the generated pyruvate is oxidized by pyruvate oxidase to produce a color reaction (λ = 570 nm). The color intensity is proportional to the amount of pyruvate produced, and therefore the PK activity can be measured. Enzyme activity was normalized to total protein content in each sample

Lactate Production Assay

Macrophages were plated at 0.5×10^5 /well in a 96-well black and clear bottom plates (Costar) and cultured overnight. The cells were stimulated by LPS for 19 h either with or without 5 h-pre-treatment of mashua extracts as described above. Lactate

production in the medium was detected by using the Lactate Assay Kit (BioVision, Mountain View, CA), according to the manufacturer's instructions.

Total RNA Preparation and Real-Time qRT-PCR Analysis

Total RNA was extracted from macrophages after LPS treatment for 6 or 19 h using the TRIzol® Reagent (Invitrogen, Carlsbad, CA), according to the manufacturer's instructions. RNA concentration was measured with a NanoDrop ND-1000 spectrophotometer (NanoDrop Technologies, Willmington, DE). The 1 μg RNA, treated with DNase I to avoid DNA contamination, was reverse-transcribed into cDNA using the SuperScript III first-strand synthesis supermix (Invitrogen, Carlsbad, CA), following the manufacturers protocol. Finally, the cDNAs were used for real-time qRT-PCR analyses, which were performed using Power SYBR Green PCR Master Mix (Applied Biosystems, Foster City, CA), following the manufacturer's instructions. cDNA amplification was carried out using a 7900 HT Sequence Detection System (Applied Biosystems, Foster City, CA). The primer sets are listed in Table 1 and were provided by Integrated DNA Technologies (IDT, Coralville, IA). The relative expression of each gene was normalized by β-Actin or by the geometrical mean of β-actin, GDHA and 18s ribosomal RNA (*96*), and was calculated following the comparative Ct method (ΔΔCt), also known as the $2^{-\Delta\Delta Ct}$ method (*97*).

Table 1 Sequences of primers used in gene expression studies

Primer	Sequence
TNFα-F	5’-ACTGGCAGAAGAGGCACTCC -3’
TNFα-R	5’-CGATCACCCCGAAGTTCA-3’
COX-2-F	5’-ACATCGATGTCATGGAACTG-3’
COX-2-R	5’-GGACACCCCTTCACATTATT-3’
IFN-β-F	5’-TCCAAGAAAGGACGAACATTCG-3’
IFN-β-R	5’-TGAGGACATCTCCCACGTCAA-3’
IL-1β-F	5’-GAGCACCTTCTTTTCCTTCATCT-3’
IL-1β-R	5’-GATATTCTGTCCATTGAGGTGGA-3’
iNOS-F	5’-GCTCGCTTTGCCACGGACGA-3’
iNOS-R	5’-AAGGCAGCGGGCACATGCAA-3’
β-Actin-F	5’-CCCAGGCATTGCTGACAGG-3’
β-Actin-R	5’-TGGAAGGTGGACAGTGAGGC-3’
PKM2-F	5’-TCGCATGCAGCACCTGATT-3
PKM2-R	5’-CCTCGAATAGCTGCAAGTGGTA-3’
PKM1-F	5’-GCTGTTTGAAGAGCTTGTGC-3’
PKM1-R	5’-TTATAAGAGGCCTCCACGCT-3’
LDHA-F	5’-CTTCCTCAGTGTCCCATGTATC-3’
LDHA-R	5’-GTGTCTGCGCTCTTCTTCA-3’
PDK1-F	5’-CCACTGAGGAAGATCGACAGAC-3’
PDK1-R	5’-AGAGGCGTGATATGGGCAATCC-3’
GLUT1-F	5’-ATGGATCCCAGCAGCAAG-3’

Table 1 Continued

GLUT1-R	5’-CCAGTGTTATAGCCGAACTGC-3’
18S ribosomal RNA-F	5’-CTTAGAGGGACAAGTGGCG-3’
18S ribosomal RNA-R	5’-ACGCTGAGCCAGTCAGTGTA-3’
GDHA-F	5’-AATGTGTCCGTCGTGGATCT-3’
GDHA-R	5’-CATCGAAGGTGGAAGAGTGG-3’

Statistical Analysis

The data were analyzed using Student's t-test or one-way analysis of variance (ANOVA) followed by Tukey-HSD test, using the software JMP Pro v10.0. Results are expressed as means ± standard errors (SE) from at least three biological repeats. Different letters show significant differences ($P < 0.05$).

Results

Total Phenolic Content of Mashua Genotypes

The total phenolic analysis indicated that the purple genotypes of mashua 203003, 203021 and 203040 contained 390, 382.4 and 313.0 mg CAE/ mg of dried extract respectively. On the other hand, the yellow genotypes of mashua 203076, 203109 and 203081 contained 58.4, 60.5 and 76.3 mg CAE/ mg of dried extract respectively. Overall, the purple genotypes of mashua contained higher phenolic content compare to the yellow genotypes.

Characterization and Identification of Compounds by LC-MS in Mashua Extracts and Fractions

Mashua 203040

HPLC/MS profiles of mashua 203040 fractions F1, F2 and F3, are illustrated in Figure 4, and the profiles of fractions F4H_2O and F4MeOH in Figure 5. The retention time, peak area, UV absorption, molecular weight, MS^2, and identification of compounds detected in mashua 203040 fractions F1, F2, F3, F4H_2O, and F4MeOH, are listed in Table 2-6, respectively. The compounds were identified according to their fragmentation data and UV absorption. In the ethyl acetate fraction (F1), compound **1** at R.T 15.95 with $[M+H]^+$ 180 yielded in MS^2 fragments at *m/z* 167, 149, 105, and 70.07, the major fragmentation of *m/z* 149 was due to the loss of benzyl isothiocyante group and this compound was assigned as 4-methoxy benzyl isothiocyanate. Compound **2** at R.T 23.70 showed UV maxima at 227, 278 with $[M+H]^+$ 166 yielded MS^2 fragments at *m/z* 147 and 121, the major fragment 121 was due to the loss of 4-hydroxy vinyl cation. Compound **3** at R.T 26.08 showed UV maxima at 227, 278 with $[M+H]^+$ 150 yielded MS^2 fragments at *m/z* 121 and 77, and this compound was identified as benzyl isothiocyanate. Compound **4** at R.T 31.60 with $[M+H]^+$ 206 yielded MS^2 fragments at *m/z* 161, 149, 136, 118, and this compound was identified as indolemethyl-isothiocyanate. Compound **5** at R.T 33.97 and compound **6** at R.T 37.11 with $[M+H]^+$ 282 and $[M+H]^+$ 369 yielded MS^2 fragments 150 and 121, and 262, respectively. Compound **5** was tentatively identified as indole methyl phenyl derivative and compound **6** remained unknown.

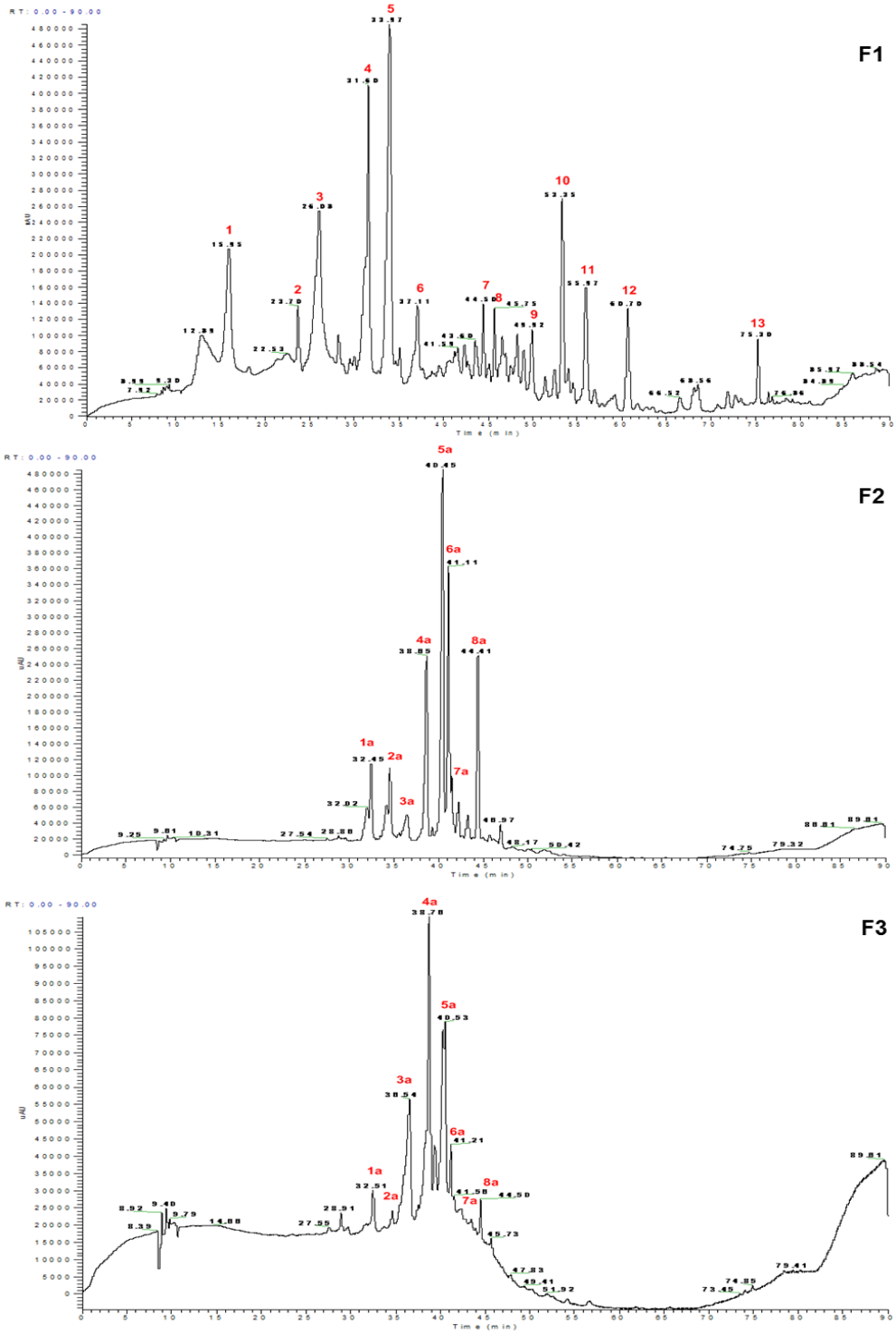

Figure 4 HPLC/MS profiles of mashua 203040 fractions F1, F2 and F3.

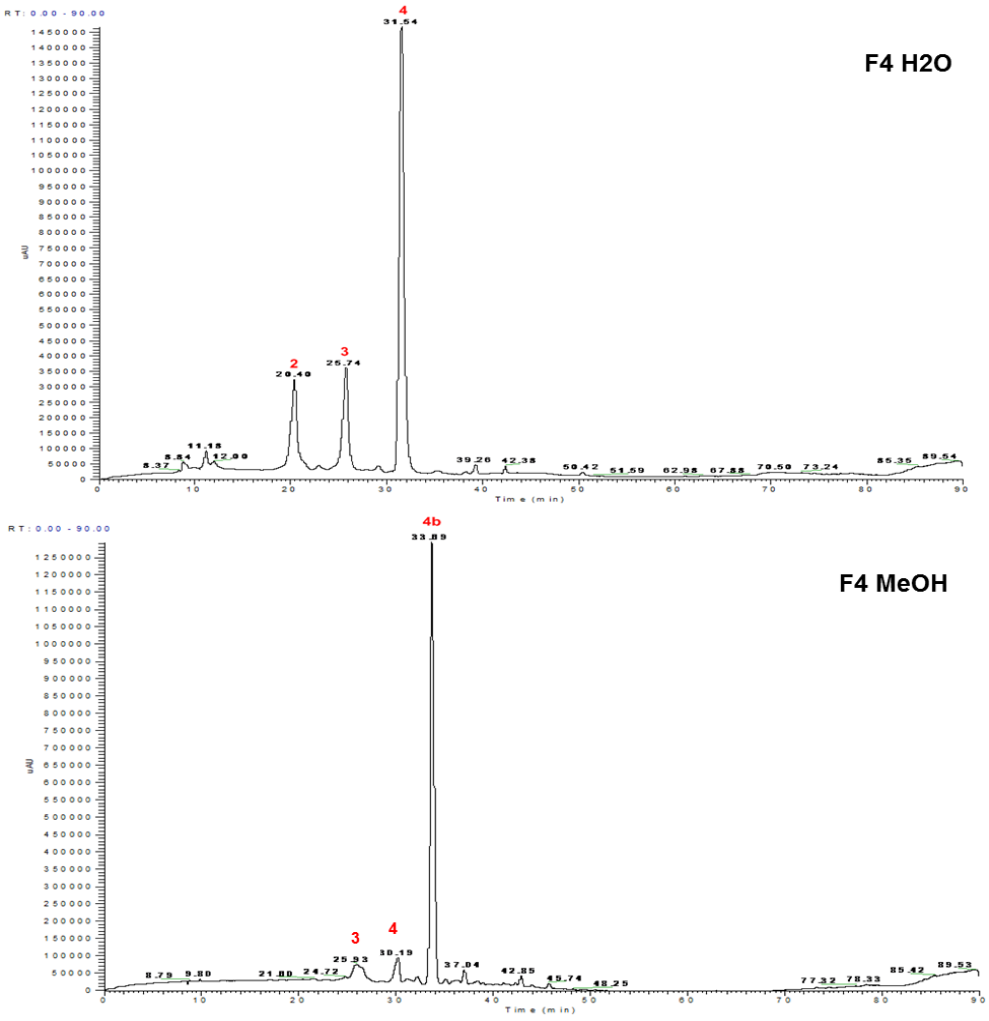

Figure 5 HPLC/MS profiles of mashua 203040 fractions F4 H_2O and F4 MeOH.

Table 2 Identification of phytochemicals from the ethyl acetate fraction (F1) from mashua 203040

Peak No	Retention time	Area	Mass [M+H]	UV	MS^n	Identification
1	15.95	6021206.1	180	227, 278	MS^2 180 : 167, 149, 105, 70.07	4-methoxy benzyl isothiocyanate
2	23.70	1392619.6	166	227, 278	MS^2 166: 147, 121	4-hydroxy benzyl isothiocyanate
3	26.08	11045159.9	150	227, 278	MS^2 150: 121, 77.0	benzyl isothiocyanate
4	31.60	11274489.1	206	227, 278	MS^2 206: 161, 149, 136, 118	Indolemethyl-isothiocyanate
5	33.97	13642787.9	282	227, 282	MS^2 282: 150, 121	unknown isothiocyante derivative
6	37.11	3407525.6	369	227, 280	MS^2 : 369 262	unknown isothiocyante derivative
7	44.50	1399933.5	579	235, 278	MS^2 : 579 457, 288	Procyanidin B2
8	45.75	1564125.5	457	235, 275	MS^2 : 457 457, 305, 169	(–)-epigallocatechin gallate
9	49.92	1642212.5	441	232, 261	MS^2 : 441 289, 169	epicatechin gallate
10	55.35	4730827.4	165	310	MS^2 : 165 127, 118	p-Coumaric acid
11	55.97	3799947.4	339	315	MS^2 : 339 190.9, 162.9, 172.9	5-pCoQA (5-p-coumaroylquinic acid)
12	60.70	3315513.2	333	315	MS^2 : 333 168, 150, 124.8	GCA (gallic-caffeic acid ester)
13	75.30	1218374	343	328	MS^2:343 160.9,134.9 202.8, 280.9, 250.9	diCA (dicaffeic acid)

Table 3 Identification of phytochemicals from the acetone fraction (F2) from mashua 203040

Peak No	Retention time	Area	Mass [M+H]	UV	MS^n	Identification
1a	32.45	2962101.5	773	330, 520	MS^2 **773** : 627, 303	delphinidin 3-sophoroside-5-rhamnoside
2a	34.55	2783552.6	465	330, 520	MS^2 **465**: 465, 303	delphinidin 3-glucoside
3a	36.02	1013766.6	611	330, 520	MS^2 **150**: 465, **303**	delphinidin 3-glucoside-5-rhamnoside
4a	38.65	3815699.9	757	330, 520	MS^2 **757**: 611, 287	cyanidin 3-sophoroside-5-rhamnoside
5a	40.45	6225991.6	449	330, 520	MS^2 **449**: 287	cyanidin 3-glucoside
6a	41.11	3961601.8	595	330, 520	MS^2 **595**: 287	cyanidin 3-rutinoside
7a	42.32	694663.7	653	330, 520	MS^2 **653**: 465, 303	delphinidin 3-glucoside-5-acetylrhamnoside
8a	44.41	2704222.1	815	330, 520	MS^2 **815**: 627, 303	delphinidin 3-sophoroside-5-acetylrhamnoside

Table 4 Identification of phytochemicals from the methanol fraction (F3) from mashua 203040

Peak No	Retention time	Area	Mass [M+H]	UV	MS^n	Identification
1a	32.45	168954.9	773	330, 520	MS^2 **773** : 627, 303	delphinidin 3-sophoroside-5-rhamnoside
2a	34.55	55115.1	465	330, 520	MS^2 **465**: 465, 303	delphinidin 3-glucoside
3a	36.02	1489770.0	611	330, 520	MS^2 **150**: 465, **303**	delphinidin 3-glucoside-5-rhamnoside
4a	38.65	1897289.2	757	330, 520	MS^2 **757**: 611, 287	cyanidin 3-sophoroside-5-rhamnoside
5a	40.45	216900.5	449	330, 520	MS^2 **449**: 287	cyanidin 3-glucoside
6a	41.11	1561713.1	595	330, 520	MS^2 **595**: 287	cyanidin 3-rutinoside
7a	42.32	196824.6	653	330, 520	MS^2 **653**: 465, 303	delphinidin 3-glucoside-5-acetylrhamnoside
8a	44.41	160946.0	815	330, 520	MS^2 **815**: 627, 303	delphinidin 3-sophoroside-5-acetylrhamnoside

Table 5 Identification of phytochemicals from the fraction F4 H_2O from mashua 203040

Peak No	Retention time	Area	Mass [M+H]	UV	MS^n	Identification
2	23.70	13753932.5	166	227, 278	MS^2 **166**: 147, 121	4-hydroxy benzyl isothiocyanate
3	25.74	13477752.8	150	227, 278	MS^2 **150**: 121, 77.0	benzyl isothiocyanate
4	31.54	53905704.4	206	227, 278	MS^2 **206**: 161, 149, 136, 118	Indolemethyl-isothiocyanate

Table 6 Identification of phytochemicals from the fraction F4 MeOH from mashua 203040

Peak No	Retention time	Area	Mass [M+H]	UV	MS^n	Identification
3	25.93	3901391.4	150	227, 278	MS^2 **150**: **121**, 77.0	benzyl isothiocyanate
4	31.54	2737010.5	206	227, 278	MS^2 **206**: 161, 149, 136, 118	Indolemethyl-isothiocyanate
4b	33.09	34552575.2	317	227, 278	MS^2 **316**: 136, 180	N,N-Di(4-methoxybenzyl)thiourea

The compound **7** at R.T 44.5 with $[M+H]^+$ 579 yielded in MS^2 fragments at *m/z* 457 and 288, which was identified as procyanidin B2. Compound **8** at R.T 45.75 with $[M+H]^+$ 457 yielded in MS^2 fragments at *m/z* 457, 305, 169, and this compound was identified as epigallocatechin gallate. Compound **9** at R.T 49.92 with with $[M+H]^+$ 441 yielded in MS^2 fragments at *m/z* 289 and 169; this compound was identified as epicatechin gallate. Procyanidin B2, epigallocatechin gallate, epicatechin gallate, gallic acid and coumaric acid derivatives were previously identified by HPLC-DAD in *Tropaeolum tuberosum* Ruız & Pavon tubers (*90*). Compound **10** at R.T 55.35 with $[M+H]^+$ 165 yielded in MS^2 fragment at *m/z* 127 and 118, and this compound was identified as p-Coumaric acid. Compound **11** with $[M+H]^+$ 339 yielded in MS^2 fragment at *m/z* 190.9, 162.9, 172.9 and this compound was identified as 5-pCoQA (5-p-coumaroylquinic acid). Compound **12** at R.T 60.70 gave $[M+H]^+$ 333 yielded MS^2 fragments 168, 150, 124.8 as this compound was assigned GCA (gallic-caffeic acid ester). Compound **13** at R.T 75.30 gave $[M+H]^+$ 343 yielded MS^2 fragments 160.9, 134.9, 202.8, 280.9, 250.9 as this compound was assigned as diCA (dicaffeic acid).

HPLC, ESI/MS and MS-MS were used to characterize anthocyanins from the acetone (F2) and methanol (F3) fractions of mashua 203040 (*98*). Peaks **1a**, **2a**, **3a**, **7a**, and **8a** showed *m*/*z* 303 as a major fragment, which indicate that the peaks contained delphinidin derivatives. Molecular ions at *m*/*z* 773 and 611 were observed in peaks **1a** and **3a**, which then were fragmented into two main molecular ion peaks at *m*/*z* 627 and 303 and *m*/*z* 465 and 303, respectively. The observation of the molecular ions at *m*/*z* 627 and 303 might have been attributed to the loss of a rhamnose molecule (146u) and a

sophorose molecule (321u), while the molecular ions at *m*/*z* 465 and 303 were generated by the loss of a rhamnose molecule (146u) and a glucose molecule (162u). Taking all the fragments into consideration, the molecules present in peaks **1a** and **3a** were identified as delphinidin 3-sophoroside-5-rhamnoside and delphinidin 3-glucoside-5-rhamnoside, respectively. Peak **2a** was found to be delphinidin 3-glucoside since it showed a molecular ion at *m*/*z* 465 with a loss of 162u that is attributed to a glucose molecule. Peak **7a** was found to be delphinidin 3-glucoside-5-acetylrhamnoside since it showed a molecular ion at *m*/*z* 653 and fragment ions at *m*/*z* 465 and 303 (*99*). The observation of the molecular fragments at *m*/*z* 465 and 303 might have been attributed to the loss of a rhamnose molecule linked to an acetyl group (146 + 42u) and the loss of a glucose molecule (162u), respectively. Peak **8a** was found to be delphinidin 3-sophoroside-5-acetylrhamnoside since it showed a molecular ion at *m*/*z* 815 and fragments at *m*/*z* 627 and 303. The observation of the molecular fragments at *m*/*z* 627 and 303 might have been attributed to the loss of a rhamnose molecule linked to an acetyl group (146 + 42u) and the loss of a sophorose molecule (324u), respectively.

Peaks **4a**, **5a**, and **6a** showed *m*/*z* 303 as a major fragment, which indicate that the peaks contained cyanidin derivatives. Peak **4a** was found to be cyanidin 3-sophoroside-5-rhamnoside since it showed a molecular ion at *m*/*z* 757 and fragment ions at *m*/*z* 611 and 287. Peaks **5a** and **6a** were identified as cyaniding 3-glucoside and cyanidin 3-rutinoside since they showed molecular ions at *m*/*z* 449 and 595, respectively. The ion fragmentation can be attributed to the loss of a glucose molecule (162u) and a

rutinose molecule (308u). The anthocyanins identified in this study are in agreement with previously reported anthocyanins in *Tropaeolum tuberosum* (*89*).

Fraction F4H_2O is rich in isothiocyanates. The isothiocyanates detected are the same as in F1, but present in higher concentrations. Compound **4** was the major peak in this fraction and was identified as indolmethyl isothiocyanate. Compounds **2** and **3** were previously identified as 4-hydroxy benzyl isothiocyanate and benzyl isothiocyanate. In F4 MeOH, compound **4b** at R.T 33.09 with $[M+H]^+$ 317 yielded MS^2 fragments at *m/z* 136 and 180 compound was identified as N,N-Di(4-methoxybenzyl)thiourea. This compound has been reported previously from glucosinolate-containing plants (*100*).

Mashua 2013081

HPLC/MS profiles of mashua 203081 fractions F1, F2 and F3, are illustrated in Figure 7, and the profiles of fractions F4H_2O and F4MeOH in Figure 8. The retention time, peak area, molecular weight, MS^2, and identification of the compounds detected in mashua 203081 fractions F1, F2, F3, F4H_2O, and F4MeOH, are listed in Table 7-11 respectively. The compounds were identified according to their fragmentation data and UV absorption. In the ethyl acetate fraction (F1), compound **1** at R.T 16.13 with $[M+H]^+$ 180 yielded in MS^2 fragments at *m/z* 167, 149, 105 and 70.07 the major fragmentation of *m/z* 149 was due to the loss of benzyl isothiocyante group and this compound was assigned as 4-methoxy benzyl isothiocyanate.

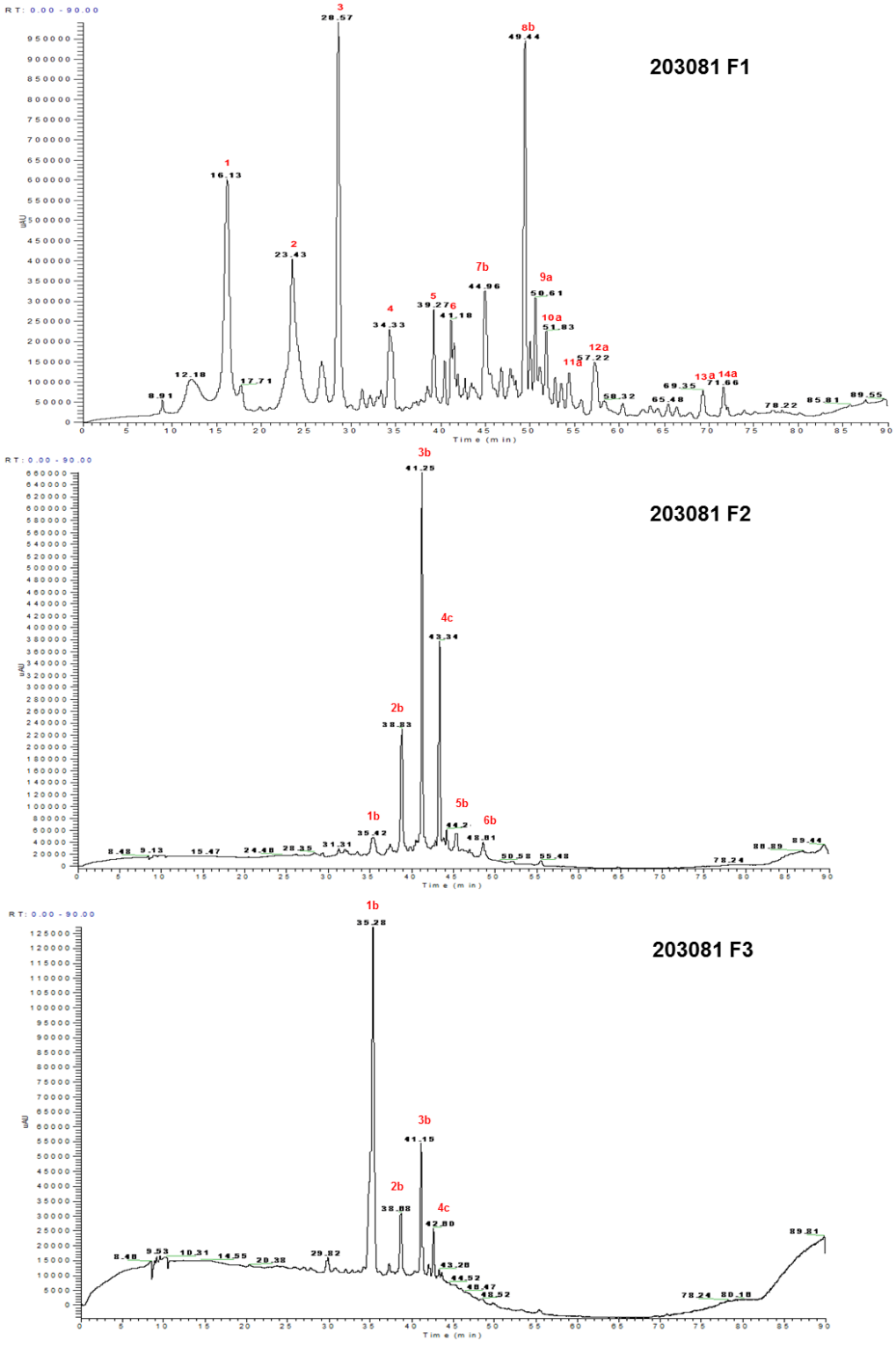

Figure 6 HPLC/MS profiles of mashua 203081 fractions F1, F2 and F3.

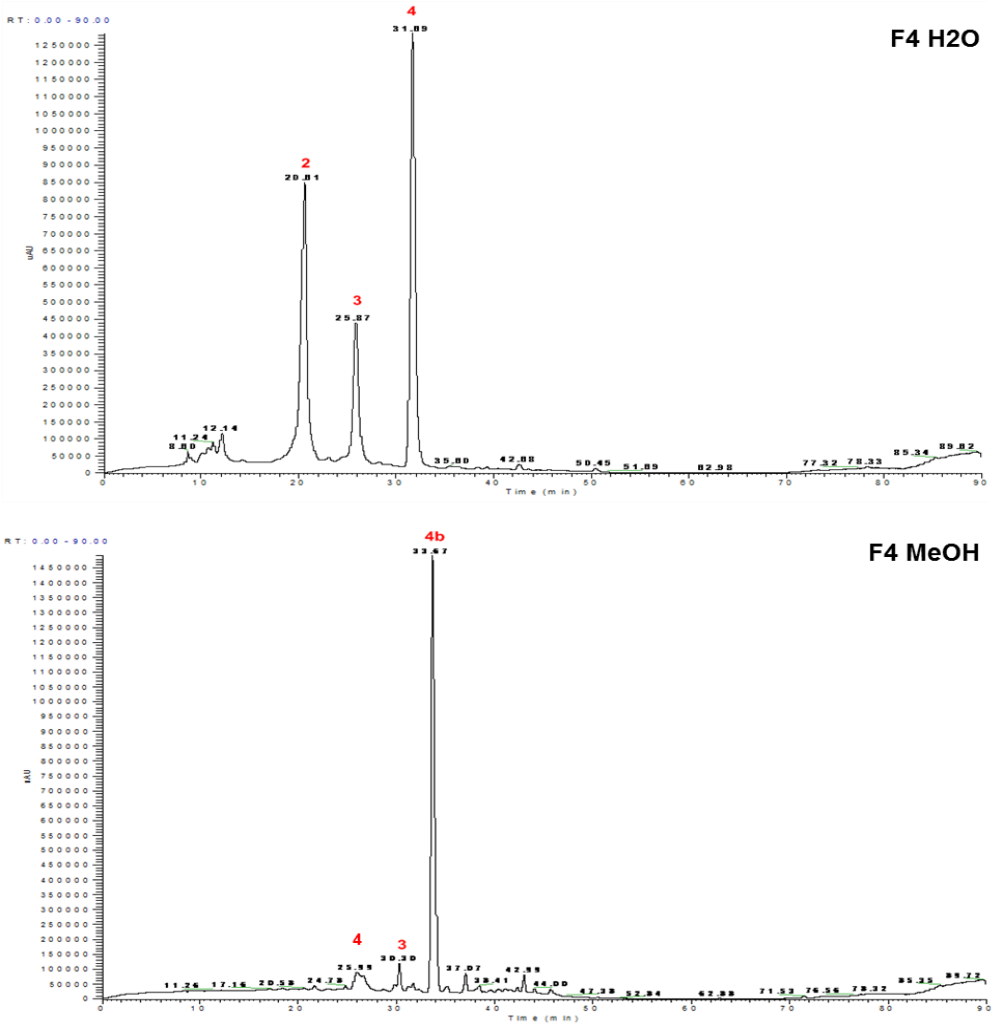

Figure 7 HPLC/MS profiles of mashua 203081 fractions F4 H_2O and F4 MeOH.

Table 7 Identification of phytochemicals from the ethyl acetate fraction (F1) of mashua 203081

Peak No	Retention time	Area	Mass [M+H]	UV	MS^n	Identification
1	16.13	26205628.6	180	227, 278	MS^2 180 : 167, 149, 105, 105, 70.07	4-methoxy benzyl isothiocyanate
2	23.43	23090689.4	166	227, 278	MS^2 166: 147, 121	4-hydroxy benzyl isothiocyanate
3	28.57	24755101.9	150	227, 278	MS^2 150: 121, 77.0	benzyl isothiocyanate
4	34.33	7200317	206	227, 278	MS^2 206: 161, 149, 136, 118	Indolemethyl-isothiocyanate
5	39.27	3510478.7	282	227, 282	MS^2 282: 150, 121	unknown isothiocyante derivative
6	41.18	6843253.8	369	227, 280	MS^2 369: 262	unknown isothiocyante derivative
7b	44.96	10260012.3	611	235, 278	MS^2 611: 345, 303, 273, 257	Rutin
8b	49.44	15212413.0	491	235, 275	MS^2 491: 481, 448, 430, 426, 403, 330, 294, 272	CQA-derivative
9a	50.61	3450294.1	503	232, 261	MS^2 503: 356, 382, 427, 447	CQA-derivative
10a	51.83	3510714.3	330	245, 263, 346, 382	MS^2 330: 330, 311, 165	quercetin dimethyl ether
11a	54.62	5618018.0	195	243, 283	MS^2 195: 135, 161	Ferulic amide

Table 7 Continued

12a	57.22	4889549.8	528	333	MS^2 528: 202, 184.8 , 178	QQCA (quinicquinic-caffeic acid ester)
13a	69.35	2095980.7	333	328	MS^2 333: 172.9 , 160.9,136.9	5-FQA (5-*O*-feruloylquinic acid)
14a	71.66	2138591.8	343	328	MS^2 343: 160.9, 134.9 202.8, 280.9, 250.9	diCA (dicaffeic acid)

Table 8 Identification of phytochemicals from the acetone fraction (F2) from mashua 203081

Peak No	**Retention time**	**Area**	**Mass [M+H]**	**UV**	**MS^n**	**Identification**
1b	35.42	1496857.1	576	231, 249	MS^2 **576**: 557, 543, 502, 418, 310, 292, 257	Not identified Tentative structure Isothiocyanate derivative
2b	38.83	3653480.9	644	232, 261	MS^2 **644**: 624, 595, 552, 521, 479, 436, 270	Not identified Tentative structure Isothiocyanate derivative
3b	41.25	9243666.0	545	230, 264	MS^2 **545**: 484	Not identified Isothiocyanate derivative
4c	43.34	4402690.8	467	230, 265	MS^2 **467**: 154	Not identified Isothiocyanate derivative
5b	44.24	62259.6	467	230, 265	MS^2 **467**: 154	Not identified Isothiocyanate derivative
6b	48.81	39616.8	467	230, 265	MS^2 **467**: 154	Not identified Isothiocyanate derivative

Table 9 Identification of phytochemicals from the methanol fraction (F3) from mashua 203081

Peak No	Retention time	Area	Mass [M+H]	UV	MS^n	Identification
1b	35.28	3150626.8	576	231, 249	MS^2 **576**: 557, 543, 502, 418, 310, 292, 257	Not identified Tentative structure Isothiocyanate derivative
2b	38.68	325949.8	644	232, 261	MS^2 **644**: 624, 595, 552, 521, 479, 436, 270	Not identified Tentative structure Isothiocyanate derivative
3b	41.15	568060.7	545	230, 264	MS^2 **545**: 484	Not identified Isothiocyanate derivative
4c	42.60	312758.3	467	230, 265	MS^2 **467**: 154	Not identified Isothiocyanate derivative

Table 10 Identification of phytochemicals from the fraction F4 H_2O from mashua 203081

Peak No	Retention time	Area	Mass [M+H]+	UV	MS^n	Identification
2	20.81	42911183.9	166	227, 278	MS^2 **166**: 147, 121	4-hydroxy benzyl isothiocyanate
3	25.87	16923893.6	150	227, 278	MS^2 **150**: 121, 77.0	benzyl isothiocyanate
4	31.89	46084341.9	206	227, 278	MS^2 **206**: 161, 149, 136, 118	Indolemethyl-isothiocyanate

Table 11 Identification of phytochemicals from the fraction F4 MeOH from mashua 203081

Peak No	Retention time	Area	Mass [M+H]	UV	MS^n	Identification
3	25.99	5728017.6	150	227, 278	MS^2 **150**: 121, 77.0	benzyl isothiocyanate
4	30.30	2504390.1	206	227, 278	MS^2 **206**: 161, 149, 136, 118	Indolemethyl-isothiocyanate
4b	33.67	38391967.3	317	227, 278	MS^2 **316**: 136, 180	N,N-Di(4-methoxybenzyl) thiourea

Compound **2** at R.T 23.43 showed UV maxima at 227, 278 with $[M+H]^+$ 166 yielded MS^2 fragments at *m/z* 147 and 121, the major fragment 121 was due to the loss of 4-hydroxy vinyl cation. Compound **3** at R.T 28.57 showed UV maxima at 227, 278 with $[M+H]^+$ 150 yielded MS^2 fragments at *m/z* 121 and 77, and this compound was identified as benzyl isothiocyanate. Compound **4** at R.T 34.33 with $[M+H]^+$ 206 yielded MS^2 fragments at *m/z* 161, 149, 136, 118, and this compound was identified as indolemethyl-isothiocyanate. Compound **5** at R.T 39.27 and compound **6** at R.T 41.18 with $[M+H]^+$ 282 and $[M+H]^+$ 369 yielded MS^2 fragments 150 and 121, and 262, respectively. Compound **5** was tentatively identified as indole methyl phenyl derivative and compound **6** remained unknown. Here for the first time we have determined the presence of isothiocyanates by MS fragmentation pattern. Some of the isothiocyantes like 4-methoxy benzyl isothiocyanate and benzyl isothiocyante were previously reported in *Tropaeolum tubersom* (*101*).

Figure 8 illustrates the structures of identified isothiocyantes in mashua 203040 and 203081. The compound **7b** at R.T 44.96 with $[M+H]^+$ 611 yielded in MS^2 fragments at *m/z* 345, 303, 273, 257, 245, 180, the major fragmentation of *m/z* 303 was due to the loss of quercetin group. Compound **7b** was identified as rutin. The compound **8b** at R.T 49.44 with $[M+H]^+$491 yielded in MS^2 fragments at *m/z* 481, 448, 430, 426, 403, 330, 294, 272, the major fragmentation of *m/z* 355 can be assigned to chlorogenic acid fragment. The *m/z* 456 can be explained on the basis of the loss of the 2 hydroxy groups as shown in the structure (Figure 9A). There were no relevant reports of this molecule, however a closely related structure of chlorogenic acid derivative have been reported as a cosmetic, which show skin-conditioning effect (*102*). The compound **9a** at R.T 50.61 with $[M+H]^+$ 503 yielded in MS^2 fragments at *m/z* 355, 382, 427 and 447 the major fragmentation of *m/z* 356 can be assigned to chlorogenic acid fragment. The *m/z* 382 can be explained on the basis of the loss of the carbonyl group which accounts the loss of 28 Da in the structure (Figure 9B). There were no relevant reports of this molecule however a closely related structure of chlorogenic acid derivative have been reported as an Itk (interleukin-2 inducible T-cell kinase), a Th2-cell target, isolated from the Australian rainforest tree *Polysciasmurrayi (103).* Compounds **10a** at R.T 51.83 and **11a** at R.T 54.62 were reported as quercetin dimethyl ether and ferulicamide based on the fragmentation and the UV pattern from the literature (*104*). Compound **12a** at R.T 57.22 gave [M+H]+ 528 yielded MS^2 fragments 202, 184.8, 178 and this compound was assigned as QQCA (quinicquinic- caffeic acid).

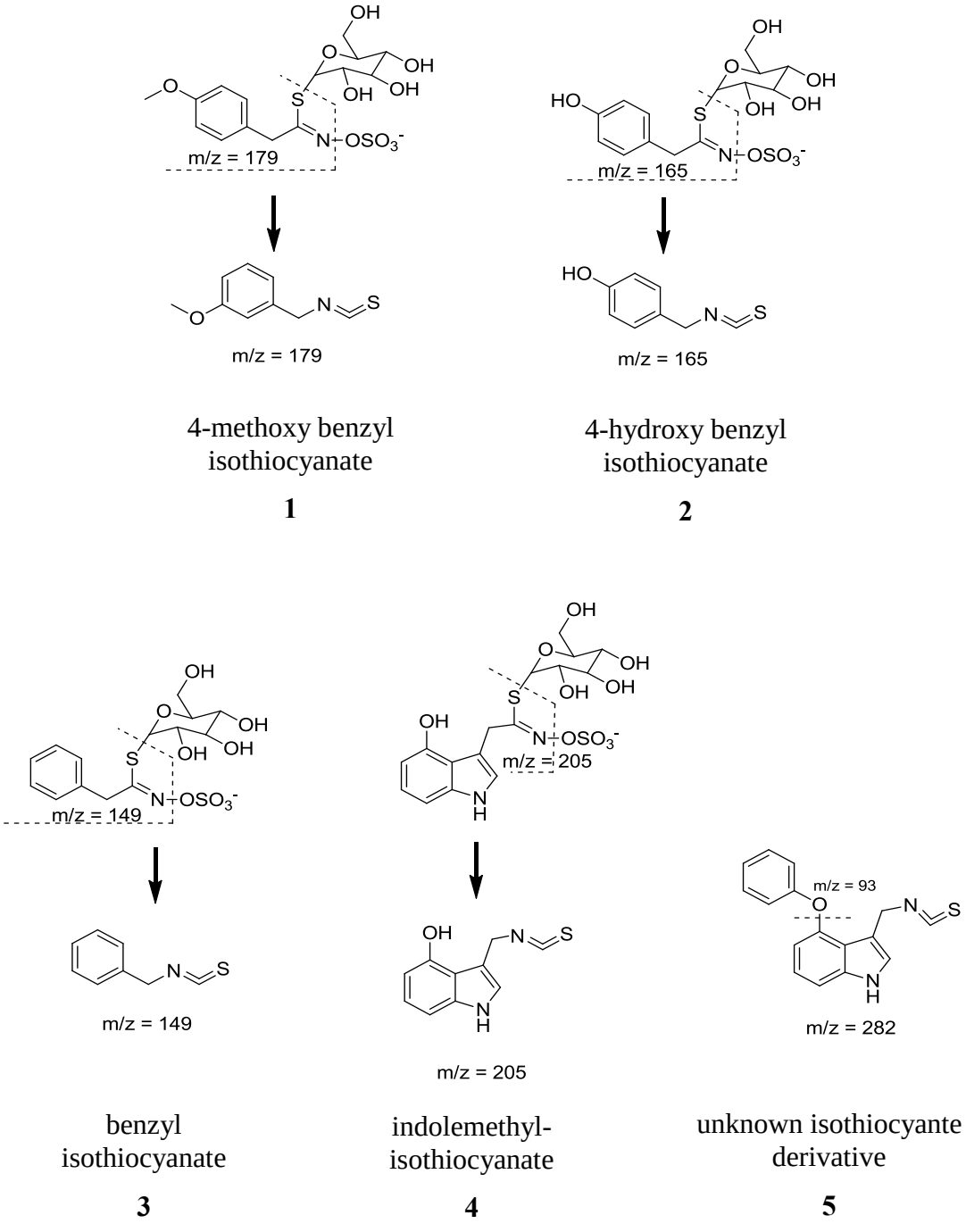

Figure 8 Structures of identified isothiocyantes in mashua 203040 and 203081.

A

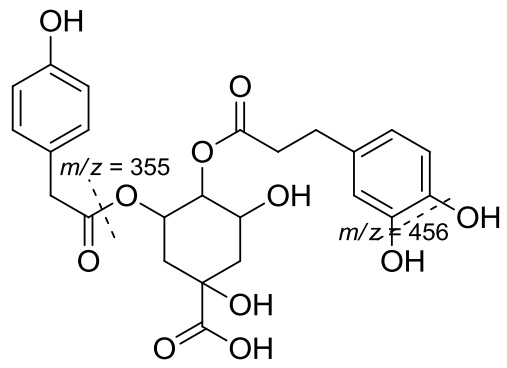

8b

B

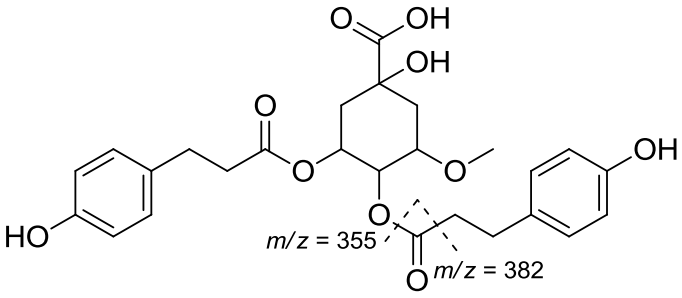

9a

Figure 9 Tentative structures of the chlorogenic acid derivative from the ethylacetate extract (F1) in mashua 203081.

Compound **13a** at R.T 69.35 gave $[M+H]^+$ 333 yielded MS^2 fragments 172.9, 160.9, 136.9 as this compound was assigned 5-FQA (5-*O*-feruloylquinicacid). Compound **14a** at R.T 71.66 gave $[M+H]^+$ 343 yielded MS^2 fragments 160.9, 134.9 202.8, 280.9, 250.9 as this compound was assigned as diCA (dicaffeic acid). For fractions F2 and F3, the peak **1b** at 35.42 (*m/z* 576) gave MS^2 fragments at 557, 543, 502, 418, 310, 292, 257, peak **2b** at 38.83 (*m/z* 644) gave MS^2 fragments at 643, 624, 595, 552, 521, 479, 436, 270, peak **3b** at 41.25 (*m/z* 545) gave MS^2 fragment at 484 and peak **4c**, **5b** and **6b** gave same (*m/z* 467) MS^2 fragment at 466, 154. There were no reports for these molecules however from the knowledge of the types of molecules formed in mashua and the high molecular weight these fragments obtained could be justified and constructed as shown in Figure 10.

Fraction F4H_2O is rich in isothiocyantes. The isothiocyanates detected are the same as in fraction F1, but present in higher concentrations. Compound **4** was the major peak in this fraction and was identified as indolmethyl isothiocyanate. Compounds **2** and **3** were previously identified as 4-hydroxy benzyl isothiocyanate and benzyl isothiocyanate. In fraction F4 MeOH, compound **4b** at R.T 33.09 with $[M+H]^+$ 317 yielded MS^2 fragments at *m/z* 136 and 180 compound was identified as N,N-Di(4-methoxybenzyl)thiourea.

Effect of Mashua Extracts on LPS-Induced ROS and NO productions

Here we assessed the effect of six mashua extracts on NO and ROS production in LPS-stimulated RAW 264.7 macrophage cell line.

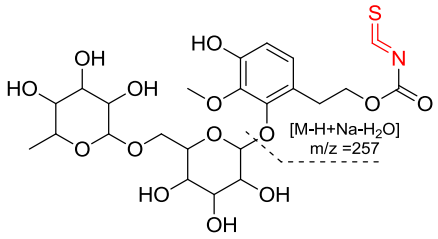

1b

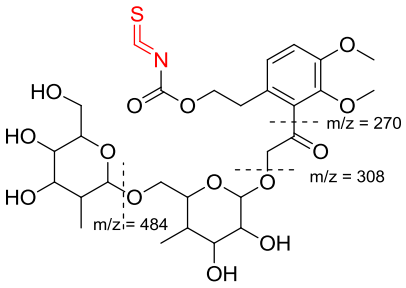

2b

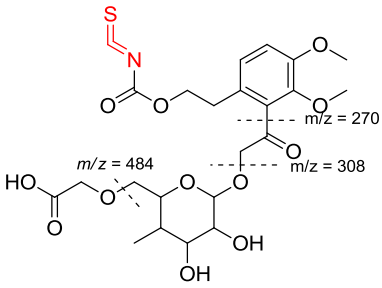

3b

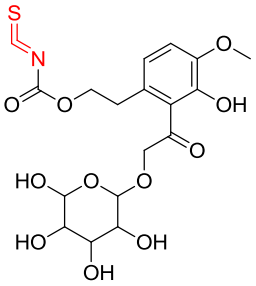

4c

Figure 10 Tentative structures of isothiocyanates from acetone (F2) and methanol (F3) extracts in mashua 203081.

The MTS assay showed that 100 µg/ml extract dose did not affect cell viability (Figure 11A), and therefore this concentration was used for the following experiments. The effects of mashua extracts on LPS-induced NO were investigated using Griess reagent on the extracellular medium. All mashua extracts suppressed NO levels (Figure 11B). The extracts of genotypes 203081 and 203040 showed the greatest reduction of NO levels. When LPS-induced ROS production was assessed using DCFA at 19 h after the LPS challenge, all genotypes, except for genotype 203076, suppressed ROS production (Figure 11C). The extracts of genotypes 203040 and 203003 showed the greatest reduction on ROS levels. Among all mashua genotypes extracts, 203081 and 203040 were among the most active extracts to reduce both NO and ROS production and thus were selected fort further study of their molecular targets.

Identification of PKM as a Potential Target of Mashua Extracts

DARTS strategy was used to identify the cell-targets of mashua extracts 203081 and 203040. DARTS, revealed a strong protected band near 60 kDa in the mashua 203081 (Figure 12A) and 203040 (Figure 12B) treated samples. In gel-digestion and MALDI-TOF analysis identified the protected band as pyruvate kinase, muscle (PKM). There are two isoforms of PKM, PKM1 and PKM2. Western blotting detection confirmed that mashua extracts could protect PKM1 and PKM2 from proteolysis induced by pronase treatment (Figure 12C), indicating binding to these proteins. To validate the biological relevance of the binding of mashua phytochemicals to PKM, we next assessed the effect of mashua extracts 203081 and 203040 on pyruvate kinase activity.

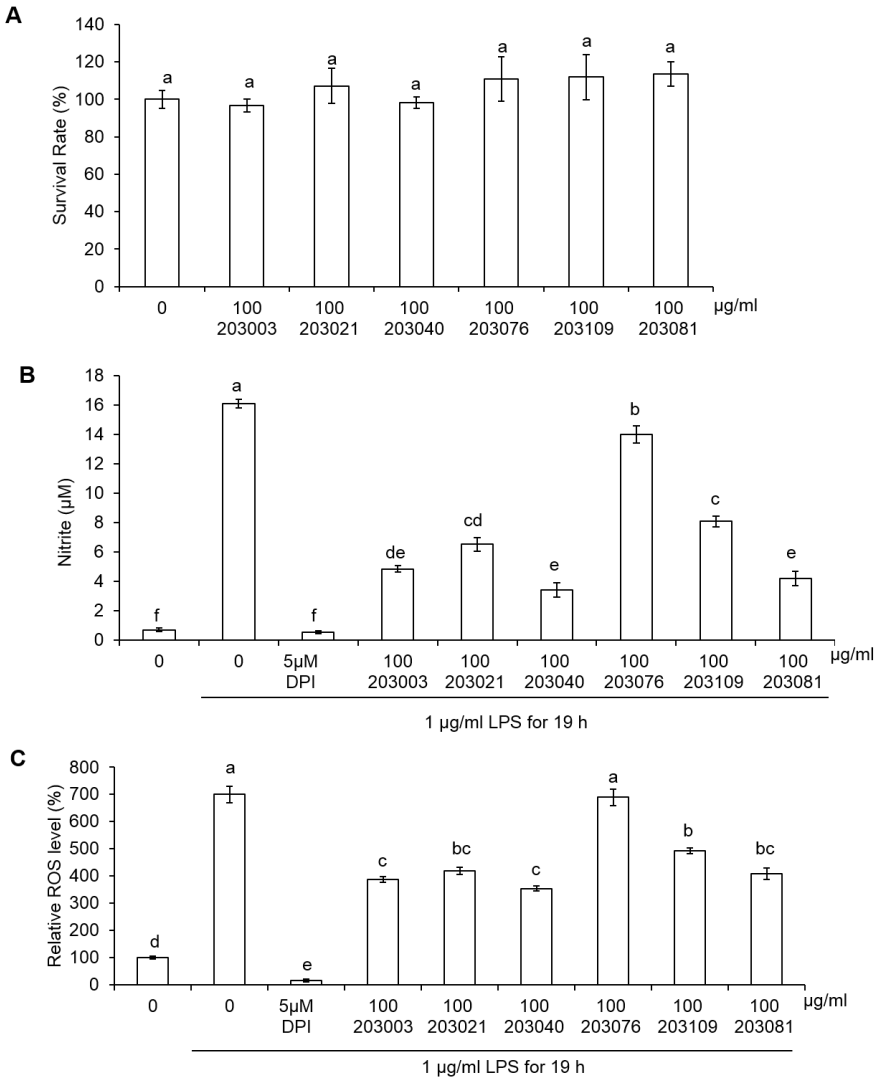

Figure 11 Effect of mashua extracts on cell viability and LPS-induced NO and ROS production. (A) Effect of mashua extracts on cell viability in macrophage cells. RAW 264.7 cells (0.5×10^5 cells/well in 96-well culture plates) were treated with 100 μg/ml mashua extract for 24 h and then the cell viability was measured by MTS assay. (B-C) Effect of mashua extracts on LPS-induced NO and ROS production. RAW264.7 cells (0.5×10^5 cells/well in 96-well culture plates) were pretreated with 100 μg/ml mashua extract for 5 h and then stimulated with LPS (1 μg/ml) for 19 h. Griess reagent was used to detect the generation of extracellular nitrite (B) and DCFA was used to determine the generation of intracellular ROS at 19 h after the LPS challenge (C). Data, obtained from four biological repeats at least, are shown as mean ± SE values. Different letters indicate significant differences by the ANOVA/Tukey-HSD ($p < 0.05$).

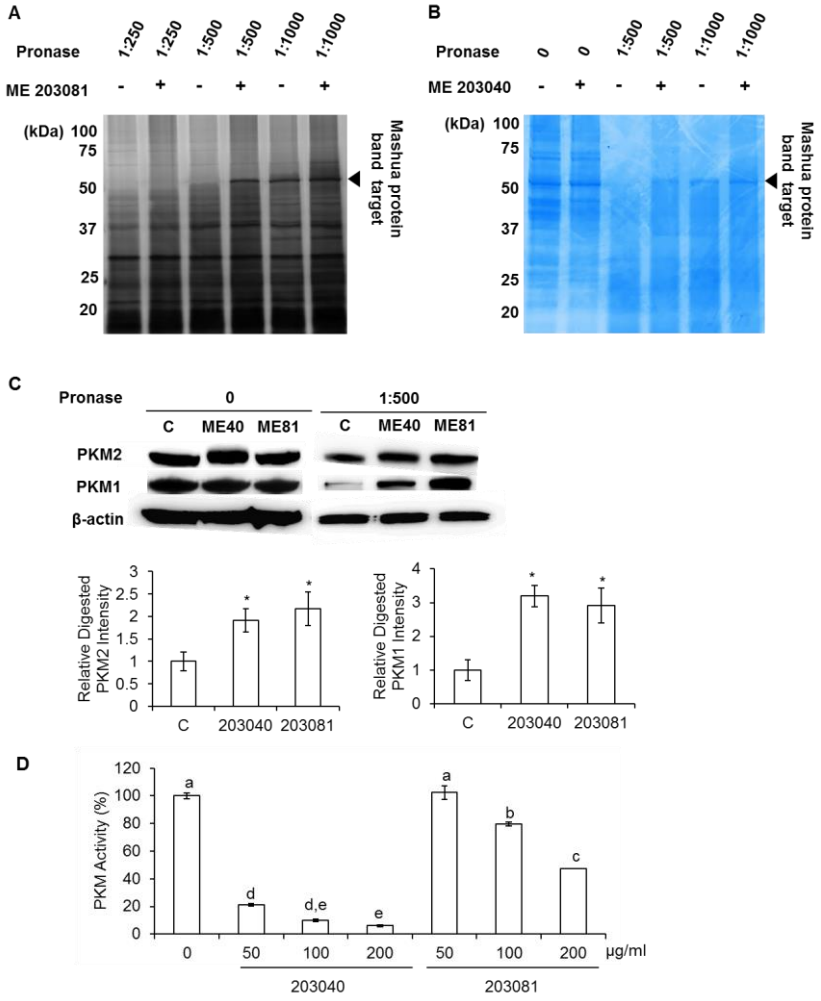

Figure 12 Identification of PKM as a potential target of mashua phytochemicals in RAW264.7 macrophages by DARTS methodology. (A-B) RAW 264.7 cell lysates were incubated with 400 µg/ml of mashua extract 203081 (A) and 203040 (B) for 3 h at RT, and then digested with pronase for 25 min at RT, followed by Silver or Coomassie blue staining. Black arrow indicates a strong band (~60 kDa) protection from pronase proteolysis by both mashua extracts. In gel-digestion and MALDI-TOF analysis identified the protected band as pyruvate kinase, muscle (PKM). (C) The protective effects of mashua extracts on PKM1 and PKM2 proteolysis were confirmed by western blot analysis using DARTS lysates. (D) Pyruvate kinase activity was measured in RAW264.7 cell lysates that where directly exposed to mashua treatments, using the pyruvate kinase activity assay kit according to the manufacturer's instructions. Data, obtained from three biological repeats at least, are shown as mean ± SE values. Different letters indicate significant differences by the ANOVA/Tukey-HSD ($p < 0.05$). Symbols indicate significant differences by Student's t test (#$p < 0.1$,*$p < 0.05$).

Pyruvate kinase activity was measured in cell lysates that were directly exposed to mashua treatments. Results showed that extract 203040 significantly ($p<0.05$) inhibited PK activity at 50, 100 and 200 µg/ml while extract 203081 inhibited only at 100 and 200 µg/ml. Overall extract 203040 was a more potent inhibitor of PK activity (Figure 12D).

Effects of Mashua Extracts on LPS- Induced Pyruvate Kinase Activity and Lactate Production

To further study PKM as target of mashua phytochemicals we next evaluated the effect of 19 h LPS stimulation in RAW 264.7 macrophages on pyruvate kinase activity and lactate production and the effect of mashua extracts on both markers. Pyruvate kinase was measured in cell lysates that had been treated with mashua during their growth. Results showed that there is a slight increase in PKM activity after cells were stimulated by LPS for 19 h. Extract 203040 at 100 µg/ml significantly inhibited PKM activity to levels comparable to the negative control. Extract 203081 also inhibited PKM activity, but at a lower extent (Figure 13A). Lactate is the end product of non-oxidative glycolysis and is produced from pyruvate in a reaction catalyzed by lactate dehydrogenase (LDH). Since PKM is involved in the production of pyruvate, lactate levels will be influenced by PKM activity rate. Results show that there is a significant increment in lactate levels after cells were stimulated by LPS for 19 h. Both extracts significantly inhibited the LPS-induced lactate production at 50 and 100 µg/ml (Figure 13B).

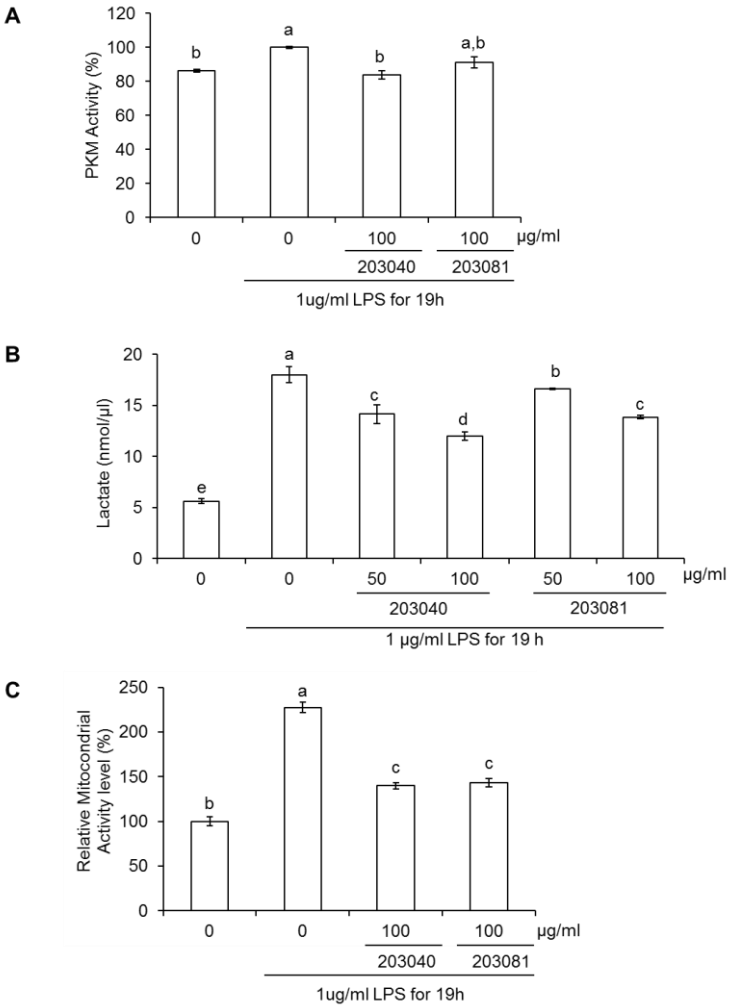

Figure 13 Effect of mashua extracts on LPS-induced lactate production and pyruvate kinase and mitochondrial dehydrogenase activity. (A) Effect of mashua extracts on pyruvate kinase activity. RAW264.7 cells (0.5×10^6 cells/well in 6-well culture plates) were pretreated with 100 µg/ml mashua extract for 5 h and then stimulated with LPS (1 µg/ml) for 19 h. Pyruvate kinase activity was measured using the pyruvate kinase activity assay kit according to the manufacturer's instructions. (B) Effect of mashua extracts on lactate production and (C) mitochondrial dehydrogenase activity. RAW264.7 cells (0.5×10^5 cells/well in 96-well culture plates) were pretreated with 100 µg/ml mashua extract for 5 h and then stimulated with LPS (1 µg/ml) for 19 h. Lactate production in the medium was detected by using the Lactate Assay Kit, and mitochondrial dehydrogenase activity was evaluated using the MTS assay kit according to the manufacturer's instructions. Data, obtained from three biological repeats at least, are shown as mean ± SE values. Different letters indicate significant differences by the ANOVA/Tukey-HSD ($p < 0.05$). Symbols indicate significant differences by Student's t test (#$p < 0.1$).

Effects of Mashua Extracts on LPS-Induced Mitochondrial Dehydrogenase Activity

The effect of mashua extracts 203081 and 203040 on LPS-induced mitochondrial dehydrogenase activity was evaluated using the MTS assay kit. In the MTS assay, tetrazolium is mainly reduced to formazan by intracellular NADH.

Some reports agree that, despite the mitochondrial NADH contribute to the reduction of tetrazolium, the formation of formazan depends primarily on the rate of glycolytic NADH production (*105, 106*). Results show that 19 h after LPS stimulation, formazan levels increased significantly when compared to the control and this effect was significantly reduced with both mashua extracts (Figure 13C). When macrophages are stimulated with LPS the rate of glycolysis increases whereas the rate of respiration decreases, and this phenomena is part of what is known as the Warburg effect (*19*). Therefore the increment in formazan levels upon LPS stimulations is likely a reflection of the increment in NADH produced in glycolysis, in addition to mitochondrial NADPH.

Effects of Mashua Extracts on LPS-Induced ROS Production in Early and Late Inflammatory Response

The effect of different doses of mashua 203081 and 203040 extracts on LPS-induced ROS production in early (6 h after LPS challenge) (Figure 14A) and late (at 19 h after LPS challenge) (Figure 14B) inflammatory response, was examined by 2′,7′-Dichlorofluorescin diacetate (DCFA). At 6 and 19 h after LPS stimulation, both extracts at doses of 25, 50 and 100 µg/ul suppressed LPS-induced ROS. The reductions of ROS by both mashua extracts was higher at 6 h compared to 19 h.

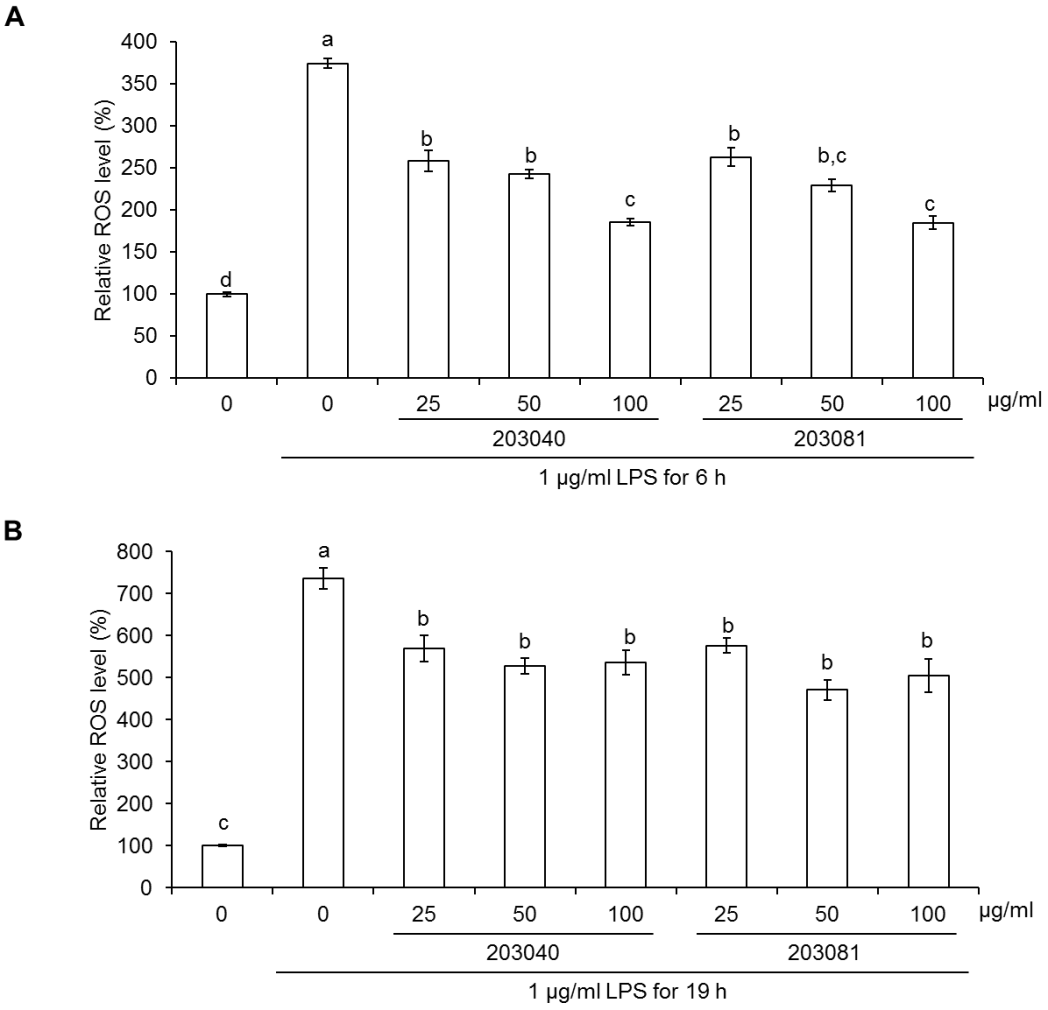

Figure 14 Effect of mashua extracts on LPS-induced ROS production in early and late inflammatory response. RAW264.7 cells (0.5×10^5 cells/well in 96-well culture plates) were pretreated with 100 μg/ml mashua extract for 5 h and then stimulated with LPS (1 μg/ml) for 6 h or 19 h. DCFA was used to determine the generation of intracellular ROS at 6 h (A) and 19 h (B) after the LPS challenge. Data obtained from a minimum of four biological repeats are shown as mean ± SE values. Different letters indicate significant differences by the ANOVA/Tukey-HSD ($p < 0.05$).

Mashua extract 203040 at concentrations of 25, 50 and 100 µg/ul reduced ROS by 29.77, 38.78 and 50.60 % respectively at 6 h after LPS challenge and by 22.67, 28.20 and 27.10 %, respectively at 19 h after LPS challenge. On the other hand, mashua extract 203081 at concentrations of 25, 50 and 100 µg/ul reduced ROS by 30.89, 35.21 and 50.47 %, respectively at 6 h after LPS challenge and by 21.69, 35.95 and 31.44 %, respectively at 19 h after LPS challenge.

Effects of Mashua Extracts on ROS Dependent LPS-Induced Gene Expressions in Early and Late Inflammatory Response

The effects of mashua extracts 203081 and 203040 on various pro-inflammatory gene expressions at 6 h (Figure 15A) and 19 h (Figure 15B) after LPS-stimulation were examined by real-time qRT-PCR analysis. Results show that LPS at 6 h promotes the expression of *IL-1β, TNFα* and *iNOS* and at 19 h the expression of *COX-2, IL-1β, TNFα, iNOS* and *IFN-β.* As shown in Figure 15B, both mashua extracts at a concentration of 100 µg/ml suppressed LPS-induced expressions of *COX-2, IL-1β* and *iNOS* at 19 h. Mashua extract 203040 suppressed the expression of *IFN-β* at 19 h. Both extracts enhanced LPS-induced expression of *TNFα* at 19 h. Furthermore, the effect of both mashua extracts on LPS-induced expressions of *IL-1β, iNOS* and *TNFα* were examined at 6 h (Figure 15A). Results show that mashua extracts 203081 and 203040 at concentration of 100 µg/ml were able to significantly suppress the expressions of *IL-1β* and *iNOS* at 6 h. Mashua extract 203081 suppressed the expression of *TNFα* at 6 h.

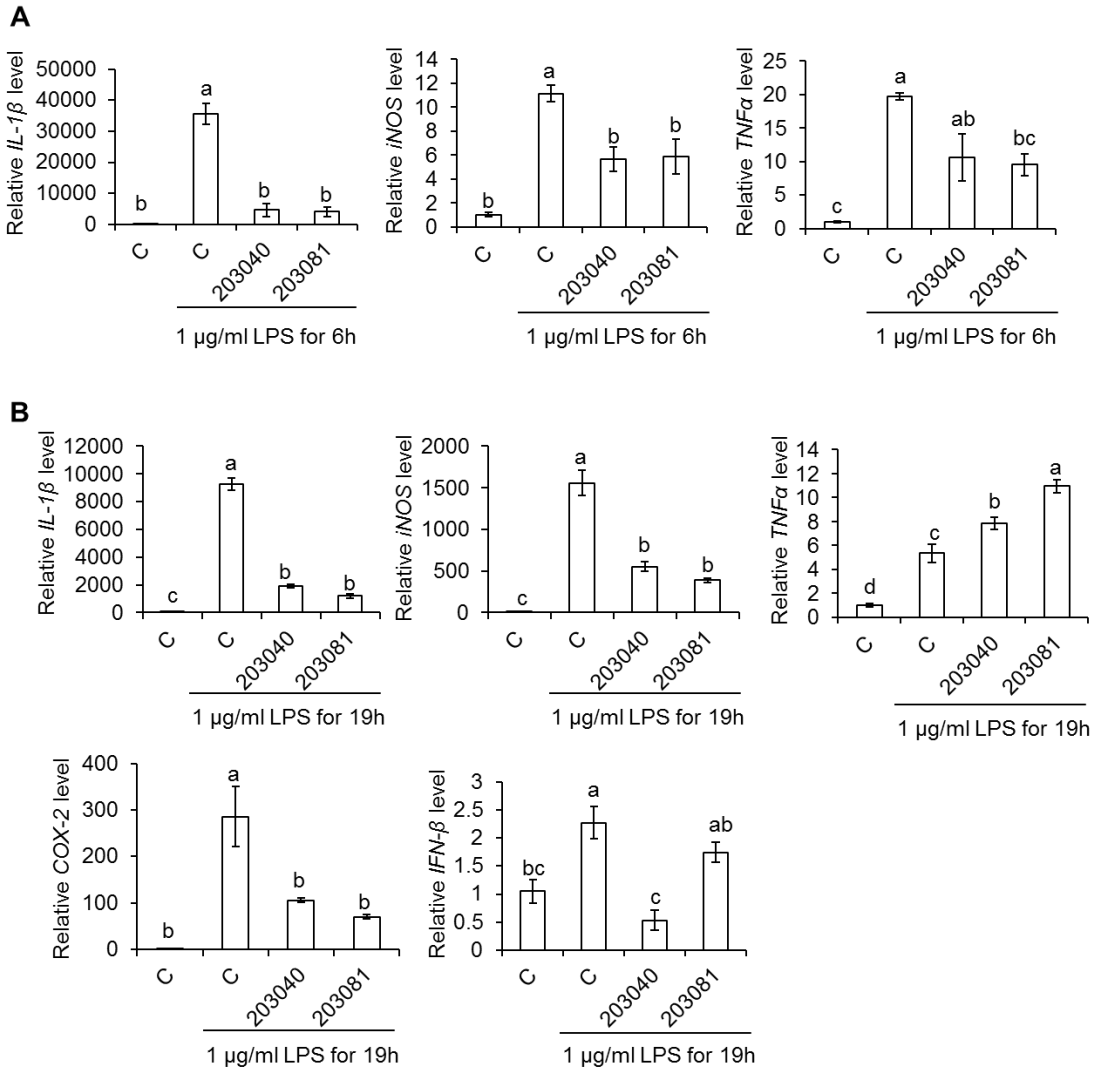

Figure 15 Effects of mashua extracts on ROS dependent LPS-induced gene expressions in early and late inflammatory response. RAW 264.7 cells (0.5×10^6 cells/well in 6-well culture plates) were pretreated with 100 μg/ml mashua extract for 5 h and then stimulated with LPS (1 μg/ml) for 6 h (A) or 19 h (B). Subsequently, total RNAs were prepared and subjected to real-time qRT-PCR analysis using specific primer sets, responsible for *TNFα*, *COX-2*, *IFN-β*, *IL-1 β* and *iNOS* genes. *β-actin* was used as the reference gene. Data obtained from triplicate repeats are shown as mean ± SE. Different letters indicate significant differences by the ANOVA/Tukey-HSD ($p < 0.05$).

ROS plays an important role in the activation of transcription factors such as NF-κB and AP-1 and therefore in the expression of genes regulated by these transcription factors (*31, 32, 107*). In previous work done in our lab, we showed that different genes respond differently to the suppression of ROS levels, some being more sensitive than others (Bang and Cisneros-Zevallos, Unpublished). This could explain why some genes (*COX-2, IL-1β, iNOS* and *IFN-β*) were suppressed at 19 h while others (*TNFα)* required a higher inhibition of ROS and were only suppressed at 6 h.

Effects of Mashua Extracts on PKM1, PKM2 and PKM2 Codependent Gene Expression in Late Inflammatory Response

The effect of mashua extracts 203081 and 203040 on the expression of PKM1, PKM2 and genes co-activated by PKM2, including *PDK1*, *GLUT1* and *LDHA* were evaluated at 6 h (Figure 16A) and 19 h (Figure 16B) after LPS-stimulation by real-time qRT-PCR analysis. Results show that LPS stimulation for 19 h, promoted the gene expression of *GLUT1,* while the expression of *PKM2, PKM1* and *LDHA* remained the same when compared to the control. The expression of *PDK1* decreased with LPS at 19 h when compared to the control. Both mashua extracts reduced significantly LPS-induced *GLUT1*expression at 19 h. For *PKM1, PKM2, LDHA* and *PDK1*, neither mashua extract had an effect on gene expression levels compared to the LPS control. Furthermore, results show that LPS stimulation for 6 h, did not affect the expression of *GLUT1* and PKM1, and reduced the expression of *PKM2, PDK1* and *LDHA.*

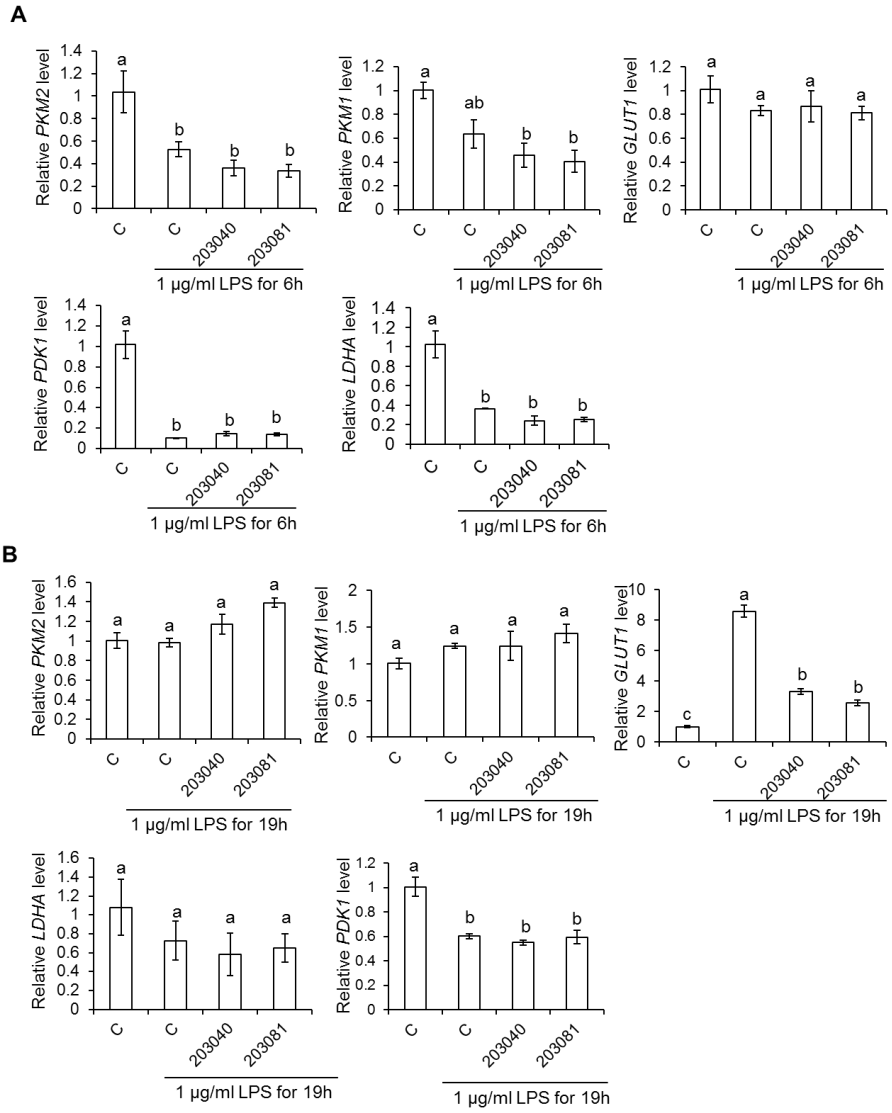

Figure 16 Effects of mashua extracts on PKM1, PKM2 and PKM2 codependent gene expression in early and late inflammatory response. RAW 264.7 cells (0.5×106 cells/well in 6-well culture plates) were pretreated with 100 μg/ml mashua extract for 5 h and then stimulated with LPS (1 μg/ml) for 6 h (A) or 19 h (B). Subsequently, total RNAs were prepared and subjected to real-time qRT-PCR analysis using specific primer sets, responsible for PKM1, PKM2, PDK1, LDHA, and GLUT1 genes. For 6h, β-actin was used as the reference gene. For 19h, the geometrical mean of three reference genes (β-actin, GDHA and 18s ribosomal RNA), was used. Data obtained from triplicate repeats are shown as mean ± SE. Different letters indicate significant differences by the ANOVA/Tukey-HSD ($p < 0.05$).

Neither mashua extract had an effect on gene expression levels compared to the LPS control. In general, this group of genes shows very low expression levels, and therefore variations in the reference gene can significantly affect these results (*96*). For this reason, for the genes analyzed at19 h after LPS-stimulation, the geometrical mean of three reference genes (β-actin, GDHA and 18s ribosomal RNA) was used to analyze the expression of these genes. For the genes analyzed at 6 h after LPS-stimulation only β-actin was use as the reference gene.

The Effect of LPS on PKM1 and PKM2 Protein Expression and PKM2 Conformation and Nuclear Translocation

The effects of LPS stimulation for 19 h on PKM1and PKM2 protein expression was investigated by western blot analysis. Results show that PKM2 protein levels remain the same after 19 h stimulation with LPS, while PKM1 expression significantly increases (Figure 17A). PKM2 can switch between a tetramer, a monomer, and a dimer, and can be located in the cytoplasm or in the nucleus. The location and conformation of PKM2 can define its function (*83*) and thus this was studied. The effect of 19 h LPS stimulation on nuclear PKM2 levels was evaluated by using a Nuclear Extract Kit (Active Motif 40010) and western blot analysis. Results show that there is not a significant change in the nuclear PKM2 protein levels upon LPS stimulation for 19 h. Moreover, neither mashua extract had an effect on the nuclear PKM2 protein levels (Figure 17B). To understand how LPS stimulation affects PKM2 conformation, croslinking analysis was performed (Figure 18).

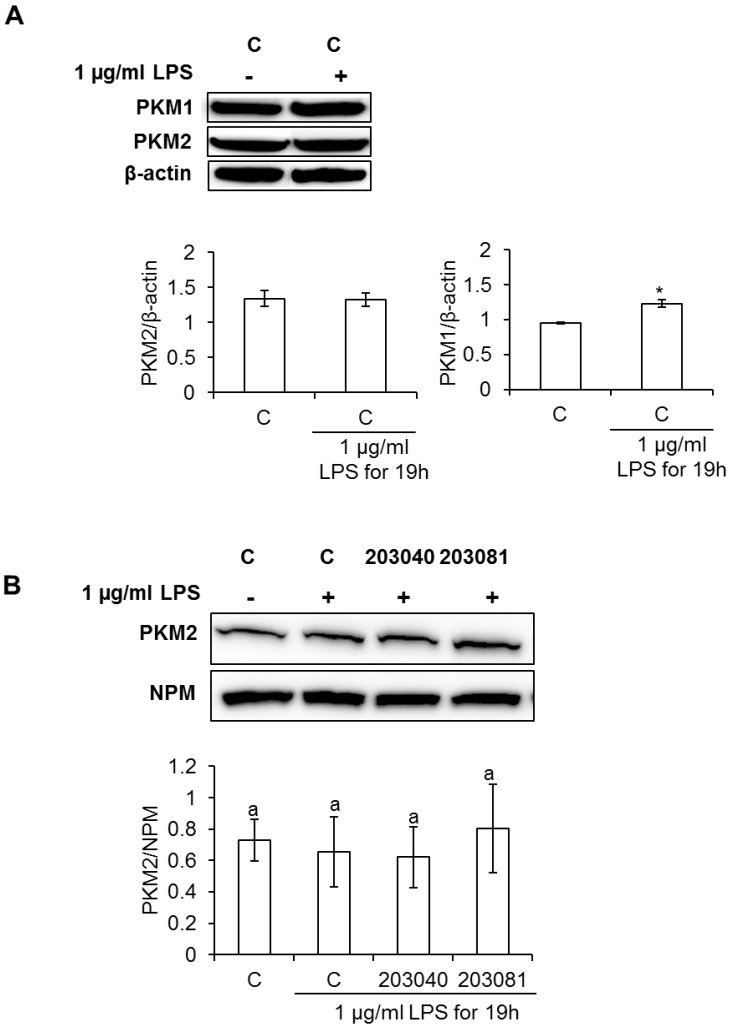

Figure 17 The effect of LPS on PKM1 and PKM2 total protein expression, and PKM2 nuclear protein expression. RAW 264.7 cells (0.5 × 106 cells/well in 6-well culture plates) were pretreated with 100 μg/ml mashua extract for 5 h and then stimulated with LPS (1 μg/ml) for 19 h. (A) For PKM1 and PKM2 protein expression, cell lysates were subjected to SDS-PAGE and Western blot analysis using specific antibodies against PKM1, PKM2 and B-actin. (B) For nuclear PKM2, nuclear fractions were isolated as described under Materials and Methods and subjected to SDS-PAGE and Western blot analysis using specific antibodies against PKM2 and NPM. The protein bands in the upper panels were detected by chemiluminescence. The histograms in the bottom panels represent the relative protein levels measured by ImageJ software. Data, obtained from at least three biological repeats, are shown as the mean ± SE. Different letters indicate significant differences by the ANOVA/Tukey-HSD ($p < 0.05$). Asterisks indicate significant differences by Student's t test ($p < 0.05$).

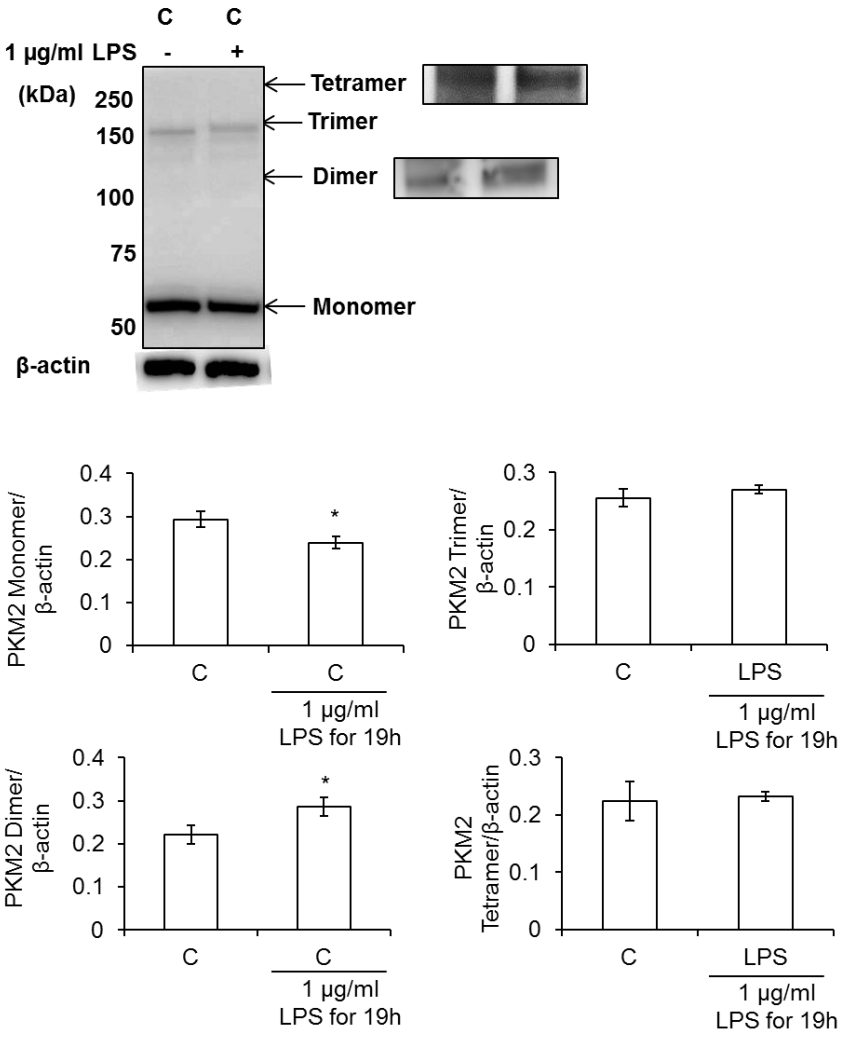

Figure 18 The effect of LPS on PKM2 conformation. RAW 264.7 cells (0.5×10^6 cells/well in 6-well culture plates) stimulated with LPS (1 µg/ml) for 19 h. For PKM2 configuration study cells were crosslinked with with 1 mM disuccinimidyl suberate as described in Material and Methods. Cell lysates were subjected to SDS-PAGE and Western blot analysis using specific antibodies against PKM2 and β-actin. The protein bands in the upper panel were detected by chemiluminescence. The histograms in the bottom panel represent the relative protein levels measured by ImageJ software. Data, obtained from at least three biological repeats, are shown as the mean ± SE. Asterisks indicate significant differences by Student's t test ($p < 0.05$).

Results show that PKM2 is mainly present as a monomer in RAW264.7 cells, and upon LPS stimulation the monomeric form significantly decreases. Moreover, a tetramer, trimer and dimer forms of PKM2 were also detected. The dimeric form of PKM2 was shown to increase with LPS at 19 h, while no significant changes were detected with the tetramer and trimer.

Effect of Mashua Fractions on LPS-Induced ROS and NO Production and Assessment of Binding to PKM2

In order to understand the identity of the mashua phytochemicals that possess anti-inflammatory properties, mashua 202040 and 203081 fractions (F1, F2, F3, F4, F4MeOH and F4H_2O) were evaluated for their effects on the LPS-induced inflammation. The MTS assay confirmed that neither 50 and 100 µg/ml doses of all fractions affected the cell survival rate more than 20%, except for 100 µg/ml F3 and 100 µg/ml F4$H_2$0 of mashua 203081 (Figure 19A) and 100 µg/ml F4$H_2$0 of mashua 203040 (Figure 20A), which were not used for the following experiments. Fractions F1 (100 µg/ml) and F3 (50 and 100 µg/ml) from mashua extract 203040 showed the highest effect on the suppression of NO (Figure 20B) and ROS (Figure 20C) at 19 h, while all the other fractions showed little or no effect. On the other hand, fractions F2 (100 µg/ml) and F3 (50 µg/ml) from mashua extract 203081 showed the highest effect on suppression of NO (Figure 19B) and ROS (Figure 19C) at 19 h, while all the other fractions showed little or no effect. Furthermore, we evaluated the binding of the fractions to PKM2 using DARTS strategy.

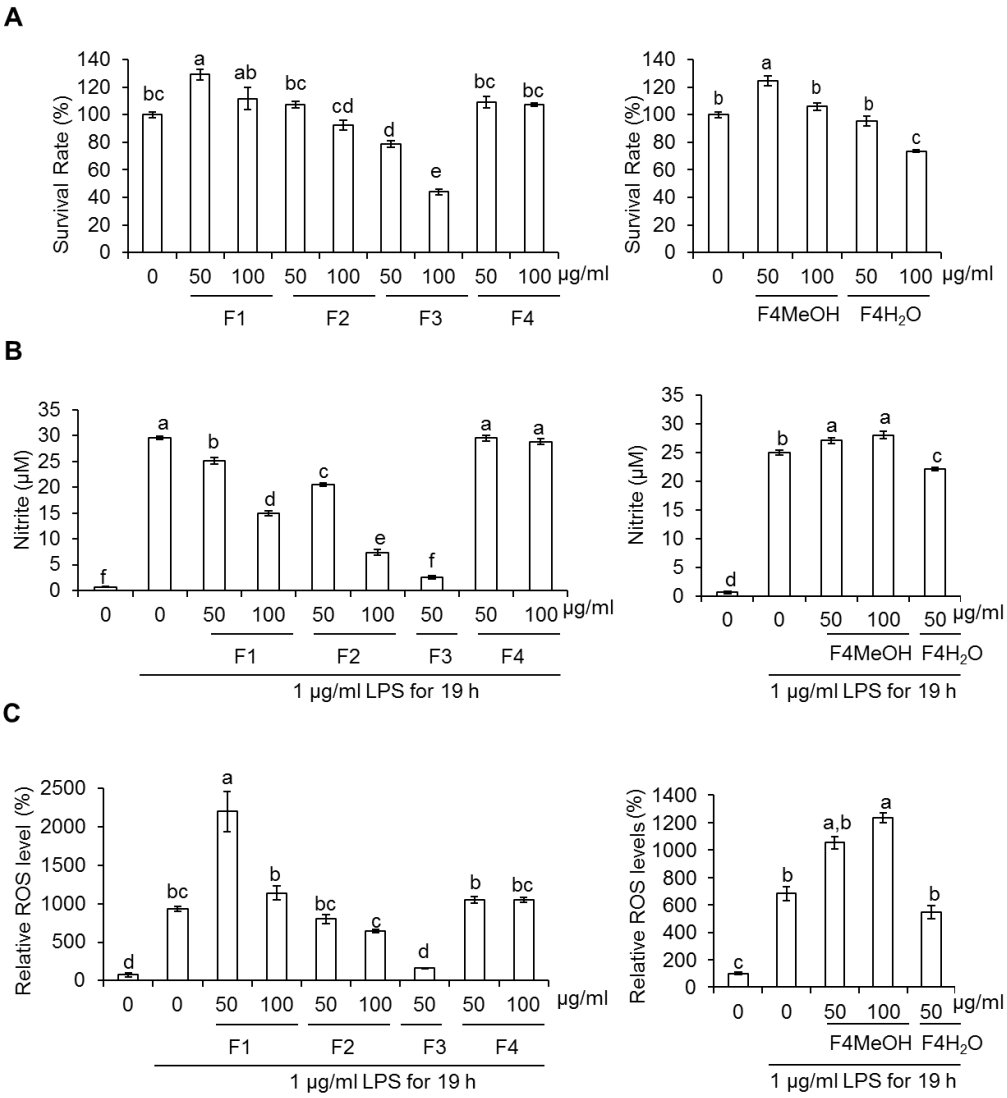

Figure 19 Effect of mashua 203081 fractions on cell viability and LPS-induced NO and ROS production. (A) Effect of mashua extracts on cell viability in macrophage cells. RAW 264.7 cells (0.5×10^5 cells/well in 96-well culture plates) were treated with 50 or 100 μg/ml mashua fractions for 24 h and then the cell viability was measured by MTS assay. (B-C) Effect of mashua fractions on LPS-induced NO and ROS production. RAW264.7 cells (0.5×10^5 cells/well in 96-well culture plates) were pretreated with 50 or 100 μg/ml mashua fractions for 5 h and then stimulated with LPS (1 μg/ml) for 19 h. Griess reagent was used to detect the generation of extracellular nitrite (B) and DCFA was used to determine the generation of intracellular ROS at 19 h after the LPS challenge (C). Data, obtained from four biological repeats at least, are shown as mean ± SE values. Different letters indicate significant differences by the ANOVA/Tukey-HSD ($p < 0.05$).

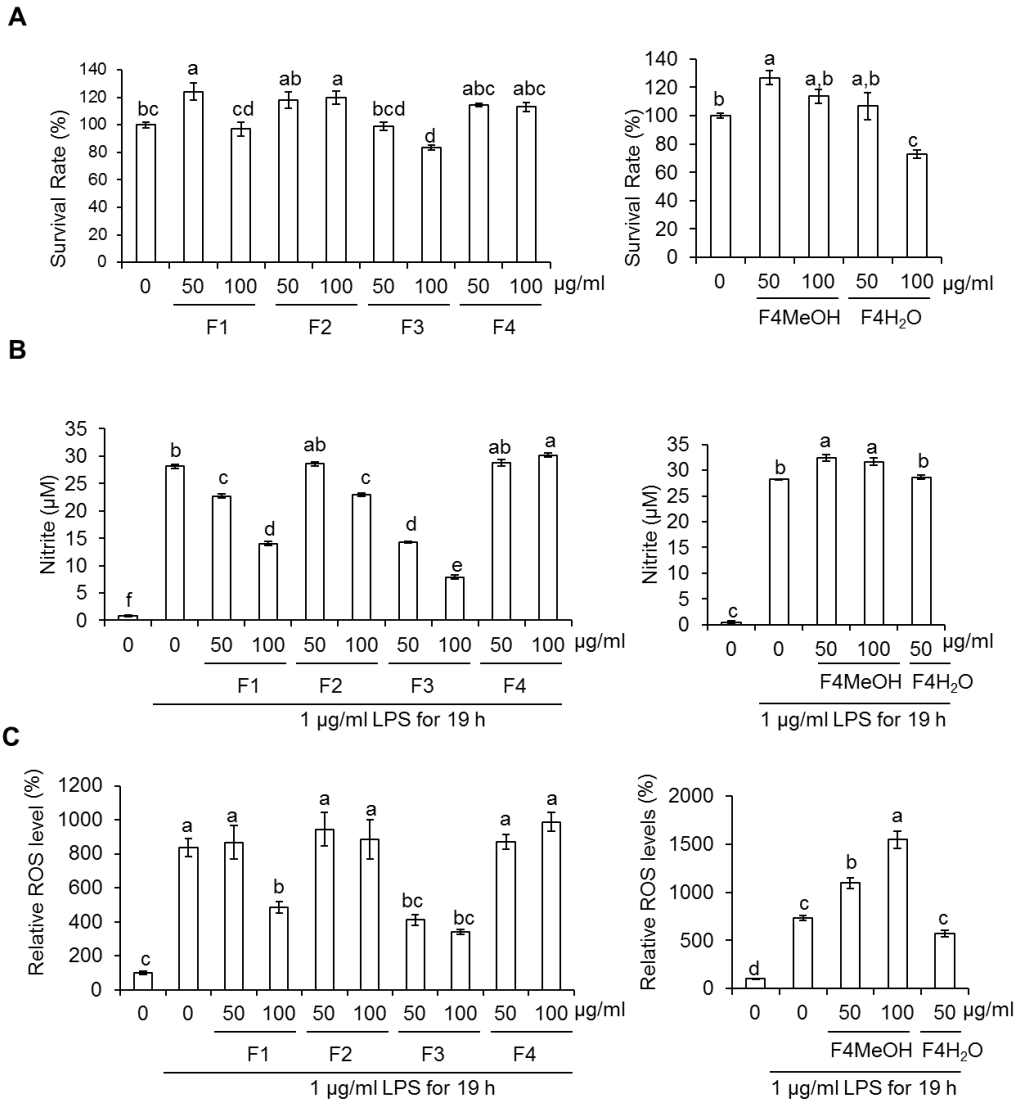

Figure 20 Effect of mashua 203040 fractions on cell viability and LPS-induced NO and ROS production. (A) Effect of mashua extracts on cell viability in macrophage cells. RAW 264.7 cells (0.5×10^5 cells/well in 96-well culture plates) were treated with 50 or 100 μg/ml mashua fractions for 24 h and then the cell viability was measured by MTS assay. (B-C) Effect of mashua fractions on LPS-induced NO and ROS production. RAW264.7 cells (0.5×10^5 cells/well in 96-well culture plates) were pretreated with 50 or 100 μg/ml mashua fractions for 5 h and then stimulated with LPS (1 μg/ml) for 19 h. Griess reagent was used to detect the generation of extracellular nitrite (B) and DCFA was used to determine the generation of intracellular ROS at 19 h after the LPS challenge (C). Data, obtained from four biological repeats at least, are shown as mean ± SE values. Different letters indicate significant differences by the ANOVA/Tukey-HSD ($p < 0.05$).

For mashua 203081 only fraction F3 protected PKM2 from proteolysis when compared to the control (Figure 21A) indicating that the phytochemicals present in this fraction are binding PMK2. Instead, for mashua 203040 fractions F1, F2 and F3 protected PKM2 from proteolysis when compared to the control (Figure 21B) indicating that phytochemicals present in F1, F2 and F3 are binding PMK2.

Discussion

Chronic inflammation can lead to the development of different conditions including diabetes, arteriosclerosis and some types of cancers (*8-11*). Macrophages play a key role in chronic inflammation and therefore have been used as a model in drug discovery studies associated with inflammation and related conditions. Dietary phytochemicals have been extensively studied in the past years for their health beneficial properties. Despite the promising results, the cellular targets of most dietary phytochemicals have not been yet reported. The lack of understanding of the mechanism of action of most dietary compounds limits their potential use as medicinal foods, supplements or drugs, and their regulation. In this study, we were able to overcome this barrier and could demonstrate that phytochemicals from two genotypes of mashua reduce LPS-induced inflammation in RAW264.7 macrophages by targeting PKM and reducing ROS. Moreover, we proposed a Warburg-like effect in the RAW264.7 macrophage cell line.

M1 or classically activated macrophages, besides energy, have a high demand for biosynthetic precursors used for synthesis of pro-inflammatory proteins.

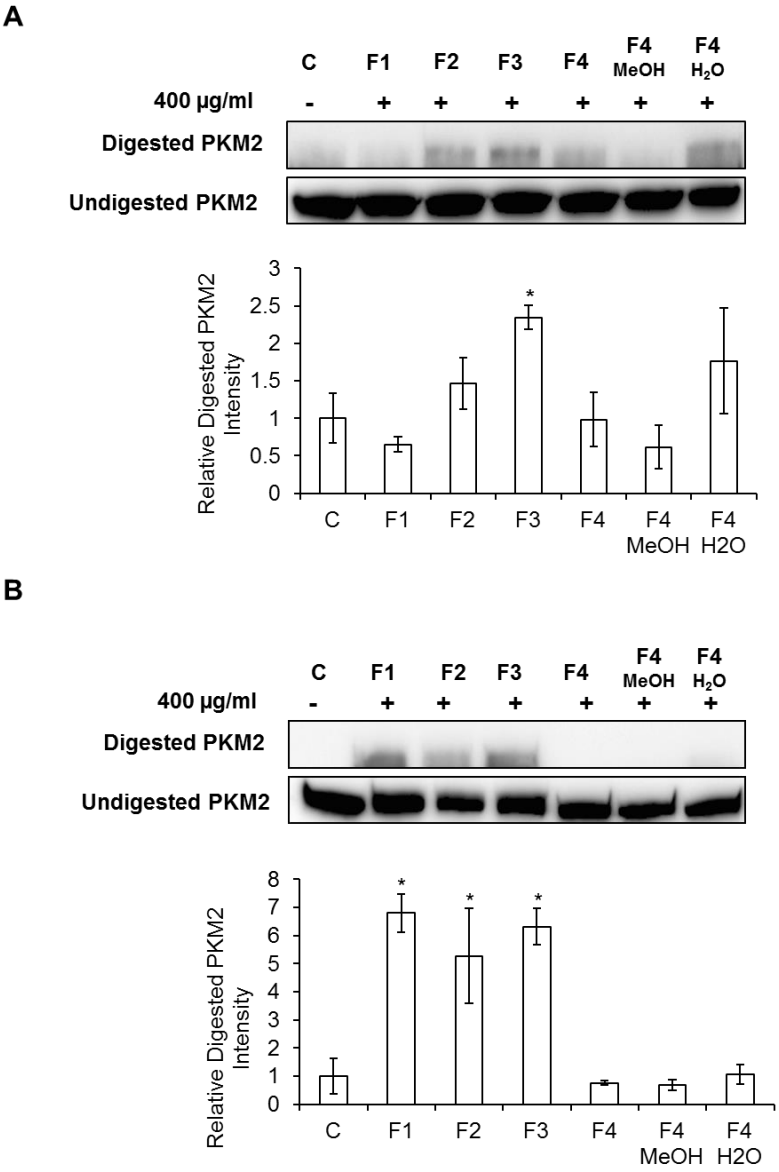

Figure 21 Assessment of binding of mashua fractions to PKM2 by DARTS methodology. RAW 264.7 cell lysates were incubated with 400 µg/ml of mashua 203081 (A) and 203040 (B) fractions for 3 h at room temperature, and then proteolized with pronase for 25 min at room temperature. DARTS cell lysates were subjected to SDS-PAGE and Western blot analysis using specific antibodies against PKM2 and β-actin. The protein bands in the upper panel were detected by chemiluminescence. The histograms in the bottom panel represent the relative protein levels measured by ImageJ software. Data, obtained from three biological repeats, are shown as the mean ± SE. Asterisks indicate significant differences by Student's t test ($p < 0.05$).

In order to meet these new needs, M1 macrophages exhibit an increase in aerobic glycolysis and a decrease in oxidative phosphorylation, known as the Warburg effect. Recently, different studies have highlighted the importance of the Warburg effect in the activation of M1 macrophages. Thus, targeting key mediators of the Warburg effect has been proposed as a promising therapeutic approach to modify inflammatory responses *(6, 19)*. An important mediator of the Warburg effect is pyruvate kinase M2 (PKM2), a protein kinase and transcriptional coactivator. PKM catalyzes the last step of glycolysis, which is the conversion of phosphoenolpyruvate (PEP) to pyruvate with the production of one molecule of ATP. There are two isoforms of PKM, PKMI and PKM2, which are produced by alternative splicing of the PKM gene (*108, 109*). The PKM1 isoform is always present as an active tetramer while the PKM2 isoform can be regulated allosterically or by posttranslational modifications, which allows it to switch between an active tetramer and a less active monomer/dimer (*108*). In undifferentiated primary macrophages, PKM2 increases upon the stimulation with LPS and plays an important role in the Warburg effect and inflammatory response. Thus, PKM2 has been proposed as a target for inflammation (*83, 110*).

In our study, we used the secondary RAW264.7 macrophage cell line as a model of inflammation. We report that LPS stimulation in this particular cell line induces several changes that are in agreement with previous reports of the Warburg effect in macrophages, as well as characteristics that are not. Thus, we proposed that LPS stimulation in RAW264.7 macrophages induce a Warburg-like effect (*111*). We found that the basal PKM2 protein level in this cell line is high, and that LPS stimulation did

not increase this level any further. In contrast, we found that PKM1 protein levels increase with LPS. Moreover, the nuclear PKM2, which is associated with a co-transcription factor function, did not change with LPS stimulation.

PKM2 together with the hypoxia-inducible factor (HF1) regulate various genes involved in the Warburg effect as well as in the inflammation response, including *LDHA, PDK1, IL-1β* and *GLUT1 (19).* The HIF1 heterodimer is formed by HIF1α and HIF1β. The HIF1β subunit is constitutively expressed in cells, while the expression of the HIF1α may be induced by a number of pathways, and its stability is highly dependent on O_2 levels (*112*). HF1α plays a key role in gene regulation under hypoxic conditions. However, it has been reported that other stimuli like LPS, can also increase HF1α expression level and activity (*113, 114*).

We observed that upon LPS stimulation in RAW264.7 macrophages, the expression of *IL-1β* increased at 6 and 19 h and the expression of *GLUT1* at 19 h but not at 6 h. This is in agreement with the fact that PKM2 is present in the nucleus, even before LPS stimulation, and that HF1α has been reported to increase with LPS. The expression of *GLUT1* seems to be a late time response since it increases only at 19 h after LPS stimulation. It is likely that the HIF-1α levels required to promote the expression of *GLUT1* are only reached at later times. ROS can promote the stabilization (*33, 115*) and enhance the transcription (*116*) of HIF-1α. Since ROS production in LPS stimulated macrophages increases with time, the levels of active HIF-1α will be higher at later times as well. *IL-1β* besides HF1α is also regulated by AP-1 (*117*). The expression of *PKM2, LDHA* did not changed, while *PDK1* decreased with LPS. It is possible that

these genes are less sensitive to HF1or that other signaling proteins are required for their expression.

The up-regulation of *GLUT1* gene expression is associated with an increased influx of glucose and glycolysis rate (*118*). The MTS results support these facts by showing that formazan levels, which are mainly associated with glycolytic NADH production (*105, 106*), increase with LPS. Also, we reported that the PKM activity increases, which is in agreement with the increased rate of glycolysis. Our results showed that PKM1 but not PKM2 increases with LPS, which indicates that PKM1 is responsible for the increment in PKM activity. PKM2 monomeric form decreases with LPS, but its dimeric form increases. It is possible that the dimeric form exerts a higher enzymatic activity, which can be attributed to the increment in PKM activity as well. Moreover, our results indicate that upon LPS stimulation lactate levels increase. Overall, we show that *GLUT1* gene expression increases, which translates into a higher influx of glucose and higher glycolysis rates. Additionally, part of the pyruvate produced will be converted to lactate.

In our report, we showed that mashua phytochemicals exert their anti-inflammatory properties by interfering with the NF-κB pathway and attenuating the Warburg-like effect possibly by the suppression of ROS and inhibition of PKM activity. The model showing the mechanism of action of mashua in RAW 264.7 is illustrated in Figure 22.

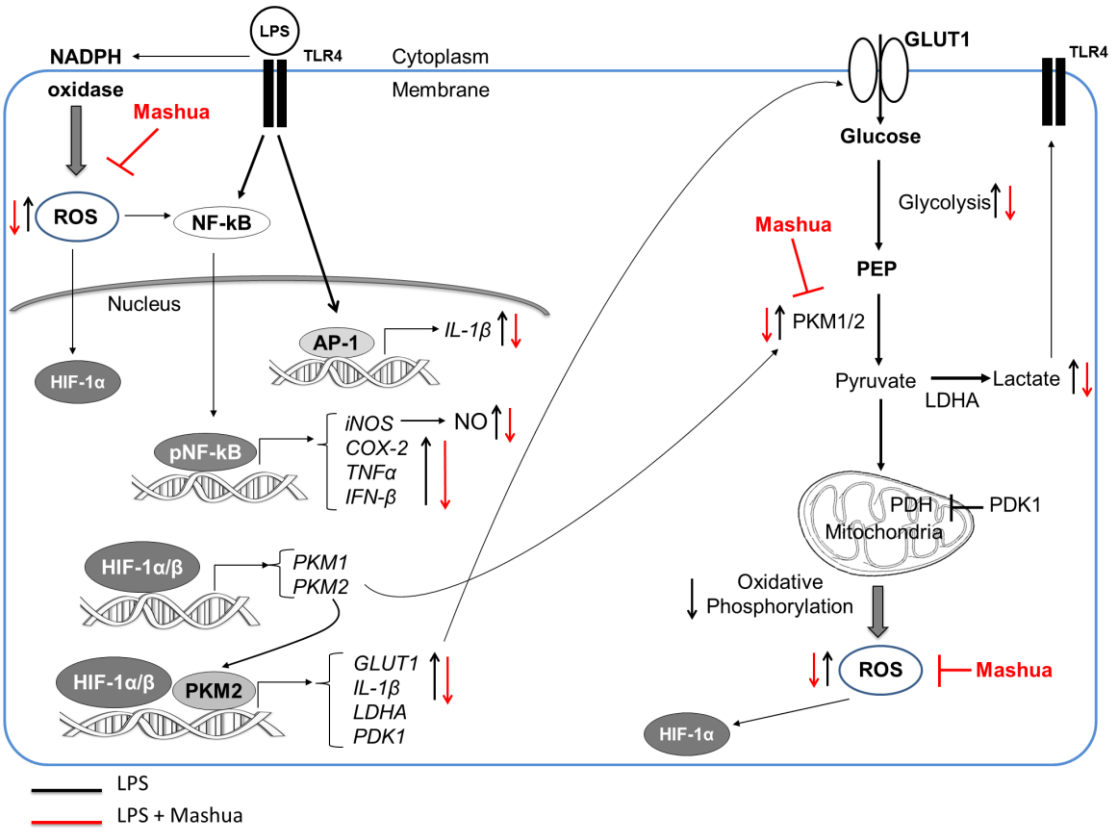

Figure 22 Anti-inflammatory role of mashua extracts.

Macrophage cells produce high levels of ROS after the LPS challenge through the NADPH oxidase and the mitochondria electron transfer chain (*28, 119*). The ROS induced by LPS has shown to mediate the LPS/TLR4 signaling pathway through different ROS-responsive signaling proteins. For instance, ROS have been reported to mediate the LPS-induced activation of NF-κB through redox mechanisms (*31, 32*). NF-κB can induce the expression of genes such as *TNFa*, *COX-2*, *IFN-β* (*17*), and eventually *iNOS* (*26, 27*). We showed that mashua phytochemicals reduced ROS levels at 6 and 19

h and consequently were able to reduce the expression of *TNFa, COX-2, IFN-β,* and *iNOS*. *TNFa* was the only gene that was only suppressed at 6 h but not at 19 h. In previous work done in our lab, we showed that different genes respond differently to the suppression of ROS levels, some being more sensitive than others (Bang and Cisneros-Zevallos, Unpublished). The reduction of ROS by both mashua extracts was higher at 6 h compared to 19 h. This could explain why some genes (*COX-2, IL-1β, iNOS* and *IFN-β*) were suppressed at 19 h while others (*TNFα)* required a higher inhibition of ROS and were only suppressed at 6 h. Additionally, the reduction of NO at 19 h could be explained by the reduction of *iNOS*, which is the enzyme responsible for its synthesis.

Furthermore, ROS can promote the stabilization and enhance the transcription of Hif-1α (*33*, *115*). Therefore the suppression of ROS by mashua extracts can reduce the transcription and stability of Hif-1α, and consequently decrease the expression of some of the genes regulated by this transcription factor. Mashua reduced the expression of *IL-1β* and *GLUT1*. The down regulation of *GLUT-1* is associated with a lower influx of glucose and glycolysis rate (*118*). Thus, the mashua extracts can suppress the LPS-induced glycolysis. The MTS results support this finding by showing that mashua suppress the LPS induced formazan levels, which are mainly associated with glycolytic NADH production (*105, 106*). Moreover, it has been reported that increasing glucose uptake by *GLUT1* is sufficient to promote a M1 macrophage phenotype, highlighting the importance of this transporter in the Warburg effect and inflammatory response (*118*)

In addition mashua exerts its anti-inflammatory properties by binding and inhibiting the activity of PKM. PKM2 has been widely studied for its role in cancer and

recently it has emerged as an important target for inflammation (*83, 84*). In the Warbug-like effect in LPS stimulated RAW264.7, we show that not only PKM2, but PKM1 also plays an important role in the Warburg effect and the respective inflammatory response. In the present study, we found that the phytochemicals of mashua exerted anti-inflammatory properties partially by inhibiting the activity of PKM and consequently reducing lactate production. In agreement with our results, a previous report showed that the PKM2 inhibitor shikonin protected mice against lethal endotoxic shock and sepsis by inhibiting PKM2 activity, lactate production, and HMGB1 release (*84*). It has been shown that lactate can further promote the inflammation processes by stimulating Toll-like receptor (TLR)-4 signaling activation in macrophages (*120*). In addition, lactate promotes macrophage activation via an autocrine HMGB1-dependent pathway (*121*). Therefore, mashua can exert its anti-inflammatory properties in part through lactate suppression caused by the inhibition of PKM activity.

In order to identify the phytochemicals from mashua that possess the anti-inflammatory properties, mashua extracts were fractionated, and these fractions were evaluated for their ability to reduce LPS-induced ROS and NO in macrophages, and to bind to PKM2. The phytochemicals responsible for ROS and NO reduction seem to be present mainly in F3 for mashua 203081, which contains isothiocyanate derivatives. This fraction contains a major compound (**1b**), tentatively identified as an isothiocyanate derivative, which may be responsible for the bioactivity of this fraction. However, further studies should be conducted to elucidate the structure of this compound. Instead, for mashua 203040, the phytochemicals responsible for ROS and NO reduction seem to

be present mainly in F1 and F3, which contain isothiocyanates and phenolics, and anthocyanins, respectively. Both isothiocyanates and anthocyanins have been shown to have anti-inflammatory and anti- oxidant properties (*122-124*). PKM2 but not PKM1 has been reported to play an important role in cancer and in M1 macrophage polarization. Thus, using DARTS methodology, we evaluated the mashua fractions that bind to PKM2. The phytochemicals responsible for the inhibition of PKM2 seem to be present mainly in F3 for 203081, which mostly contain isothiocyanate derivatives. Instead for mashua 203040 the compounds in F1, F2 and F3, which correspond to both phenolics and isothiocyanates seem to be responsible for the inhibition of PKM2. In a recent report phenolics have been reported to inhibit PKM2 activity (*34*), however to our knowledge this is first time isothiocyanates are reported to bind to PKM2.

In conclusion we evaluated the anti-inflammatory properties of mashua extracts and we identify PKM as a potential target of its phytochemicals through the use of DARTS methodology. However, further studies should be done to confirm the binding of mashua to PKM. In, additional studies should be conducted to confirm that mashua exerts its anti-inflammatory properties by binding and inhibiting the activity of PKM and not through interfering in other steps of PKM regulation. We also showed that mashua extracts exert their anti-inflammatory properties and attenuate the Warburg effect by suppressing ROS levels and consequently interfering with different ROS-responsive signaling proteins. Finally we showed that the bioactive compounds in mashua are both phenolics and isothiocyanates.

CHAPTER III

IDENTIFICATION OF CYCLOOXYGENASE-2 (COX-2) INHIBITORS FROM ACEROLA (*MALPIGHIA EMARGINATA*) USING A COMBINED ASSAY-GUIDED FRACTIONATION AND DRUG AFFINITY RESPONSIVE TARGET STABILITY (DARTS) METHODS

Overview

The leaves of acerola (*Malpighia emarginata*) have shown to have anti-inflammatory properties and to inhibit prostaglandin production in macrophages. The objective of this study was to identify the bioactive compounds acting as COX-2 inhibitors in acerola leaf extracts using bioassay-guided fractionation and DARTS methodology. The leaf extract (F4) was fractionated using solid-phase extraction with C18 cartridges into three fractions (F1, F2 and F3). The leaf extract and fractions 2 and 3 inhibited ($P<0.05$) COX-2 activity. LC-MS and NMR analysis revealed that F3 contains a major compound with glycerol/glycolipid/sphingolipid type structure which could be responsible for the COX-2 inhibitory properties of this fraction. F2 showed the highest COX-2 inhibitory effect among the fractions, and also showed binding to COX-2 by DARTS methodology and therefore its fractions (F2A, F2B, and F2C) were further tested for their ability to bind and inhibit COX-2 activity. All subfractions inhibited COX-2 activity but only F2C showed binding by DARTS after 25 min of pronase digestion. However, after 10 min of pronase digestion F2A and F2C showed binding by

DARTS, possibly indicating that the phytochemicals from F2A bind reversibly to COX-2, whereas the ones from F2C bind irreversibly. GC-MS profiling revealed F2A contains alkenes while F2B contains terpenes, which could account for the COX-2 inhibitory properties of these sufractions. LC-MS and GC-MS profiling revealed that F2C contains flavonoids and small amounts of terpenes. F2C was further fractionated into F2C1, F2C2, F2C3 and F2C4. Interestingly, only fraction F2C4 with aliphatic triterpene like compounds inhibited COX-2 activity. These results indicate that compounds with glycolipid/sphingolipid type structures, terpenes and alkenes are possibly responsible for the COX-2 inhibitory properties of acerola leaves.

Introduction

Over the years, many bioactive extracts and compounds from natural resources have been used for the development of new drugs, nutraceuticals or functional foods. The identification of bioactive extracts and compounds should ideally include the elucidation of cellular targets and associated pathways where these exert their activity. However, most studies have focused on the phenotypic changes, in the cell or organism, induced by a compound or an extract, instead of focusing on the identification of specific proteins targeted by these compounds. The reasoning behind this deficit is mostly due to the technical difficulty of finding appropriate methods to elucidate molecular targets. There are numerous target identification techniques described to date; however, affinity chromatography has been the most widely used method for target identification (69, 70). In affinity chromatographic purification, proteins from a cell lysate or tissue homogenate are incubated with an affinity matrix conjugated with the bioactive compound followed

by eluting the bound proteins and resolving them by electrophoresis on an SDS-PAGE gel. Subsequently, the purified target proteins can be identified by peptide microsequencing or, most commonly, by modern degradative mass spectrometric techniques (*125*). Despite the technological advances, affinity-based target identification techniques continue to be limited due to the necessity of derivatization of the small molecules without losing their bioactivity (72). For instance, conjugation to affinity matrices (a covalent attachment of target compounds to a polymeric solid support) can induce chemical and structural changes of the bioactive compound leading to the loss of native properties of the compound (*125*). Recently, it was reported that DARTS, drug affinity responsive target stability, methodology can identify the direct binding of compounds to protein targets, without requiring any chemical modification of the compound. The DARTS approach is based on the concept that small molecules can stabilize the structure of their target proteins and result in protease resistance. DARTS is unique in that the small molecules are used without the need for chemical derivatization or even knowing the chemical identity or purity of the compound (72, 74, 78).

Bioassay-guided fractionation has been frequently used in the discovery of bioactive compounds. In this approach, fractions generated from an extract are tested for their ability to induce desirable biochemical or cellular responses; the fractions giving a positive test are further processed until the bioactive compounds are isolated (*126*). One of the major limitations of using bioassay guided fractionation is that bioactive compound search is restricted to the availability of the bioassays; many potential protein targets like receptors, enzymes, kinases, transcription factors and others might not have

available assays associated to them or these assays might be hard to implement. One possible way to overcome this limitation is the use of the DARTS methods applied to screening, thus compounds binding to specific target molecules could potentially be identified.

Malphigia emaprginata, commonly known as “acerola”, is a fruit-bearing small evergreen tree that belongs to the Malpighiaceae family. Acerola is indigenous to the Lesser Antilles, Central America, and northern parts of South America, but nowadays it is cultivated globally. Brazil is one of the largest producers of acerola in the world (*127*). Acerola fruit is well known for its high Vitamin C content that can range from 695- 4827 mg/100 g of raw fruit (*128*). Studies on the phytochemical composition of acerola fruit have indicated the presence of anthocyaninins, flavonols, phenolic acids (*129*), and carotenoids (*130*). The fruit of acerola has been shown to possess antioxidant, anti hyperglycaemic (*131*), anti-inflammatory (*132*), anti-cancer, and antimicrobial activities (*133*). Despite the numerous reports on acerola fruits, there is only one study done on the chemistry of acerola leaf (*134*). Recently, our group characterized the phenolics and non-polar compounds from acerola leaf and reported the anti-inflammatory properties of acerola leaf extract and fractions for the first time (Bang et al., Unpublished). Moreover, we reported that phytochemicals from the leaves of acerola are able to reduce significantly LPS- induced prostaglandin levels in RAW264.7 macrophages (Unpublished).

The objective of this study was to identify the bioactive compounds from acerola extracts using bioassay-guided fractionation and DARTS methodology. Since our

previous work showed that acerola leaf extracts inhibited prostaglandin production in macrophage cells, we specifically focused in the present study on elucidating the bioactive compounds acting as COX-2 inhibitors. In addition, DARTS was evaluated as a screening method by the parallel comparison of the results obtained by bioassay fractionation using a commercial COX-2 kit.

In this study we present a proof of concept by which using a combined classical bioassay guided fractionation targeting COX-2 activity is confirmed simultaneously by COX-2 binding using the DARTS method.

Materials and Methods

Freeze dried acerola leaves of the genotype BRS-238 were supplied by EMPRAPA, Fortaleza, Brazil. Upon arrival at Texas A&M University, the samples were frozen and kept at −80 °C until use. The following chemicals were used in the experiments: Lipopolysaccharide (LPS), Dulbecco's Modified Eagle's Medium (DMEM)/low glucose, penicillin/streptomicyn mixture, DMSO and Fetal Bovine Serum (FBS) were purchased from Sigma (St. Louis, MO). Glucose and sodium bicarbonate were purchased from Acros Organics (Fair Lawn, NJ) and sodium bicarbonate from Mallinckrodt Chemicals (Phillipsburg, NJ), respectively. COX Inhibitor Screening Assay Kit was purchased from Cayman (Ann Arbor, MI). M-PER mammalian protein extraction reagent and Halt phosphatase inhibitor cocktail were purchased from Thermo Scientific (Rockford, IL). Protease inhibitor cocktail tablets and pronase were purchased from Roche Diagnostics (Indianapolis, IN). Antibodies against COX-2 and β-Actin were purchased from Cell Signaling Technology (Danvers, MA). Macrophages RAW 264.7

(cell line TIB-71™) were acquired from the American Type Culture Collection (ATCC) (Manassas, VA).

Crude extract (F4) preparation

A 1 g aliquot of the lyophilized acerola leaf powder was dissolved in MeOH and stirred at 4°C for 24 h. The extract was centrifuged and concentrated at 4000 rpm (2147*g*) and 45 °C until all of the volatile solvents were evaporated in a Centrivap concentrator connected to a cold trap (Labconco, Kansas City, MO).

TLC Analysis, Fractionation (Fractions F3 – F1) and Subfractionation (F2A, F2B, F2C)

The acerola leaf fractions or subfractions were spotted on a TLC plate to determine the possible presence of terpenoids using the Liebermann Burchard test and anisaldehyde/sulphuric acid spray reagent (*135*). The crude extract (F4) was fractionated using solid-phase extraction with C18 cartridges by a modified procedure previously reported (*136*). A schematic representation of the flow chart showing the elution of the fraction with different solvents is illustrated in Figure 23. Briefly, the crude extract (F4) (849 mg) was dissolved in minimum amount of MeOH/H_2O solution (1ml) and then adjusted to pH 7.0 with 5 N NaOH. A total of 1 mL of extract was loaded in SEP Pack C18 cartridge (55–105 μm, Waters Corp., Milford, MA, USA) previously conditioned to pH 7.0 with 20 mL of 100% methanol and 50 mL of nanopure water (pH 7.0). The neutral phenolics and other compounds were absorbed in the cartridge, while the phenolic acids were not. The cartridge was washed with 50 mL of water (pH 7.0).

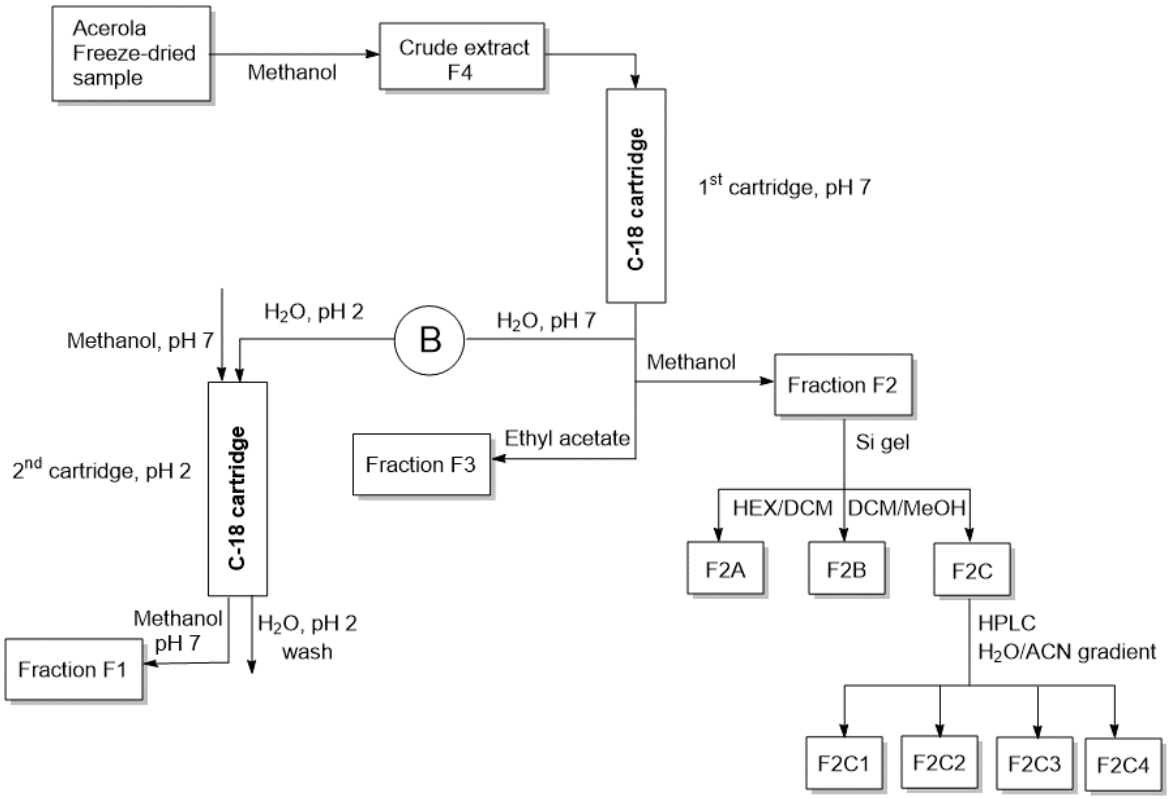

Figure 23 Extraction, fractionation and subfractionation scheme used for acerola leaves.

The water from the wash containing the phenolic acids that were not absorbed in the cartridge was adjusted to pH 2.0. This mixture was loaded into a second cartridge previously conditioned at pH 2.0 with 50 mL of methanol and 50 mL of nanopure water at pH 2.0. Phenolic acids bound to the matrix of the second cartridge were later eluted with 50 mL of methanol (F1). Subsequently, the compounds in the first cartridge were eluted with 50 mL of MeOH and with 50 mL of ethyl acetate to obtain fractions F2 and F3, respectively. All the fractions (F1 (61.2 mg) , F2 (481 mg) and F3 (131 mg) were eluted with low boiling point solvents and were completely evaporated at 45°C using a

speed vac (Labconco, Kansas City, MO). Fraction F2 (481 mg) was further fractionated as shown in Figure 23. Briefly, fraction 2 was subjected to Silica gel chromatography (10 × 200 cm, 80 g) eluted with 150 ml of hexane, 150 ml dichloromethane and 150 ml methanol in increasing polarity to obtain fractions F2A (20 mg), F2B (82 mg), F2C (215 mg), respectively.

Fractionation of F2C by Reverse Phase HPLC

F2C (215mg) was dissolved in 5ml MeOH, 1 ml of the extract was pipetted out and filled in each 1 ml HPLC vial (43 mg/ml). This extract was then injected in the waters 515 series machine equipped with 996 PDA detector, and a semi preparative phenomenex -C18 column (10 × 250 mm, 5 μm) for reverse phase HPLC analysis. The eluents were acetonitrile/methanol (1:1), formic acid (0.5:99.5, v/v) (phase A) and formic acid–water (0.5:99.5, v/v) (phase B). The applied elution conditions were: 0-2 min, 0% A, 100% B; 3-5 min, 10%A, 90% B, 5-10 min, 20% A, 80% B; 10-20 min, 35% A, 65% B; 20-30 min, 45% A, 55% B – 65% A, 35% B over period of 10 min; 31-40 min 70% A, 30% B - 100 % A over the period of 10 min; 40-44 min was held isocratic, 100% A; 45-50 min 0% A, 100 % to the starting condition at 25°C at a flow rate of 2.0mL/min. Extracts were repeatedly injected (each time 100 ul of the extract) in the HPLC and the fractions were collected with the help of fraction collector (ISCO, Lincoln, NE) over the period of time 0-10 min (F2C1) 15 mg, 10-20 min (F2C2) 13 mg, 20-30 min (F2C3) 21 mg and 30-45 min (F2C4) 12 mg (Figure 23). The HPLC chromatogram of F2C is illustrated in Figure 24.

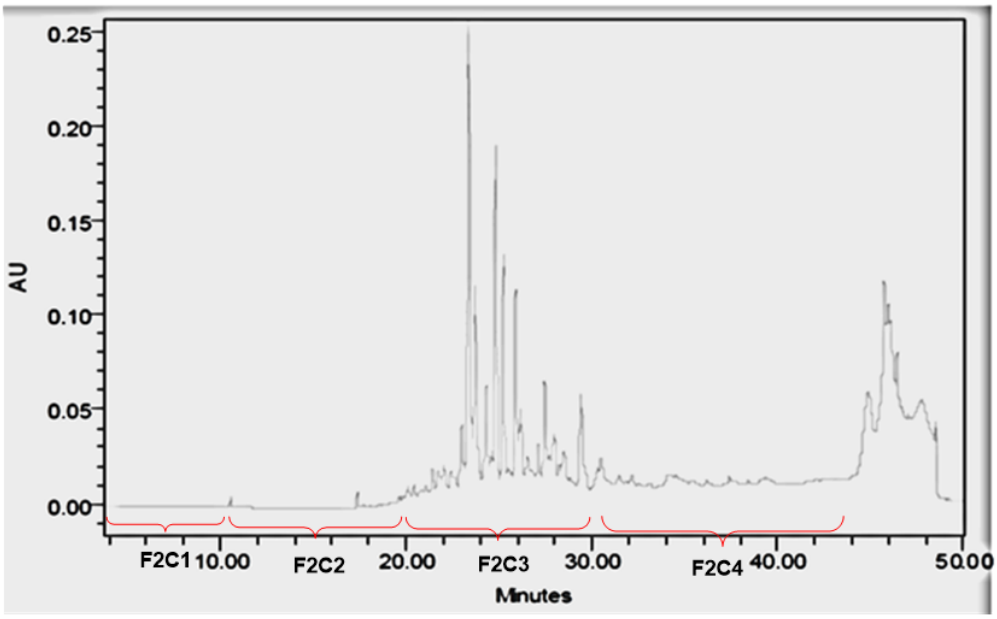

Figure 24 HPLC chromatogram of fraction F2C

Chromatography and HPLC Conditions for Compound Isolation from F3

Column chromatography was performed with silica gel (200−400 mesh, Alfa Aesar Ltd.) and reversed-phase C18 silica gel (250 mesh, Merck). Precoated TLC sheets of silica gel 60 GF254 (Silicycle Co., Ltd.) were used. Normal phase chromatography was done by Si column Astec, Advance science technologies (10 × 250 mm, 5 µm). The solvent system was composed of solvent A (hexane), solvent B (IPA) in the gradient 0-2 min, 0% A, 100% B; 3-5 min, 95%A, 5% B, 5-20 min, 80% A, 20% B; 21-28 min, 65% A, 35% B; 28-30 min, 20% A, 80% B ; 31-33 min 10% A, 90% B; 34-36 min was held isocratic, 100% B; 36-37 min 100% A to the starting condition and was held for 3 more minutes with 100 % A at 25°C at a flow rate of 2 mL/min. The concentration of the extract (F3) was 10 mg/ml and was injected (30 ul) in the HPLC repeatedly till all

volumes were used up. These conditions were used to isolate the glycolipid compound from fraction 3.

LC-MS Analysis and Conditions for Phenolics and Compound Isolation from F2

The LC-MS system used is a Surveyor (Thermo Scientific, USA) coupled to Surveyor DAD. The eluents were acetonitrile/methanol (1:1), formic acid (0.5:99.5, v/v) (phase A) and formic acid–water (0.5:99.5, v/v) (phase B). The applied elution conditions were: 0-2 min, 2% A, 98% B; 3-5 min, 5%A, 95% B, 5-30 min, 20% A, 80% B; 30-72min, 35% A, 65% B; 72-83 min, 100% A, 0% B; 83-85 min was held isocratic, 100% A; 87-90 min 2% A, 98% to the starting condition. The chromatograms were monitored at 330, 280, 210 nm; and complete spectral data were recorded in the range 200–600 nm. A reversed-phase Phenomenex (Torrance, USA) Luna C_{18} column (150 mm×4.6 mm i.d. and particle size 3 µm) with a Waters Nova-Pack C_{18} guard column (10 mm×3.9 mm i.d, 4 µm) was used and a flow of 200 µL/min from the DAD eluent was directed to the ESI interface using a flow-splitter. Nitrogen was used as desolvation gas at 275°C and a flow rate of 60 L/h, and no cone gas was used. Mass spectra were obtained on a MS Finnigan LCQ Deca XP Max, Ion trap mass spectrometer coupled at the exit of the diode array detector and equipped with a *Z*-spray ESI source, and run by Xcalibur version 1.3 software (Thermofinnigan-Surveyor, San José, USA). A potential of 1.5 kV was used on the capillary for negative ion mode. The source block temperature was held at 250 °C. These conditions were used for the characterization of phenolic compounds and for the isolation of three phenolic peaks from the extract of acerola leaf.

GCMS Conditions

GC-MS was performed on Ultra GC/DSQ (ThermoElectron, Waltham, MA). Rxi-5ms was used as a gas chromatographic column with dimensions of 60 m length, 0.25 mm i.d., and 0.25 μm film thickness (Restek; Bellefonte, PA). Helium was used as a carrier gas at constant flow of 1.5 ml/min. Split (1:50) injections were used. Transfer line and ion source were held at 250°C. The column temperature was maintained at 50°C for 5 min and raised to 320°C at 20°C/min. Mass spectra were acquired in full scan mode in the range of 30-500 *m/z*.

NMR Specstroscopy

^{1}H and ^{13}C NMR spectra were recorded on a Bruker Avance II 500 spectrometer operating at 500.130 MHz for ^{1}H and at 125.758 MHz for ^{13}C, and using a gradient-equipped inverse 5 mm triple probe with p/2 pulses of 6.5, and 14.5 ms, respectively. The standard Bruker Topspin 2.1 software under Windows 7.0 was used throughout. A total of 2mg of the pure compound was dissolved in deuterated solvent. All experiments were performed at 22 uC in deuterated solvents. Scifinder we used to search the structures.

Cell Culture

Raw 264.7 macrophages were grown in the DMEM-low glucose (pH 7.2 – 7.4) including 4 g/l glucose, 3.7 g/l sodium bicarbonate, 10% fetal bovine serum (FBS) and antibiotics (100 units/ml penicillin and 100 μg/ml streptomycin) in a humidified atmosphere with 5% CO_2 at 37°C. Cells were used at a passage of 3 to 8 in this study.

DARTS

The target identification using drug affinity responsive target stability (DARTS) methodology was based on the protocol by Lomenick et al. 2011. Macrophages were plated at 2 $\times 10^6$ cells/well in 150 x 25 mm clear plates and cultured overnight. LPS (1 µg/ml) was added for 24 h. Cells were washed twice with DPBS and then lysed with M-PER (Pierce) supplemented with protease and phosphatase inhibitors. Protein concentrations were determined by the Pierce BCA protein assay kit (Thermo Fisher Scientific, Rockford, IL). Lysates were incubated with 400 µg/ml of acerola leaf extract (F4), fraction 2 and subfractions (F2A, F2B and F2C) or DMSO (control) for 3 h at room temperature. Each sample was then divided into two aliquots, each of which underwent proteolysis with pronase or mock proteolysis, for 25 or 10 min at room temperature. A 1:1000 ratio of pronase versus cell lysates protein concentration was used for proteolysis. Proteolysis was stopped by addition of loading buffer (950 µl 2X laemmli buffer + 50 µl β-mercaptoethanol) to each sample at a ratio of 1:1 followed by western blot analysis.

Western Blot

A volume of 20 µl containing 15-20 µg of non-digested protein was loaded in each well of a 10 % polyacrylamide gel. The same volume (20 µl) was used for digested proteins. The gels were transferred by wet blotting onto PVDF membranes (Millipore, Bedford, MA). The membranes were blocked with 5 % skim milk in Tris-buffered saline with 1% Tween-20 (TBS-T) for 1 h with gentle shaking. Membranes were then incubated overnight with a specific primary antibody against COX-2 (1:1000) and Actin

(1:5000) at 4 °C. The membranes were washed four times with TBS-T and incubated for 1 h at room temperature with the secondary antibody conjugated with horseradish peroxidase (HRP) at 1:5000 dilution. Specific bands were developed using a SuperSignal West Femto enhanced chemiluminescence (ECL) Western blotting detection kit (Pierce, Thermo Fisher Scientific, Inc., Rockford, IL) and the signals were captured by Chemi Doc XRS (Bio-Rad Laboratories, Hercules, CA). Bands were quantified using densitometry with Image J software (NIH, Bethesda, MD).

COX-2 Inhibitory Assay

The COX-2 inhibitory assay was carried out using the COX Inhibitor Screening Assay Kit following the manufacturer's instructions (Cayman Chemical, Ann Arbor, MI). Briefly, 10 µl of heme and 10 µl COX-2 (human recombinant) enzyme were added to test tubes containing 160 µl COX reaction buffer. The mixture was vortexed and exposed to either 200 µg/ ml acerola compounds or to 0.5% DMSO (control) for 10 min at 37 °C. This was followed by the addition of 10 µl arachidonic acid with further incubation for 2 min. Finally, 10 µl of hydrochloric acid (1 M) was added to stop the COX reaction followed by the addition of 20 µl stannous chloride ($SnCl_2$) solution. This assay measures $PGE_{2\alpha}$ derived from $SnCl_2$ reduction of PGH_2 produced in the COX-2 reaction, by an enzyme immunoassay kit.

Statistics Analysis

The data were analyzed using Student's t-test or one-way analysis of variance (ANOVA) followed by Tukey-HSD test, using the software JMP pro v10.0. Results are

expressed as means ± standard errors (SE) from at least three biological repeats. . Different letters show significant differences ($P < 0.05$).

Results

Structure Elucidation of Compounds from Acerola Leaf Fractions by NMR Analysis

In a previous experiment done by our lab (Bang et al., Unpublished), flavonoids from acerola leaf extract (F4) were characterized by HPLC-MS chromatography and MS/MS fragmentation (as shown in Appendix A) indicating mainly the presence of quercetin and kaempferol *O*-glycosides. The identified compounds (1 to 11), and additional data are shown in Appendix B. Additionally, GC-MS analysis demostrated the presence of terpenes, alkenes and lipidic compounds. The GC-MS chromatogram of F4 is shown in Appendix C and the identified compounds are shown in Appendix D.

Following the fractionation scheme of the previous report, acerola leaf extract (F4) was fractionated into fractions F1, F2, and F3. The HPLC-MS chromatograms of these fractions are illustrated in Appendix E. In this study, compound 5, which was found to be present in F4 and F2, was further characterized using HRESIMS and 2D NMR. The molecular formula of compound 5 was determined as $C_{31}H_{36}O_{19}$ on the basis of HRESIMS *m/z* 711.1851 $[M-H]^-$ (calcd. *m/z* 711.6061 $[M-H]^-$) and ESI-MS *m/z* 713 [M+H]+. The IR spectrum showed the characteristic absorption bands of hydroxyl (3250 cm^{-1}), carbonyl (1665 cm^{-1}), and phenyl groups (1576 cm^{-1}). Fragmentation of 711$[M-H]^-$ by the MS/MS gave fragment $[M-H-132]^-$ 579 indicating a loss of a pentose sugar, followed by $[M-H-132-162]^-$ 417+42 [ACN adduct] 459 indicating that the second sugar

was a hexose and finally gave a fragment at *m/z* 285 [M-H-132-162-132]$^-$ indicating that the second pentose sugar is attached to the kaempferol ring (Figure 25).

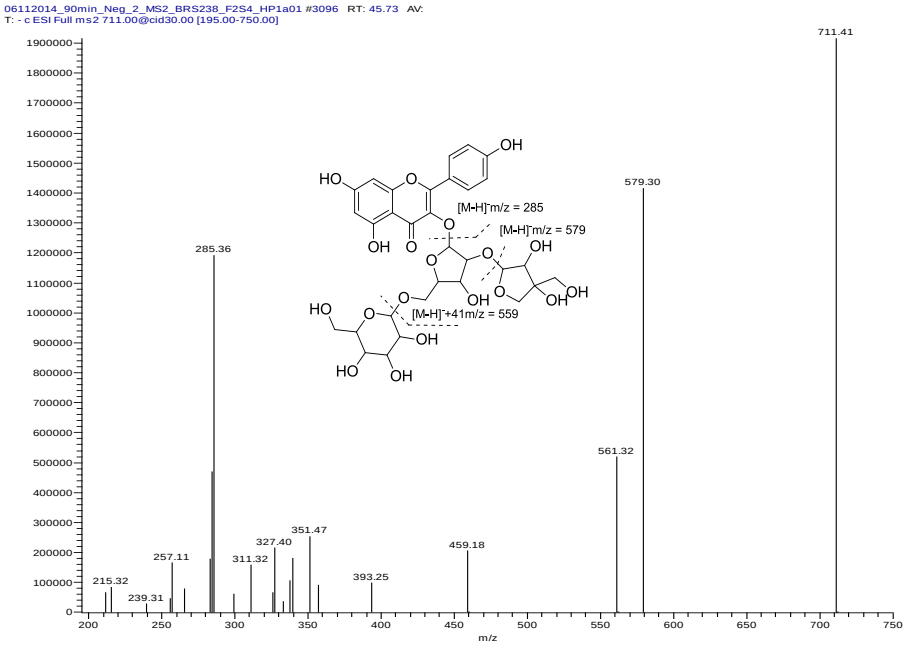

Figure 25 MS/MS fragmentation of compound **5**

The structural information concerning the attachment position of aforementioned moieties was determined based on MS fragmentation and 2D-NMR analysis. Further confirmation of the structure is explained by NMR analysis below and data is shown in Table 12. The aromatic region of the ^{1}H-NMR spectrum of compound 5 showed four signals, namely, two broad singlets (δ 6.19 and δ 6.40) for the protons in ring A and two doublets (AA'BB' system) for ring B (δ 6.89 and δ 8.13, both with J = 8.6 Hz), which are typical for a kaempferol aglycone (*137*).

Table 12 NMR data of compound **5**

Position	^{1}HNMR[a]	^{13}CNMR[b]	HSQC	^{1}H-^{1}H COSY	HMBC
2	-	158.5	Cq	-	-
3	-	134.9	Cq	-	-
4	-	179.7	Cq	-	-
4a	-	158.4	Cq	-	-
5	-	161.5	Cq	-	-
6	6.19 (d, *J* = 2.5)	99.8	CH	-	7, 8, 5, 4a
7	-	165.9	Cq	-	
8	6.40 (d, *J* = 2.5)	94.8	CH	-	6, 7, 8, 8a, 4a
8a	-	109.5	Cq	-	
1´	-	122.9	Cq	-	
2´	8.13 (d, *J* = 2.6)	132.3	CH	2´, 6´	3´, 1´, 6´, 4´
3´	6.89 (d, *J* = 8.9)	116.3	CH	2´, 5´	1´, 2´, 4´, 5´
4´	-	163.1	Cq	-	
5´	6.89 (d, *J* = 8.6)	116.3	CH	3´, 6´	1´, 2´, 4´, 5´
6´	8.13 (d, *J* = 2.6)	132.3	Cq	2´, 5´	3´, 1´, 6´, 4´
Ara-O-3					
1´´	5.34 (d, *J* = 7.8)	101.2	CH	2´´	3, 2´´, 3´´, 4´´
2´´	3.93 (dd, *J* = 3.5, 1.5)	76.9	CH	1´´, 3´´	1´´´, 2´´, 3´´, 4´´
3´´	3.65 (dd, *J* = 1.5, 3.5)	75.5	CH	2´´, 4´´	1´´, 2´´, 4´´, 5´´
4´´	3.78 (dd, *J* = 3.5, 1.5)	70.8	CH	3´´, 5´´	2´´, 3´´, 1´´, 5´´
5a´´	3.68 (dd, *J* = 7.8, 3.5)	66.9	CH_2	4´´	1´´´, 4´´, 3´´
5b´´	3.17				
Api-O-					
1´´´	5.45 (d, *J* = 1.5)	110.9	CH	2´´´	2´´, 2´´´, 3´´´, 4´´´
2´´´	4.05 (d, *J* = 1.5)	75.2	CH	1´´´, 3´´´	1´´´, 3´´´, 4´´´, 5´´´
3´´´	-	80.8	Cq	-	

Table 12 Continued

4´´´	3.62-3.64 (d, *J* = 7.8)	75.1	CH_2	-	1´´´, 2´´´, 3´´´, 5´´´
5´´´	3.61 (s)	68.5	CH_2	-	2´´´, 3´´´, 4´´´
Glu-Ara					
1´´´´	4.01 (d, *J* = 7.8)	104.5	CH	2´´´´	2´´´´, 3´´´´, 5´´´´
2´´´´	3.10 (dd, *J* = 7.8, 9.5)	74.0	CH	1´´´´, 3´´´´	1´´´´, 3´´´´, 4´´´´
3´´´´	3.65 (dd, *J* = 7.5, 9.5)	69.5	CH	4´´´´, 5´´´´	1´´´´, 2´´´´, 4´´´´, 5´´´´
4´´´´	3.59 (dd, *J* = 3.5, 1.5)	74.4	CH	3´´´´, 5´´´´	2´´´´, 3´´´´, 5´´´´, 6´´´´
5´´´´	4.04 (ddd, *J* = 1.5, 5.0, 7.0)	78.1	CH	4´´´´, 6´´´´	1´´´´, 3´´´´, 4´´´´, 6´´´´
6a´´´´	3.75 (dd, *J* = 10.0, 6.5)	66.9	CH_2	5´´´´	4´´´´, 5´´´´
6b´´´´	3.65 (dd, *J* = 7.8, 3.5)				

[a]d_4-MeOH, 300 MHz. [b]d_4-MeOH , 125 MHz

The middle region of the spectrum exhibited three anomeric signals due to the sugar units at δ 5.34, δ 5.45, and δ 4.04. The coupling constant of the anomeric proton of the pentose at δ 5.34 (*J* = 7.7 Hz) and for the hexose at δ 4.04 (*J* = 7.7) Hz was in accordance with a β-glycosidic linkage, while the coupling constant of another anomeric proton was for api-pentose (*J* = 1.5 Hz) indicated an α-glycosidic linkage (*138*). A further seventeen protons were identified between δ 3.31 and δ 4.04 due to the sugar units. The HMBC experiment of compound 5 exhibited a correlation of the anomeric proton H-1" of α-D-arabinopyranose (δ 5.34) with C-3 (δ_{C3} 135.7), indicating the linkage of this sugar with the aglycone moiety. The interglycosidic linkage is shown by the

correlation of the H-1''' (δ 5.44) of α-D-apiose with the C-2" (δ C2" 76.9) of β-D-arabinopyranose and by the correlation of the H-1'''' (δ 4.04) of β-D-glucopyranose with H-4" (CH_2 – (66.1) of β-D-arabinopyranose, hence confirming that two sugars are attached to the same pentose β-D-arabinopyranose, which is attached directly to kaempferol. Overall, the structure was confirmed on the basis of 2D NMR, and the new molecule was assigned as kaempferol-3-*O*-β-D-[-arabinopyranosyl-(1'''→2")-*O*-α-L-apiose-(1''''→5")-*O*-β-Dglucopyranoside (Figure 26).

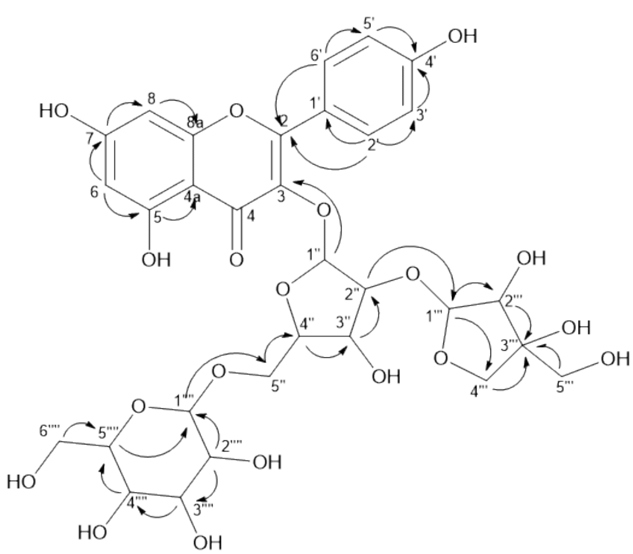

Figure 26 HMBC and ^1H-^1H COSY correlations of compound **5**

In the previous report it was shown that fraction 3 possibly contained lipid-like glycosides. To understand the chemistry of the compounds present in F3, the fraction was subjected to normal phase chromatographic separation with IPA/Hex mobile phase using Si column Astec, Advance science technologies (10 × 250 mm, 5 μm) over 40 min. One major compound F3A1 (6.5 mg) was isolated at R.T 21.4 min. Compound F3A1 gave a pinkish spot turning to violet on TLC while heating with anisaldehyde/sulphuric spray reagent indicating the possibility of conjugated glycol-lipids. Moreover, the NMR spectrum for this compound was taken to elucidate the structure of this compound. The ^{1}H NMR spectrum indicated again the presence of olefinic signals between δ_H 5.24-5.42 ppm, oxygenated signals between δ_H 3.55-4.40 ppm, and α-methylene & further aliphatic signals between δ_H 2.8-0.8 ppm. The ^{13}C NMR spectrum showed the presence of 3 carbonyl signals (δ_C 173.8, 173.5, 174.4), 6 methine signals from the olefin (δ_C 137.9, 130.2, 129.9, 128.3, 128.2, 127.9, 127.8, 127.1), an anomeric/acetal signal at δ_C 103.6 ppm, further 7 oxygenated signals containing 4 (-CH-O) signals and 3 (CH_2-O) signals (δ_C 73.1, 72.3, 71.7, 70.0, 68.4, 67.9, 62.2, 62.1) and several aliphatic methylene carbon signals and methyl carbon signals (δ_C 34.1, 31.9, 31.5, 30.9, 29.7, 29.6, 29.6, 29.6, 29.6, 29.5, 29.4, 29.3, 29.2, 29.2, 29.1, 29.1, 29.1, 29.0, 27.2, 25.6, 25.5, 25.3, 24.9, 24.8, 22.7, 22.6, 20.5, 14.3, 14.1, 14.1). Intensity of the olefinic and aliphatic signals were higher than that of oxygenated (sugars) signals and this gave a tentative substructure for a glycolipid/sphingolipid type structure (Figure 27).

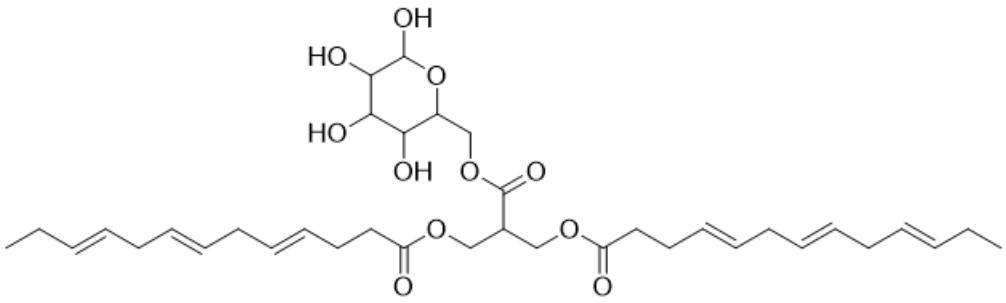

Figure 27 Structure of the isolated glycolipid from fraction F3A1

Several studies on glycolipids reported them as having specific biological activities, e.g., anti-tumor (*139*), anti-inflammatory (*140*), and anti-viral (*141*) properties.

Chemistry Analysis of F2 Fractions (F2A, F2B and F2C)

F2 obtained from the RPC_{18} cartridge was subjected to Silica gel chromatography (10 × 200 cm, 80 g) (eluted with hexane, dichloromethane and methanol in increasing polarity, step gradient) to obtain subfractions F2A, F2B, and F2C. The GC-MS chromatograms of F2A, F2B, and F2C are illustrated in Figure 28 and the potential compounds and additional data are shown in Tables 13-15, respectively. F2A was non-polar and hexane soluble fraction mainly consisting of fatty acids, volatile terpenes, simple phenols, etc. Further chemical components of F2A were revealed by GC-MS analysis. GCMS profile of fraction F2A identified 5-tetradecene, Cyclopropane Nonanoic acid, [2-butyl-], Cyclotetracosane, 5-Eicosene Androstane-3,17-diol[3β-5α 1,2-Benzene dicarboxylic acid, butyl-7-ol, Hexadecanoic acid 1-octadecanol, Phytol, 1,4 cyclo-octadiene Cyclohexane, 1,2-dimethyl-3-pentyl-4-propyl, Cyclotracosane and Dibutyl phthalate (Table 13).

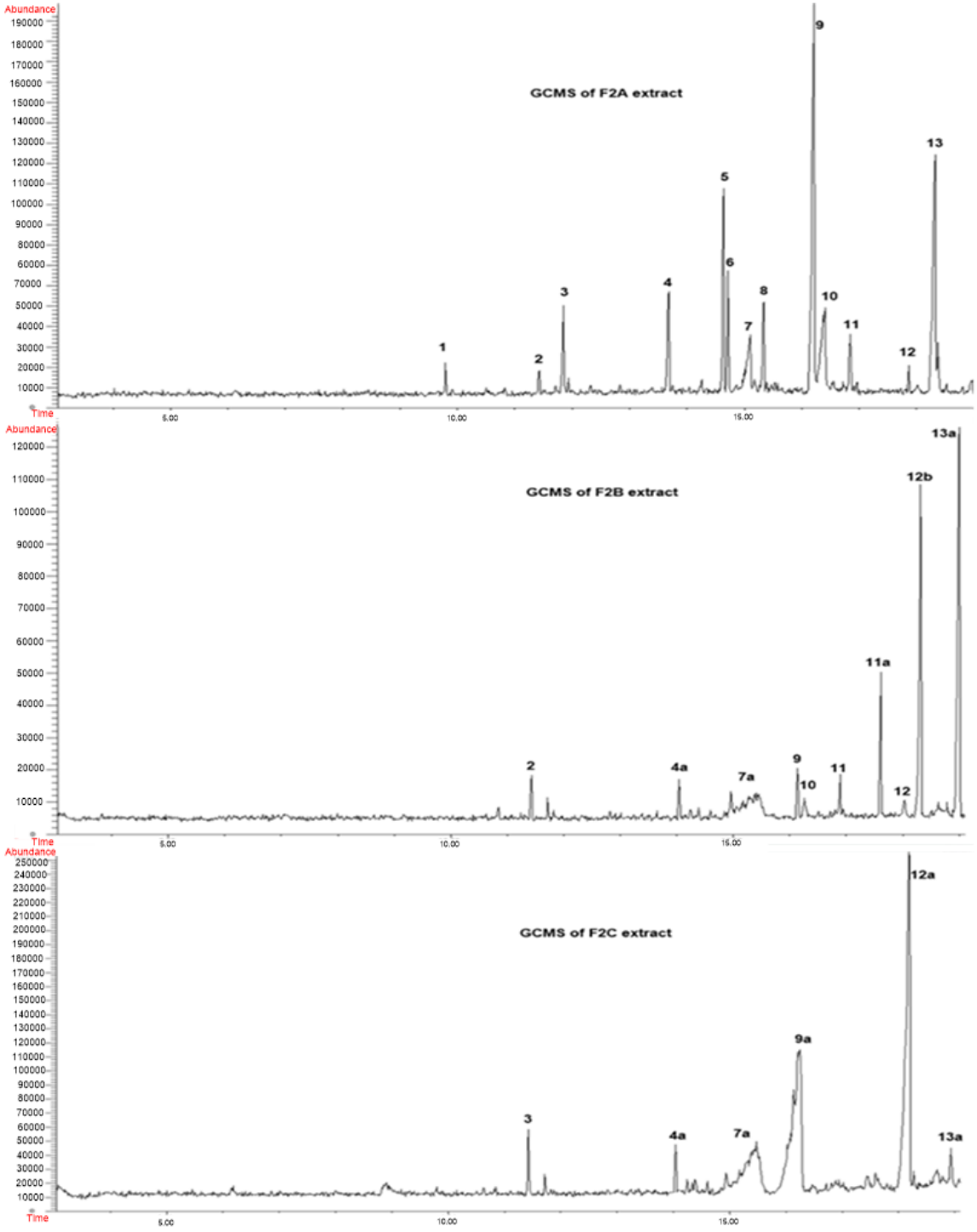

Figure 28 GCMS data of fraction F2A, F2B and F2C

Table 13 GC-MS data of F2A extract

Peak Nos	Retention time	MW	Identification	Type of compound
1	9.793	196	5-tetradecene	Alkene
2	11.416	322	Cyclopropane Nonanoic acid, [2-butyl-]	Lipid
3	11.844	336	Cyclotetracosane	Cycloalkane
4	13.664	280	5-Eicosene	Alkene
5	14.629	292	Androstane-3,17-diol[3β-5α	Diterpene
6	14.717	334	1,2-Benzene dicarboxylic acid, butyl-7-ol	Phenolic acid
7	15.090	256	Hexadecanoic acid	Lipid
8	15.331	270	1-octadecanol	Alcohol
9	16.186	296	Phytol	Diterpene alcohol
10	16.373	108	1,4 cyclo-octadiene	Cyclo alkene
11	16.855	224	Cyclohexane 1,2-dimethyl-3-pentyl-4-propyl	Substituted cycloalkane
12	16.844	336	cyclotracosane	Cyclo alkane
13	18.303	278	Dibutyl phthalate	Aromatic alkane

Table 14 GC-MS of F2B extract

Peak No	Retention time	MW	Identification	Type of compound
2	11.416	322	Cyclopropane Nonanoic acid, [2-butyl-]	Lipid
4a	14.039	170	10-undecen-1ol	Alcohol
7a	15.134	168	Geranic acid	monoterpene
9	16.133	296	Phytol	Diterpene
10	16.373	108	1,4 cyclo-octadiene	Cyclo alkene
11a	16.890	541	-	Tritepene
12	17.614	544	-	Triterpene
12b	18.305	530	-	tritepene
13a	18.996	498	-	triterpene

Table 15 GC-MS of F2C extract

Peak No	Retention time	MW	Identification	Type of compound
2	11.416	322	Cyclopropane Nonanoic acid, [2-butyl-]	Lipid
4a	14.039	170	10-undecen-1ol	Alcohol
7a	15.134	168	Geranic acid	Monoterpene
9a	15.442	196	2,6-octadien-1-ol-3,7,dimethyl acetate	Alkene ester
12a	16.177	533	-	Triterpene
13a	18.151	543	-	Triterpene

Identified compounds belong to the class of lipid, cycloalkane, alkene, diterpene, and saturated alcohol. F2B was the middle polar fraction mainly comprising of triterpenes/sterols. TLC of this fraction gave a bluish violet color with anisaldehyde sulphuric acid spray on heating which again confirmed the presence of terpenoids. GC-MS profile of F2B mainly identified the following compounds; GCMS profile of fraction F2B mainly identified as Cyclopropane Nonanoic acid, [2-butyl-],10-undecen-1ol, Geranic acid, Phytol, 1,4 cyclo-octadiene and higher molecular weight terpenoids. Identified compounds mainly belong to the class of monoterpenes and triterpenes (Table 14). The crude ^{1}HNMR of F2B also revealed the olefinic protons and saturated aliphatic methines, N-methyl and aliphatic singlet methyls, hence the compound belongs to the triterpenoid class (Appendix F). F2C was obtained as a polar fraction from the silica gel column. The LC-MS profiles of F2C, F2, and F4 were similar, and the compounds identified in F4 were seen in the fraction F2C as well. GCMS profile of fraction F2C identified very few compounds in small amounts and were mainly identified as Cyclopropane Nonanoic acid, [2-butyl-]10-undecen-1ol, Geranic acid, 2,6-octadien-1-ol-3,7,dimethyl acetate and higher molecular weight terpenoids. Identified compounds mainly belong to the class of monoterpene and triterpene Table 15.

Chemical Analysis of F2C Subfractions (F2C1, F2C2, F2C3, and F2C4)

The LC-MS chromatograms of F2C, F2C1, F2C2, F2C3 and F2C4 are illustrated in Figure 29 and the potential compounds and additional data are shown in Table 16, respectively.

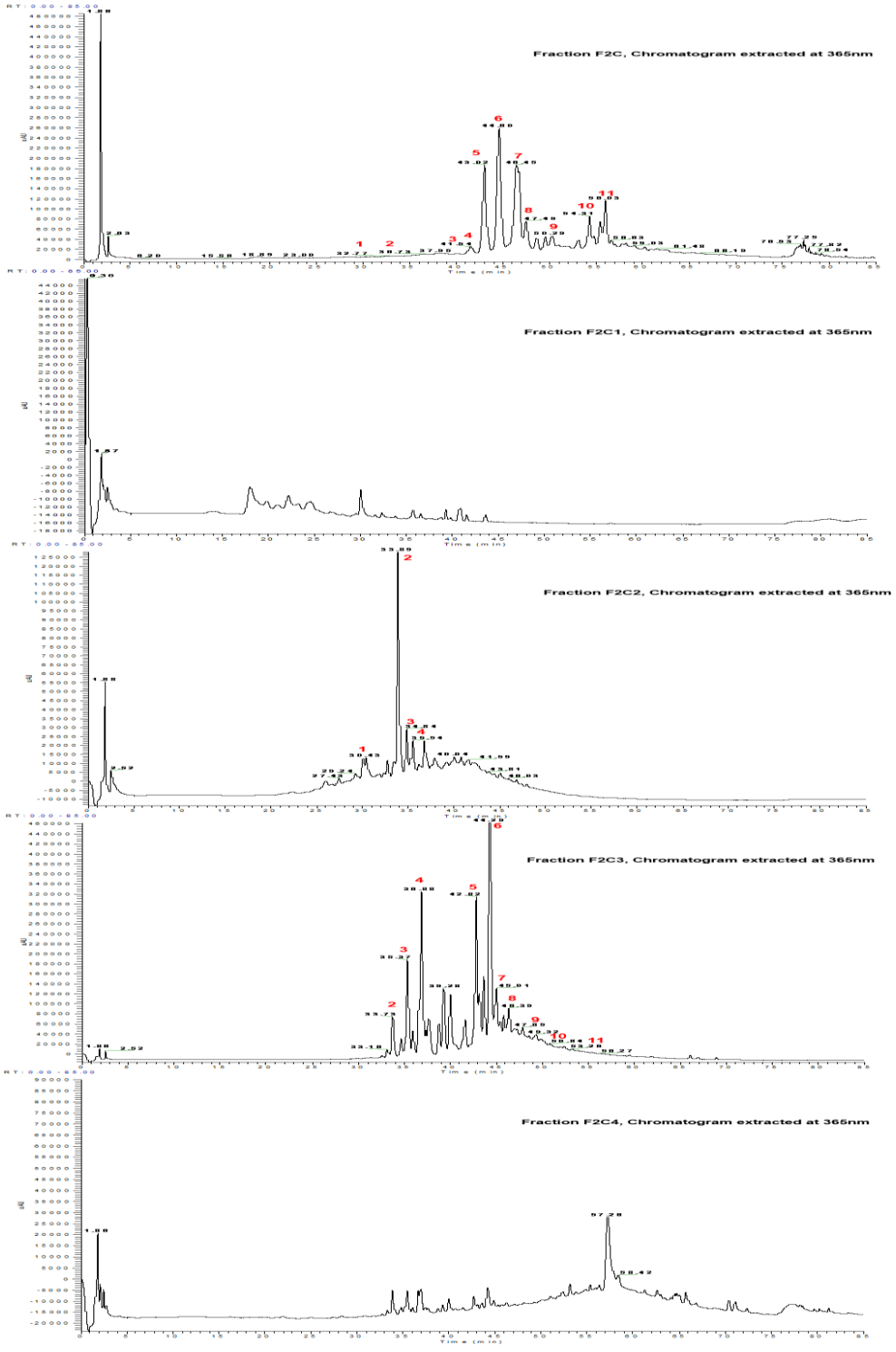

Figure 29 LCMS chromatogram of sub-fractions obtained from fraction F2C

Table 16 Identified components from F2C fractions (F2C2, F2C2, F2C3, and F2C4)

Peak no	~R.T range	UV	MS [M-H]-	MS^2	Identification
1	30.0	253, 328, 352	755	755, 609, 301	Quercetin 3-O-rhamnosyl-(1→2)-[rhamnosyl-(1→6)]-glucoside
2	33.7	242, 271, 382	593	447, 441, 301	Quercetin 3-O-dirhamnoside
3	35.4	242, 265, 299, 353	609	301	Rutin
4	36.8	242, 266, 307, 348	463	301, 151	Quercetin 3-*O*-glucoside
5	42.8-43.0	242, 266, 345	711	579, 463, 396, 329, 287	Identified by NMR [Kaempferol derivative]
6	44.3-44.6	242, 266, 347	579	447, 287	kaempferol 3-[β-D-xylofuranosyl-(1→6)-β-D-galactopyranoside]
7	45.0-46.4	242, 266, 345	579	447, 287	kaempferol 3-[β-D-xylofuranosyl-(1→6)-β-D-galactopyranoside] (isomer)
8	46.4-47.5	253, 328, 354	725	725, 579, 287	Kaempferol 3-*O*-robinobioside-7-*O*-arabinofuranoside
9	49.3-50.3	230, 242, 270, 312	451	451, 386, 329, 303, 287, 256, 245, 228	Kaempferol 3-*O*-glucoside
10	50.8-54.3	253, 328, 354	739	739, 579, 287	Kaempferol 3-*O*-(rhamnosyl-glucoside)-7-*O*-rhamnoside
11	56.0-56.3	230, 242, 270, 315	769	769, 317, 609	Isorhamnetin 3-*O*-rhamnoside-7-*O*-(rhamnosyl-hexoside)

The identification of flavonoids was achieved by comparison of MS^2 fragmentation pattern, UV spectra (nm), and retention time (RT) with data reported in the literature. The MS^2 data mining process began with the identification of aglycone fragment in order to determine the flavonoid backbone of each compound, thus quercetin ([M-H] *m/z* 301 uma), isorhamnetin ([M-H] *m/z* 315 uma), and kaempferol ([M-H] *m/z* 285 uma) were found. The next step was to determine the number and type of sugar units attached to each flavonoid skeleton. The MS^2 analysis of the precursor ions from **1**, **2**, **3** and **9** yielded major MS^2 fragment at *m/z* 301, thus, these compounds were tentatively identified as quercetin *O*-glycosides. The fragmentation pattern of compound **1**, at *m/z* 755 $[(M-H)]^-$, yielded ions at *m/z* 596 $[(M-H)-162]^-$, *m/z* 609 $[(M-H)-146]^-$, and *m/z* 301 $[(M-H)-162-146-146]^-$. The tri-glycoside **1** identified as quercetin 3-*O*-rhamnosyl-rutinoside and the fragmentation pattern reported (*142*) is similar to data obtained in this study. Compound **2**, precursor ion at *m/z* 593 $[(M-H)]^-$, generated fragments at *m/z* 447 $[(M-H)-146]^-$ and *m/z* 301 $[(M-H)-146-162]^-$, and compound **3**, precursor ion at *m/z* 609$[(M-H)+7]^-$, showed fragments at *m/z* 467 $[(M-H)-146]^-$ and *m/z* 301 $[(M-H)-146-162]^-$. Both compounds were classified as di-glycosides. Compound **3** was identified as quercetin 3-*O*-rutinoside (rutin), a well-known flavonoid, previously described in *Opuntia species* (*143, 144*). Compound **4** gave $[M-H]^-$ *m/z* at 463 and the MS^2 analysis of precursor ion at *m/z* 463, yielded the fragments at *m/z* 301 $[(M-H)-162]^-$. Compound **4** was identified as quercetin 3-*O*-glucoside, according to the fragmentation pattern in the literature (*145*).

The MS^2 fragmentation pattern of compounds 5-11 showed fragments at *m/z* 285, allowing tentatively to identify these compounds as kaempferol *O*-glycosides. Compound **5** gave $[M-H]^-$ *m/z* 711; yielded fragments at *m/z* 579 $[M-H-132]^-$ and *m/z* 285 $[M-H-132-146-132]^-$ and its structure was identified with NMR as mentioned previously. Compounds **6** and **7**, both with same precursor ion at *m/z* 579 $[(M-H)]^-$ but different RT, yielded similar fragment *m/z* 285 $[(M-H)-146-162]^-$, thus these compounds are isomers comparing these data with MS^2 fragments and UV spectra reported in the literature (*146*). Compound **8** and **10** gave $[M-H]^-$ *m/z* 725 and MS^2 fragments for 725 yielded fragments at 579 $[M-H]-146]^-$ and at *m/z* 447 [M-H]-146-132] and at *m/z* [M-H]-146-132-162]. According to these fragments, three different sugar units, such as hexose (162 uma), a deoxyhexose (146 uma) and a pentose (132 uma) are attached to a kaempferol molecule. The compound **10** with precursor ion at *m/z* 739 $[(M-H)\ ]^-$ yielded fragments at *m/z* 579 $[(M-H)-146-18]^-$, *m/z* 598.5$[(M-H)-146]^-$ and *m/z* 285 $[(M-H)-146-146-162]^-$. These tri-glycosides were identified as kaempferol 3-O-robinobioside-7-alpha-L-arabinofuran-oside (8) and kaempferol 3-*O*-(rhamnosyl-hexoside)-7-*O*-rhamnoside II (10). Ginestra et.al. reported similar kaempferol 3-*O*-tri-glycos-ides in *O. ficus-indica* stems (*143*). The compound **11** was identified as isorhamnetin *O*-glycoside due to the presence of a fragment ion at *m/z* 317. The compound **11**, precursor ion at *m/z* 770 $[(M-H)]^-$, yielded fragments at *m/z* 609 $[(M-H)-162]^-$and at *m/z* 317 $[(M-H)-162-132-162]^-$. This compound, a tri-glycoside according to these fragments, was identified as isorhamnetin 3-*O*-(pentosyl-glucoside)-7-*O*-glucoside. The fragmentation pattern of this compound was similar to the flavonoid present in honey (*147*).

Additionally, F2C1, F2C2, F2C3 and F2C4 were subjected to GCMS analyses, no peaks were observed in fractions F2C1, F2C2 and F2C3. TLC of HPLC fraction F2C4 showed positive in the Liebrmann-Buchhard test for terpenoids and anisaldehyde/ sulphuric acid spray reagent for general flavonoids and terpenoids. The GC-MS chromatograms of F2C4 is illustrated in Figure 30 and the potential compounds and additional data are shown in Table 17, respectively GC-MS analysis shows that F2C4 contains some terpenoids, which is shown by the *m/z* 162, 533 and 543 and 401 could not be identified from the library database. A crude ^{1}H NMR revealed the presence of aliphatic, acetyl, oxygenated and olefinic signals between δ_H 5.5-0.9 ppm. Further purification and detailed NMR analysis and characterization will reveal the components in the active fraction.

Figure 30 GCMS data of F2C4 extract

Table 17 GC-MS of F2C4 extract

Peak Nos	Retention time	MW	Identification	Type of compound
11b	18.29	162.9	NI	-
12a	18.35	533	NI	-
13a	18.53	543	NI	-
13b	19.01	401	NI	

Binding and Inhibition of COX-2 Activity by Acerola Leaf Extract and Fractions

The effect of acerola leaf extract (F4) and fractions (F1, F2, and F3) on COX-2 activity is shown in Figure 31. The acerola leaf extract and fractions 2 and 3 at two concentrations significantly reduced the COX-2 activity when compared to the control. Among all treatments, F4 and F2 had the highest inhibitory effect on COX2 activity, and thus were selected to confirm the binding to COX-2 by DARTS methodology. DARTS results followed by western blot analysis showed that F2 and F4 protected COX-2 from proteolysis, indicating binding of the phytochemicals present in F4 and F2 fractions to COX-2 (Figure 32).

Binding and Inhibition of COX-2 Activity by Acerola F2 Subfractions

The phytochemicals present in F2 bound to COX-2 and showed the highest inhibitory effect of COX2 activity among all the fractions. In order to identify the group of phytochemicals responsible for inhibiting COX2 activity, F2 was further fractionated into F2A, F2B, and F2C. The effect of F2 subfractions (F2A, F2B, and F2C) on COX-2 activity is shown in Figure 33.

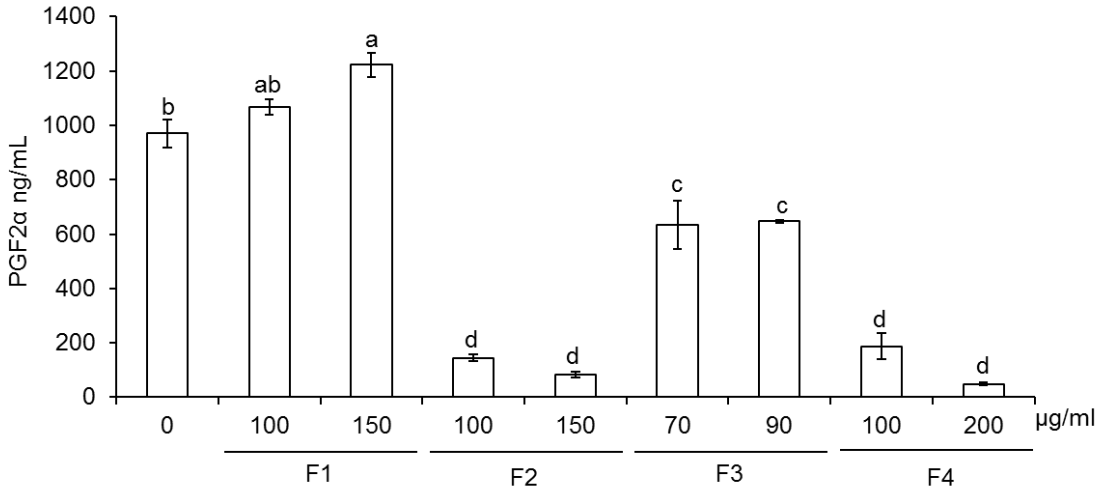

Figure 31 Effect of acerola leaves extract and fractions on COX-2 enzyme activity. According to the instruction of the COX Inhibitor Screening Assay Kit (Cayman Chemical, Ann Arbor, MI), COX-2 enzyme was incubated with acerola leaves extract (F4) or fractions (F1, F2 or F3) and then its activity was examined by measuring the level of PGE2α. Data, obtained from at least three biological repeats are shown as mean ± SE values. Different letters indicate significant differences by the ANOVA/Tukey-HSD ($p < 0.05$).

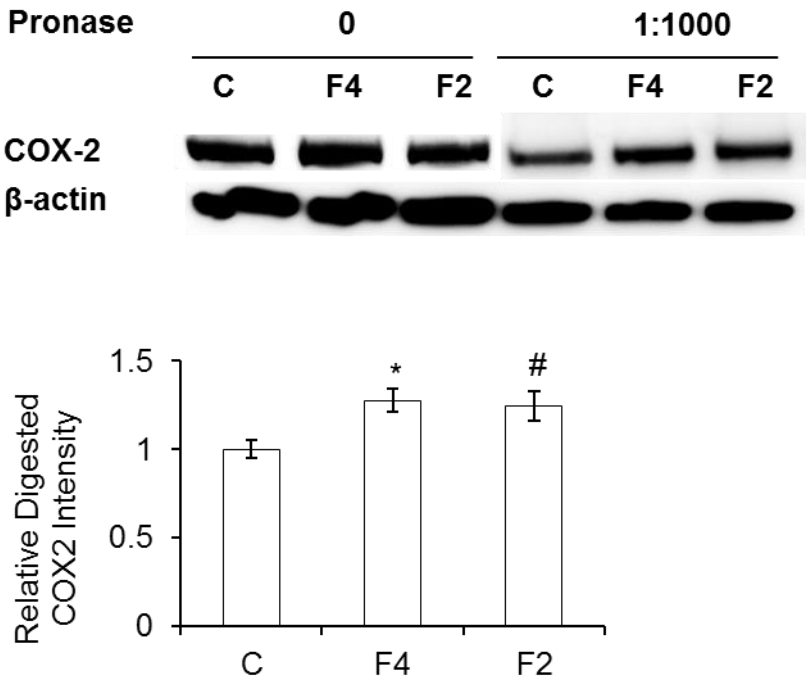

Figure 32 Evaluation of the binding of phytochemicals from acerola leaf extract (F4) or fraction (F2) to COX-2 by DARTS methodology. RAW 264.7 cell lysates were incubated with 400 µg/ml of acerola leaf extract (F4) or fraction (F2) for 3 h at room temperature, and then proteolized with pronase for 25 min at room temperature, followed by Western blot analysis. Data, obtained from three biological repeats at least, are shown as mean ± SE values. Symbols indicate significant differences by Student's t test (#$p < 0.1$,*$p < 0.05$).

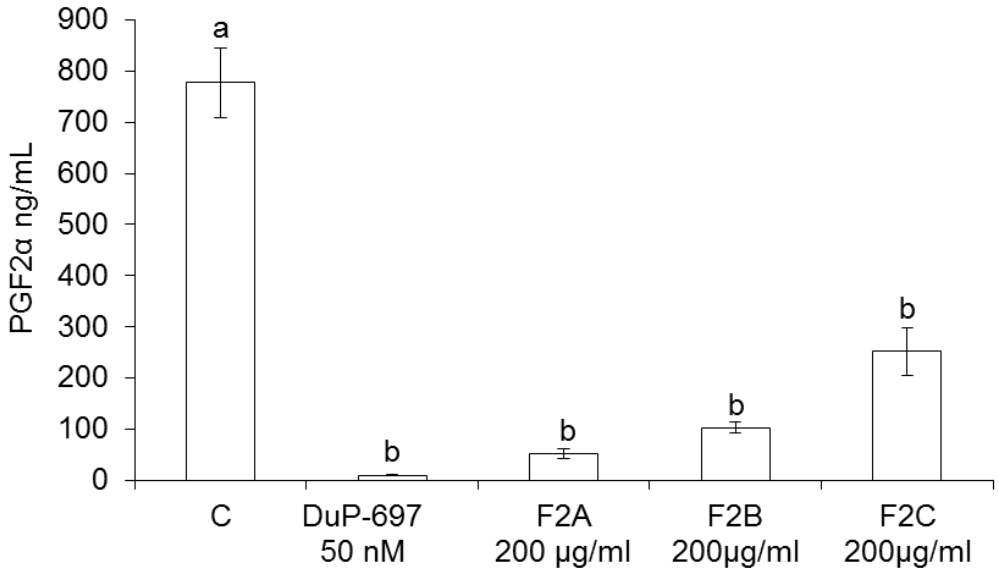

Figure 33 Effect of acerola F2 fractions on COX-2 enzyme activity. According to the instruction of the COX Inhibitor Screening Assay Kit (Cayman Chemical, Ann Arbor, MI), COX-2 enzyme was incubated with 200 µg/ml of F2 fractions (F2A, F2B or F2C) or 50 nM DuP-697, and then its activity was examined by measuring the level of PGE2α. Data, obtained from at least three biological repeats are shown as mean ± SE values. Different letters indicate significant differences by the ANOVA/Tukey-HSD ($p < 0.05$).

Results showed that all fractions at 200 µg/ml significantly inhibit COX2 activity. To assess the binding of these subfractions to COX-2, DARTS methodology was performed. Results showed that after 25 min of pronase digestion, only F2C protected COX-2 protein band when compared to the control, while F2A and F2B did not show a protection (Figure 34A). However, when the time was reduced to 10 min, both F2A and F2C protected COX-2 protein band when compared to the control (Figure 34B).

Inhibition of COX-2 Activity by Acerola F2C Subfractions and by Individual Phenolics of Acerola Leaf

The phytochemicals present in F2C bound to COX-2 and showed an inhibitory effect of COX2 activity. In order to identify the group of phytochemicals responsible for inhibiting COX2 activity, F2C was further fractionated into F2C1, F2C2, F2C3, and F2C4. The effect of F2C subfractions (F2C1, F2C2, F2C3, and F2C4) on COX-2 activity is shown in Figure 35. Interestingly, only F2C4 showed COX-2 inhibitory activity, indicating the presence of the phytochemicals with COX-2 inhibitory properties in this subfraction. Three major phenolics from acerola leaf fraction F2C were isolated as P1 (compound **5**), P2 (compound **6**) and P3 (compound **7**) and its COX-2 inhibitory properties were evaluated. Figure 36 shows that none of the isolated phenolics inhibited COX-2.

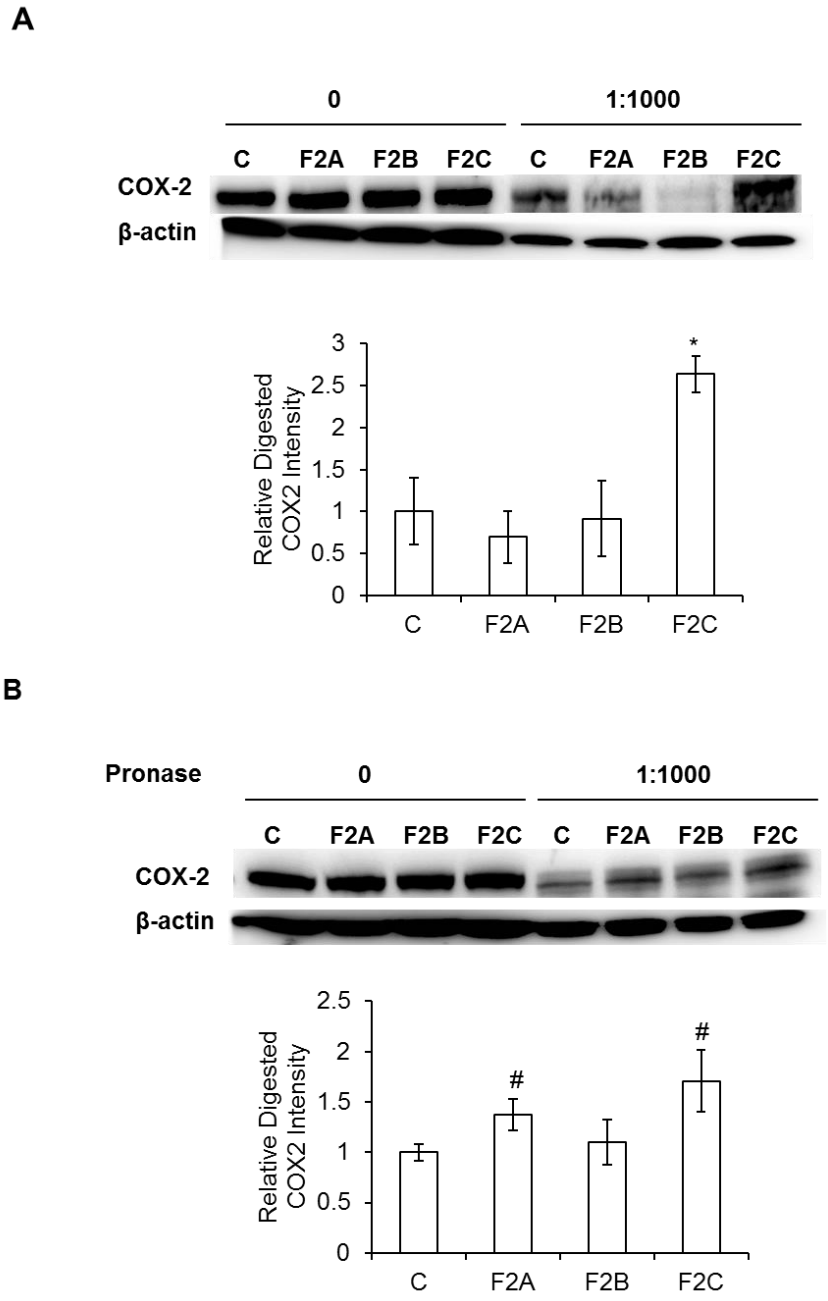

Figure 34 Evaluation of the binding of phytochemicals from acerola F2 fractions (F2A, F2B or F2C) to COX-2 by DARTS methodology. RAW 264.7 cell lysates were incubated with 400 µg/ml of acerola F2 fractions (F2A, F2B or F2C) for 3 h at room temperature, and then proteolized with pronase for 25 min (A) or 10 min (B) at room temperature, followed by Western blot analysis. Data, obtained from three biological repeats at least are shown as mean ± SE values. Symbols indicate significant differences by Student's t test (#$p < 0.1$,*$p < 0.05$).

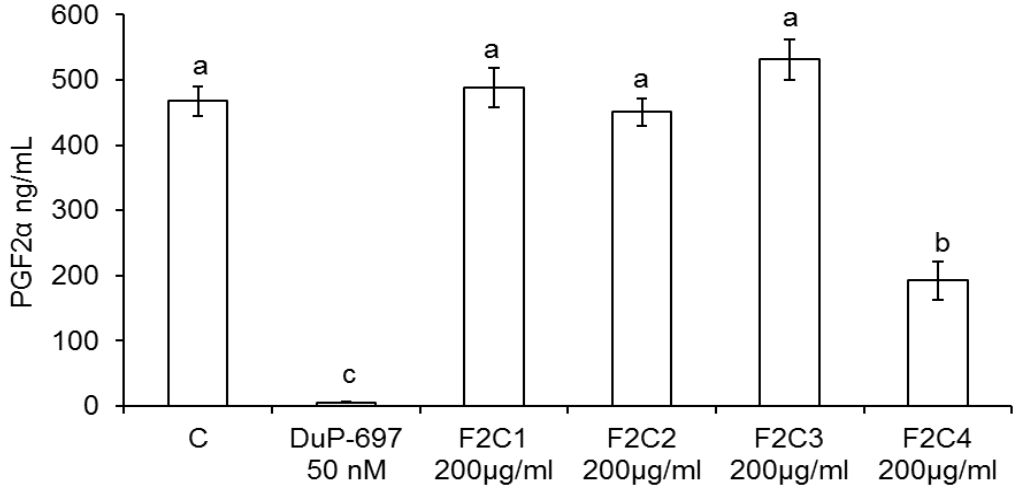

Figure 35 Effect of acerola F2C fractions on COX-2 enzyme activity. According to the instruction of the COX Inhibitor Screening Assay Kit (Cayman Chemical, Ann Arbor, MI), COX-2 enzyme was incubated with 200 µg/ml of F2C fractions (F2C1, F2C2, F2C3 or F2C4) or 50 nM DuP-697, and then its activity was examined by measuring the level of PGE2α. Data, obtained from at least three biological repeats are shown as mean ± SE values. Different letters indicate significant differences by the ANOVA/Tukey-HSD ($p < 0.05$).

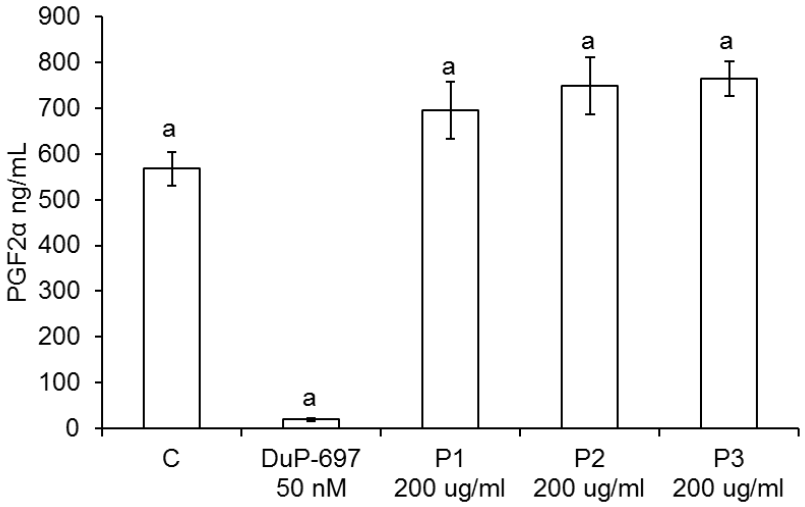

Figure 36 Effect of acerola penolics COX-2 enzyme activity. P1(Compound **5**), P2 (Compound **6**) and P3 (compound **7**). According to the instruction of the COX Inhibitor Screening Assay Kit (Cayman Chemical, Ann Arbor, MI), COX-2 enzyme was incubated with 200 µg/ml of F2C fractions (F2C1, F2C2, F2C3 or F2C4) or 50 nM DuP-697, and then its activity was examined by measuring the level of PGE2α. Data, obtained from at least three biological repeats are shown as mean ± SE values. Different letters indicate significant differences by the ANOVA/Tukey-HSD ($p < 0.05$).

Discussion

Cyclooxygenase (COX) is an enzyme that is responsible for the formation of prostanoids, including prostaglandins, prostacyclin, and thromboxane (*148, 149*).It includes two isoforms, COX-1 and COX-2, whose expressions are regulated differently; COX-1 is expressed constitutively and is responsible for the supply of prostaglandins which maintain the integrity of the gastric mucosa and provide adequate vascular homeostasis whereas COX-2 expression is induced by an inflammatory stimulus, hormones, and growth factors (*150-152*). The COX-2 isoform is mainly responsible for

the production of prostanoids in inflammation and in proliferative diseases, such as cancer (*152*). Thus, COX-2 has become an important target in inflammation and related diseases (*153*).

In previous work from our group, we showed that acerola leaf extracts and fractions reduce prostaglandin E2 (PGE2) levels in LPS-stimulated RAW 264.7 (Not Published) macrophages. COX catalyzes the synthesis of prostaglandin H2 (PGH2) from arachidonic acid, and Prostaglandin E Synthase uses PGH2 to produce PGE2 (*154*). Since COX2 is involved in the production of PGE2, we decided to evaluate this enzyme as a target of the phytochemicals present in acerola leaves. In this study, we used bioassay-guided fractionation and DARTS to identify the bioactive compounds acting as COX-2 inhibitors from acerola leaf. In this strategy, the COX-2 inhibitory activity of extracts or fractions was evaluated by an enzymatic assay and the binding of this phytochemicals to COX-2 was identified using DARTS. The results of this study showed that acerola leaf extract and fractions 2 and 3, contain phytochemicals that inhibit COX2 activity. LC-MS and NMR analysis revealed that F3 contains a main compound with glycerol/glycolipid/sphingolipid type structure. Several studies have shown that compounds with similar structures inhibit COX-2 (*155, 156*), and thus this compound could be responsible for the COX-2 inhibitory properties of F3. On the other hand, the previous report showed that F2 contains quercetin and kaempferol *O*-glycosides, terpenes and alkenes (Bang et al., Unpublished). Since F2 showed the highest COX-2 inhibitory effect among the fractions, and also showed binding to COX-2 by DARTS, its fractions (F2A, F2B, and F2C) were further tested for their ability to bind

and inhibit COX-2 activity. Our results showed that all subfractions inhibit COX-2 activity but only F2C protected COX-2 protein band after 25 min of pronase digestion in DARTS methodology (Figure 34 A). The binding of a small molecule to an enzyme can be reversible or irreversible (*157*), which may affect the target protein protection in DARTS methodology. If the rate of binding and unbinding of the small molecule remains constant or somewhat constant, the small molecules that bind reversibly, may protect the target protein only in short protease digestion times, while irreversible molecules may protect it in short and long digestion times. The fact that all F2 fractions inhibited COX-2 activity, but only F2C showed binding by DARTS, lead us to hypothesize that the phytochemicals in F2A and F2B might bind reversibly to COX-2. To proof this concept, we reduce the proteolysis time to 10 min in DARTS methodology. Results showed that F2A and F2C protected COX-2 protein band at 10 min (Figure 34 B), indicating that the phytochemicals in F2A may bind reversibly to COX2 while the phytochemicals in F2C may bind irreversibly. However the type of binding of these phytochemicals to COX2 should be validated with further studies. The fraction F2B did not protect COX-2 protein band at 25 or 10 min. It is possible that due to the reversible binding of its phytochemicals, a band protection could only be observed in less than 10 min of protease digestion or that the binding to COX2 by this phytochemicals did not protect the enzyme from protease digestion.

GC-MS profiling revealed that F2A contains alkenes and terpenes, while F2B contains mainly terpenes. Both alkenes and terpenes have been shown to inhibit COX2 activity (*158*, *159*) and could account for the COX-2 inhibitory properties of these

sufractions. The LCMS profile of F2C was similar to the previously reported profiles of F2 and F4, and indicated the presence of flavonoids. In addition, the GC-MS profiling revealed F2C contain small amounts of terpenoids. In order to further identify the bioactive phytochemicals, F2C was fractionated into F2C1, F2C2, F2C3 and F2C4. Interestingly, only fraction F2C4 containing aliphatic triterpene like compounds inhibited COX-2 activity. These results indicate that terpenes are responsible for the COX-2 inhibitory properties of F2C. In agreement with these results, the three major phenolics isolated from acerola leaf F2C did not show COX-2 inhibitory properties.

In this study we showed that acerola leaves have potential COX-2 inhibitors, which were identified by bioassay-guided fractionation and DARTS methodology. The phytochemicals responsible for the inhibition of COX-2 seem to belong to the terpene, alkene and glycolipid/sphingolipid groups of compounds. Additionally, two new compounds, a kampeferol glycoside and a glycolipid like compound from acerola leaf, were identified in this study. Moreover, we showed that DARTS methodology can be used as a screening technique if different digestion times are considered. In addition, DARTS may provide information on the type of binding of small molecules to their protein target, however this would need to be verified by other methodologies.

CHAPTER IV

CONCLUSIONS

In conclusion, we demonstrated that the extracts from mashua have anti-inflammatory properties *in vitro*. Through the DARTS methodology, PKM was identified as a potential target of mashua 203040 and 203081 extracts. In addition, mashua extracts exerted their anti-inflammatory properties and attenuated the Warburg-like effect by suppressing ROS levels and consequently interfering with different ROS-responsive signaling proteins including NF-κB and HIF. The compounds in mashua responsible for the anti-inflammatory properties are both phenolics and isothiocyanates.

Additionally, we showed that LPS-challenged RAW264.7 macrophages exhibit a Warburg-like effect. RAW264.7 cell line are frequently used as a model in inflammation studies and the Warburg effect has been shown to be crucial for macrophage activation. Thus, this study defines some of the changes that RAW264.7 cell line exhibits in relation to the to the Warburg effect, upon the challenge with LPS.

Furthermore, we showed that acerola leaves have potential COX-2 inhibitors, which were identified by bioassay-guided fractionation and DARTS methodology. The phytochemicals responsible for the inhibition of COX-2 seem to belong to the terpene, alkene and glycolipid/sphingolipid groups of compounds. Moreover, two new compounds, a kampeferol glycoside and a glycolipid like compound from acerola leaf, were identified in this study.

Finally, we showed that DARTS methodology can be used to identify putative protein targets of phytochemicals present in plant extracts. In addition, DARTS could be used as a screening technique if different digestion times are considered. Also, DARTS may provide information on the type of binding of small molecules to their protein target, however this would need to be verified by other methodologies.

Further studies should be done to identify the specific compound or combination of compounds responsible for the anti- inflammatory properties of mashua and acerola leaf. In addition, the anti-inflammatory properties of mashua tuber and acerola leaf should be evaluated in other cells such as adipocytes or endothelial cells due to the important role of these cells in the development of differed metabolic diseases. Moreover, the beneficial properties of both plants should be evaluated *in vivo* and a recommended consumption dose, to obtain those benefits, should be established.

Finally different strategies to make DARTS methodology more sensitive should be explored. Also, the proposed concept of the reversible and irreversible binding of small molecules in DARTS should be validated by using known drugs.

REFERENCES

1. Medzhitov, R. Origin and physiological roles of inflammation. *Nature* **2008,** *454*, 428-435.

2. Chalkiadaki, A.; Guarente, L. High-fat diet triggers inflammation-induced cleavage of SIRT1 in adipose tissue to promote metabolic dysfunction. *Cell Metabolism* **2012,** *16*, 180-188.

3. Hanada, T.; Yoshimura, A. Regulation of cytokine signaling and inflammation. *Cytokine and Growth Factor Reviews* **2002,** *13*, 413-421.

4. Fang, F. C. Antimicrobial reactive oxygen and nitrogen species: concepts and controversies. *Nature Reviews. Microbiology* **2004,** *2*, 820-832.

5. Moser, B.; Willimann, K. Chemokines: role in inflammation and immune surveillance. *Annals of the Rheumatic Diseases* **2004,** *63*, 84-89.

6. Kelly, B.; O'Neill, L. A. J. Metabolic reprogramming in macrophages and dendritic cells in innate immunity. *Cell Research* **2015,** *25*, 771-784.

7. Kopf, M.; Bachmann, M. F.; Marsland, B. J. Averting inflammation by targeting the cytokine environment. *Nature Reviews. Drug Discovery* **2010,** *9*, 703-718.

8. Hotamisligil, G. Inflammation and metabolic disorders. *Nature* **2006,** *444*, 860-867.

9. Rocha, V. Obesity, inflammation, and atherosclerosis. *Nature Reviews. Cardiology* **2009,** *6*, 399-409.

10. Glass, C. Mechanisms underlying inflammation in neurodegeneration. *Cell* **2010,** *140*, 918-934.

11. Coussens, L. Inflammation and cancer. *Nature* **2002,** *420*, 860-867.

12. Calay, E. S.; Hotamisligil, G. S. Turning off the inflammatory, but not the metabolic, flames. *Nature Medicine* **2013,** *19*, 265-267.

13. Terzić, J.; Grivennikov, S.; Karin, E.; Karin, M. Inflammation and colon cancer. *Gastroenterology* **2010,** *138*, 2101-2114.

14. Raposo, T. P.; Beirão, B. C. B.; Pang, L. Y.; Queiroga, F. L.; Argyle, D. J. Inflammation and cancer: Till death tears them apart. *The Veterinary Journal* **2015,** *205*, 161-174.

15. Wynn, T. Macrophage biology in development, homeostasis and disease. *Nature* **2013,** *496*, 445-455.

16. Biswas, S. K.; Mantovani, A. Macrophage plasticity and interaction with lymphocyte subsets: cancer as a paradigm. *Nature Immunology* **2010,** *11*, 889-896.

17. Biswas, Subhra K.; Mantovani, A. Orchestration of metabolism by macrophages. *Cell metabolism* **2012,** *15*, 432-437.

18. Mantovani, A.; Sica, A.; Sozzani, S.; Allavena, P.; Vecchi, A.; Locati, M. The chemokine system in diverse forms of macrophage activation and polarization. *Trends in Immunology* **2004,** *25*, 677-686.

19. Palsson Mcdermott, E. The Warburg effect then and now: From cancer to inflammatory diseases. *BioEssays* **2013,** *35*, 965-973.

20. Heiden, M. G. V.; Cantley, L. C.; Thompson, C. B. Understanding the Warburg effect: The metabolic requirements of cell proliferation. *Science* **2009**, *324*, 1029-1033.

21. Chawla, A.; Nguyen, K. D.; Goh, Y. P. S. Macrophage-mediated inflammation in metabolic disease. *Nature Reviews. Immunology* **2011,** *11*, 738-749.

22. Nikolaou, K.; Sarris, M.; Talianidis, I. Molecular pathways: The complex roles of inflammation pathways in the development and treatment of liver cancer. *Clinical Cancer Research* **2013,** *19*, 2810-2816.

23. Yu, H.; Pardoll, D.; Jove, R. STATs in cancer inflammation and immunity: a leading role for STAT3. *Nature Reviews. Cancer* **2009,** *9*, 798-809.

24. Baker, R. G.; Hayden, M. S.; Ghosh, S. NF-kB, inflammation, and metabolic disease. *Cell Metabolism* **2011,** *13*, 11-22.

25. Pasparakis, M. Regulation of tissue homeostasis by NF-kappaB signalling: implications for inflammatory diseases. *Nature Reviews. Immunology* **2009,** *9*, 778-788.

26. Chan, E. D.; Riches, D. W. H. IFN-γ + LPS induction of iNOS is modulated by ERK, JNK/SAPK, and p38mapk in a mouse macrophage cell line. *American Journal of Physiology* **2001,** *280*, C441-C450.

27. Jacobs, A. T.; Ignarro, L. J. Lipopolysaccharide-induced expression of interferon-β mediates the timing of inducible nitric-oxide synthase induction in RAW 264.7 macrophages. *Journal of Biological Chemistry* **2001,** *276*, 47950-47957.

28. Mittal, M.; Siddiqui, M. R.; Tran, K.; Reddy, S. P.; Malik, A. B. Reactive oxygen species in inflammation and tissue injury. *Antioxidants & Redox Signaling* **2014,** *20*, 1126-1167.

29. Oktyabrsky, O. N.; Smirnova, G. V. Redox regulation of cellular functions. *Biochemistry* **2007,** *72*, 132-145.

30. Naik, E.; Dixit, V. M. Mitochondrial reactive oxygen species drive proinflammatory cytokine production. *The Journal of Experimental Medicine* **2011,** *208*, 417-420.

31. Song, J. D.; Lee, S. K.; Kim, K. M.; Kim, J. W.; Kim, J. M.; Yoo, Y. H.; Park, Y. C. Redox factor-1 mediates NF-κB nuclear translocation for LPS-induced iNOS expression in murine macrophage cell line RAW 264.7. *Immunology* **2008,** *124*, 58-67.

32. Kabe, Y.; Ando, K.; Hirao, S.; Yoshida, M.; Handa, H. Redox regulation of NF-κB activation: Distinct redox regulation between the cytoplasm and the nucleus. *Antioxidants and Redox Signaling* **2005,** *7*, 395-403.

33. Jung, S.N.; Yang, W. K.; Kim, J.; Kim, H. S.; Kim, E. J.; Yun, H.; Park, H.; Kim, S. S.; Choe, W.; Kang, I.; Ha, J. Reactive oxygen species stabilize hypoxia-inducible factor-1 alpha protein and stimulate transcriptional activity via AMP-activated protein kinase in DU145 human prostate cancer cells. *Carcinogenesis* **2008,** *29*, 713-721.

34. van Duijnhoven, F. J.; Bueno de Mesquita, H. B.; Ferrari, P.; Jenab, M.; Boshuizen, H. C.; Ros, M. M.; Casagrande, C.; Tjønneland, A.; Olsen, A.; Overvad, K.; Thorlacius-Ussing, O.; Clavel-Chapelon, F.; Boutron-Ruault, M. C.; Morois, S.; Kaaks, R.; Linseisen, J.; Boeing, H.; Nöthlings, U.; Trichopoulou, A.; Trichopoulos, D. Fruit, vegetables, and colorectal cancer risk: The european prospective investigation into cancer and nutrition. *American Journal of Clinical Nutrition* **2009,** *89*, 1441-1452.

35. Aune, D.; Chan, D. S. M.; Lau, R.; Vieira, R.; Greenwood, D. C.; Kampman, E.; Norat, T. Dietary fibre, whole grains, and risk of colorectal cancer: systematic review and dose-response meta-analysis of prospective studies. *British Medical Journal* **2011,** *343*, 1062-1082.

36. Gan, Y.; Tong, X.; Li, L.; Cao, S.; Yin, X.; Gao, C.; Herath, C.; Li, W.; Jin, Z.; Chen, Y.; Lu, Z. Consumption of fruit and vegetable and risk of coronary heart disease: a meta-analysis of prospective cohort studies. *International Journal of Cardiology* **2015,** *183*, 129-137.

37. Hu, D.; Huang, J.; Wang, Y.; Zhang, D.; Qu, Y. Fruits and vegetables consumption and risk of stroke: a meta-analysis of prospective cohort studies. *Stroke* **2014,** *45*, 1613-1619.

38. Xun, P.; Qin, B.; Song, Y.; Nakamura, Y.; Kurth, T.; Yaemsiri, S.; Djousse, L.; He, K. Fish consumption and risk of stroke and its subtypes: accumulative evidence from a meta-analysis of prospective cohort studies. *European Journal of Clinical Nutrition* **2012,** *66*, 1199-1207.

39. He, K.; Song, Y.; Daviglus, M. L.; Liu, K.; Van Horn, L.; Dyer, A. R.; Greenland, P. Accumulated evidence on fish consumption and coronary heart disease mortality: a meta-analysis of cohort studies. *Circulation* **2004,** *109*, 2705-2711.

40. Harvey, A. Strategies for discovering drugs from previously unexplored natural products. *Drug Discovery Today* **2000,** *5*, 294-300.

41. Grau Alfredo, R. O. D.; Nieto Cabrera, C.; Hermann, M. In Mashua Tropaeolum tuberosum Ruíz & Pav; International Potato Center, Lima, Peru/International Plant Genetic Resources Institute: Rome, Italy, 2003.

42. Scalbert, A.; Andres-Lacueva, C.; Arita, M.; Kroon, P.; Manach, C.; Urpi-Sarda, M.; Wishart, D. Databases on food phytochemicals and their health-promoting effects. *Journal of Agricultural and Food Chemistry* **2011**, *59*, 4331-4348.

43. Crozier, A.; Clifford, M. N.; Ashihara, H. In Plant secondary metabolites : occurrence, structure and role in the human diet. edited by Alan Crozier, Michael N. Clifford, Hiroshi Ashihara. Oxford ; Ames, Iowa : Blackwell Pub., 2006.

44. Liu, R. H. Potential synergy of phytochemicals in cancer prevention: mechanism of action. *Journal of Nutrition* **2004**, *134*, 3479-3485.

45. Bellik, Y.; Boukraâ, L.; Alzahrani, H. A.; Bakhotmah, B. A.; Abdellah, F.; Hammoudi, S. M.; Iguer-Ouada, M. Molecular mechanism underlying anti-inflammatory and anti-allergic activities of phytochemicals: an update. *Molecules* **2013,** *18*, 322-353.

46. Scharf, G.; Prustomersky, S.; Knasmuller, S.; Schulte-Hermann, R.; Huber, W. W. Enhancement of glutathione and g-glutamylcysteine synthetase, the rate limiting enzyme of glutathione synthesis, by chemoprotective plant-derived food and beverage components in the human hepatoma cell line HepG2. *Nutrition and Cancer* **2003,** *45*, 74-83.

47. Gülçin, İ. Antioxidant properties of resveratrol: A structure-activity insight. *Innovative Food Science & Emerging Technologies* **2010,** *11*, 210-218.

48. Du, Y.; Guo, H.; Lou, H. Grape seed polyphenols protect cardiac cells from apoptosis via induction of endogenous antioxidant enzymes. *Journal of Agricultural and Food Chemistry* **2007,** *14,* 9-16.

49. Rangkadilok, N.; Sitthimonchai, S.; Worasuttayangkurn, L.; Mahidol, C.; Ruchirawat, M.; Satayavivad, J. Evaluation of free radical scavenging and antityrosinase activities of standardized longan fruit extract. *Food and Chemical Toxicology* **2007,** *45,* 328-336.

50. Leopoldini, M.; Russo, N.; Toscano, M. Molecular basis of working mechanism of natural polyphenolic antioxidants. *Food Chemistry* **2011,** *125,* 288-306.

51. Chen, Y.; Tsai, Y. H.; Tseng, S. H. The potential of tetrandrine as a protective agent for ischemic stroke. *Molecules* **2011,** *16,* 8020-8032.

52. Virgili, F.; Kobuchi, H.; Packer, L. Procyanidins extracted from pinus Maritima (Pycnogenol®): Scavengers of free radical species and modulators of nitrogen monoxide metabolism in activated murine raw 264.7 macrophages. *Free Radical Biology and Medicine* **1998,** *24,* 1120-1129.

53. Akhtar, N.; Haqqi, T. M. Epigallocatechin-3-gallate suppresses the global interleukin-1beta-induced inflammatory response in human chondrocytes. *Arthritis Research and Therapy* **2011,** *13,* 328-336.

54. Jang, D. S.; Cuendet, M.; Hawthorne, M. E.; Kardono, L. B. S.; Kawanishi, K.; Fong, H. H. S.; Mehta, R. G.; Pezzuto, J. M.; Kinghorn, A. D. Prenylated flavonoids of the leaves of macaranga conifera with inhibitory activity against cyclooxygenase-2. *Phytochemistry* **2002,** *61,* 867-872.

55. Likhitwitayawuid, K.; Sawasdee, K.; Kirtikara, K. Flavonoids and stilbenoids with COX-1 and COX-2 inhibitory activity from Dracaena loureiri. *Planta Medica* **2002,** *68*, 841-843.

56. Kim, C.-S.; Kawada, T.; Kim, B.-S.; Han, I.-S.; Choe, S.-Y.; Kurata, T.; Yu, R. Capsaicin exhibits anti-inflammatory property by inhibiting IkB-a degradation in LPS-stimulated peritoneal macrophages. *Cellular Signalling* **2003,** *15*, 299-306.

57. Hong, M. H.; Kim, M. H.; Chang, H. J.; Kim, N. H.; Shin, B. A.; Ahn, B. W.; Jung, Y. D. (-)-Epigallocatechin-3-gallate inhibits monocyte chemotactic protein-1 expression in endothelial cells via blocking NF-kappaB signaling. *Life Sciences* **2007,** *80*, 1957-1965.

58. Cheon, M. S.; Yoon, T.; Lee, D. Y.; Choi, G.; Moon, B. C.; Lee, A. Y.; Choo, B. K.; Kim, H. K. Chrysanthemum indicum Linné extract inhibits the inflammatory response by suppressing NF-κB and MAPKs activation in lipopolysaccharide-induced RAW 264.7 macrophages. *Journal of Ethnopharmacology* **2009,** *122*, 473-477.

59. Hämäläinen, M.; Nieminen, R.; Vuorela, P.; Heinonen, M.; Moilanen, E., Anti-inflammatory effects of flavonoids: genistein, kaempferol, quercetin, and daidzein inhibit STAT-1 and NF-κB activations, whereas flavone, isorhamnetin, naringenin, and pelargonidin inhibit only NF-κB activation along with their inhibitory effect on iNOS expression and NO production in activated aacrophages. *Mediators of Inflammation* **2007,** *2007*, 4567-4587.

60. Takahashi, A.; Yamamoto, N.; Murakami, A. Cardamonin suppresses nitric oxide production via blocking the IFN-γ/STAT pathway in endotoxin-challenged peritoneal macrophages of ICR mice. *Life Sciences* **2011,** *87*, 337-342.

61. Gresele, P.; Pignatelli, P.; Guglielmini, G.; Carnevale, R.; Mezzasoma, A. M.; Ghiselli, A.; Momi, S.; Violi, F. Resveratrol, at concentrations attainable with moderate wine consumption, stimulates human platelet nitric oxide production. *Journal of Nutrition* **2008,** *138*, 1602-1608.

62. Non, L.; Duong, D.; Peehl, D. M. Chemopreventive anti-inflammatory activities of curcumin and other phytochemicals mediated by MAP kinase phosphatase-5 in prostate cells. *Carcinogenesis* **2007,** *28*, 1188-1196.

63. Jung, C. H.; Kim, J. H.; Hong, M. H.; Seog, H. M.; Oh, S. H.; Lee, P. J.; Kim, G. J.; Kim, H. M.; Um, J. Y.; Ko, S. G. Phenolic-rich fraction from Rhus verniciflua Stokes (RVS) suppress inflammatory response via NF-κB and JNK pathway in lipopolysaccharide-induced RAW 264.7 macrophages. *Journal of Ethno Pharmacology* **2007,** *110*, 490-497.

64. Arango, D.; Morohashi, K.; Yilmaz, A.; Kuramochi, K.; Parihar, A.; Brahimaj, B.; Grotewold, E.; Doseff, A. I. Molecular basis for the action of a dietary flavonoid revealed by the comprehensive identification of apigenin human targets. *Proceedings of the National Academy of Sciences* **2013**, *110*, 2153-2162.

65. Efferth, T.; Koch, E. Complex interactions between phytochemicals. The multi-target therapeutic concept of phytotherapy. *Current Drug Targets* **2011,** *12*, 122-132.

66. Ziegler, S.; Pries, V.; Hedberg, C.; Waldmann, H. Target identification for small bioactive molecules: finding the needle in the haystack. *Angewandte Chemie (International Ed. In English)* **2013,** *52*, 2744-2792.

67. Tashiro, E.; Imoto, M. Target identification of bioactive compounds. *Bioorganic & Medicinal Chemistry* **2012,** *20,* 1910-1921.

68. Schenone, M.; Dančík, V.; Wagner, B. K.; Clemons, P. A. Target identification and mechanism of action in chemical biology and drug discovery. *Nature Chemical Biology* **2013,** *9*, 232-240.

69. Sleno, L.; Emili, A. Proteomic methods for drug target discovery. *Current Opinion in Chemical Biology* **2008,** *12*, 46-54.

70. Sato, S.-i.; Murata, A.; Shirakawa, T.; Uesugi, M. Review: Biochemical Target Isolation for Novices: Affinity-Based Strategies. *Chemistry & Biology* **2010,** *17*, 616-623.

71. MacKinnon, A. L.; Garrison, J. L.; Hegde, R. S.; Taunton, J. Photo-leucine incorporation reveals the target of a cyclodepsipeptide inhibitor of cotranslational translocation. *Journal of the American Chemical Society* **2007,** *129*, 14560-14561.

72. Lomenick, B. Identification of direct protein targets of small molecules. *ACS Chemical Biology* **2011,** *6*, 34-46.

73. Terstappen, G. C.; Schlüpen, C.; Raggiaschi, R.; Gaviraghi, G. Target deconvolution strategies in drug discovery. *Nature Reviews. Drug Discovery* **2007,** *6*, 891-903.

74. Lomenick, B. Target identification using drug affinity responsive target stability (DARTS). *Proceedings of the National Academy of Sciences of the United States of America* **2009,** *106,* 21984-21989.

75. Henzler-Wildman, K.; Kern, D. Dynamic personalities of proteins. *Nature* **2007,** *450*, 964-972.

76. Pace, C. N.; McGrath, T.; Substrate stabilization of lysozyme to thermal and guanidine hydrochloride denaturation. *The Journal of Biological Chemistry* **1979,** *255*, 3862-3865.

77. Makowski, L.; Rodi, D. J.; Mandava, S.; Minh, D. D. L.; Gore, D. B.; Fischetti, R. F. Molecular crowding inhibits intramolecular breathing motions in proteins. *Journal of Molecular Biology* **2008,** *375*, 529-546.

78. Lomenick, B.; Jung, G.; Wohlschlegel, J. A.; Huang, J. Target identification using drug affinity responsive target stability (DARTS). *Current Protocols in Chemical Biology* **2011,** *3*, 163–180.

79. Pai, M. Y.; Lomenick, B.; Hwang, H.; Schiestl, R.; McBride, W.; Loo, J. A.; Huang, J. Drug affinity responsive target stability (DARTS) for small-molecule target identification. *Methods in Molecular Biology* **2015,** *1263*, 287-298.

80. Derry, M. M.; Somasagara, R. R.; Raina, K.; Kumar, S.; Gomez, J.; Patel, M.; Agarwal, R.; Agarwal, C. Target identification of grape seed extract in colorectal cancer using drug affinity responsive target stability (DARTS) technique: Role of endoplasmic reticulum stress response proteins. *Current Cancer Drug Targets* **2014,** *14*, 323-336.

81. Wang, N.; Wang, Z.; Peng, C.; You, J.; Shen, J.; Han, S.; Chen, J. Dietary compound isoliquiritigenin targets GRP78 to chemosensitize breast cancer stem cells via β-catenin/ABCG2 signaling. *Carcinogenesis* **2014,** *35*, 2544-2554.

82. Eskew, J. D.; Sadikot, T.; Morales, P.; Duren, A.; Dunwiddie, I.; Swink, M.; Zhang, X.; Hembruff, S.; Donnelly, A.; Rajewski, R. A.; Blagg, B. S. J.; Manjarrez, J. R.; Matts, R. L.; Holzbeierlein, J. M.; Vielhauer, G. A. Development and characterization of a novel C-terminal inhibitor of Hsp90 in androgen dependent and independent prostate cancer cells. *BMC Cancer* **2011,** *11*, 468-468.

83. Palsson-Mcdermott, E. Pyruvate kinase M2 regulates Hif-1α activity and IL-1β induction and is a critical determinant of the Warburg effect in LPS-activated macrophages. *Cell Metabolism* **2015,** *21*, 347-347.

84. Yang, L.; Xie, M.; Yang, M.; Yu, Y.; Zhu, S.; Hou, W.; Kang, R.; Lotze, M. T.; Billiar, T. R.; Wang, H.; Cao, L.; Tang, D. PKM2 regulates the Warburg effect and promotes HMGB1 release in sepsis. *Nature Communications* **2014,** *5*, 4436-4436.

85. Ortega, O. Glucosinolate survey of cultivated and feral mashua (Tropaeolum tuberosum Ruíz & Pavón) in the cuzco region of Peru. *Economic Botany* **2006,** *60*, 254-264.

86. Ramallo, R.; Ramallo, J.-P.; Wathelet, E.; Le Boulenga, E.; Torres, M.; Marlier, J. F.; Ledent, A.; Guidi, Y. Glucosinolates in isano (Tropaeolum tuberosum) tubers: qualitative and quantitative content and changes after maturity. *Journal of the Science of Food and Agriculture* **2004,** *84*, 701-706.

87. Johns, T., Isothiocyanates and thioureas in enzyme hydrolysates of Tropaeolum tuberosum. *Phytochemistry* **1981,** *20*, 2687-2689.

88. Chirinos, R.; Chirinos, D.; Campos, N.; Costa, C.; Arbizu, R.; Pedreschi, Y. Phenolic profiles of andean mashua (Tropaeolum tuberosum Ruiz & Pavan) tubers: Identification by HPLC-DAD and evaluation of their antioxidant activity. *Food Chemistry* **2008,** *106*, 1285-1298.

89. Chirinos, R. High-performance liquid chromatography with photodiode array detection (HPLC-DAD)/HPLC-mass spectrometry (MS) profiling of anthocyanins from andean mashua tubers (tropaeolum tuberosum Ruiz and Pavon) and their contribution to the overall antioxidant activity. *Journal of Agricultural and Food Chemistry* **2006,** *54*, 7089-7097.

90. Chirinos, R.; Campos, D.; Costa, N.; Arbizu, C.; Pedreschi, R.; Larondelle, Y. Phenolic profiles of andean mashua (tropaeolum tuberosum Ruíz & Pavón) tubers: Identification by HPLC-DAD and evaluation of their antioxidant activity. *Food Chemistry* **2008,** *106*, 1285-1298.

91. Johns, T. Anti-reproductive and other medicinal effects of Tropaeolum tuberosum. *Journal of Ethnopharmacology* **1982,** *5*, 149-161.

92. Chirinos, R.; Chirinos, D.; Campos, M.; Warnier, R.; Pedreschi, J. F.; Rees, Y. Antioxidant properties of mashua (Tropaeolum tuberosum) phenolic extracts against oxidative damage using biological in vitro assays. *Food Chemistry* **2008,** *111*, 98-105.

93. Chirinos, R. Effect of genotype, maturity stage and post-harvest storage on phenolic compounds, carotenoid content and antioxidant capacity of Andean mashua

tubers (Tropaeolum tuberosum Ruiz & Pavón. *Journal of the Science of Food and Agriculture* **2007,** *87*, 437-446.

94. Swain, T., The phenolic constituents of Prunus domestica. I.-The quantitative analysis of phenolic constituents. *Journal of the Science of Food and Agriculture* **1959,** *10*, 63-68.

95. Nair, V. Protective role of ternatin anthocyanins and quercetin glycosides from butterfly pea (clitoria ternatea leguminosae) blue flower petals against lipopolysaccharide (LPS)-induced inflammation in macrophage cells. *Journal of Agricultural and Food Chemistry* **2015,** *63*, 6355-6365.

96. Vandesompele, J. Accurate normalization of real-time quantitative RT-PCR data by geometric averaging of multiple internal control genes. *Genome Biology* **2002,** *3*, 1-34.

97. Schmittgen, T. D. Analyzing real-time PCR data by the comparative C-T method. *Nature Protocols* **2008,** *3*, 1101-1108.

98. Giusti, M. M.; Rodríguez-Saona, L. E.; Griffin, D.; Wrolstad, R. E. Electrospray and tandem mass spectroscopy as tools for anthocyanin characterization. *Journal of Agricultural and Food Chemistry* **1999,** *47*, 4657-4664.

99. Alcalde-Eon, C.; Saavedra, G.; de Pascual-Teresa, S.; Rivas-Gonzalo, J. C., Liquid chromatography–mass spectrometry identification of anthocyanins of isla oca (Oxalis tuberosa, Mol.) tubers. *Journal of Chromatography A* **2004,** *1054*, 211-215.

100. El-Migirab, S.; Berger, Y.; Jadot, J. Isothiocyanates, thioureas and thiocarbamates from *Pentadiplandra brazzeana. Phytochemistry* **1977,** *16*, 1719-1721.

101. Johns, T.; Towers, G. N., Isothiocyanates and thioureas in enzyme hydrolysates of tropaeolum tuberosum. *Phytochemistry* **1981,** *20*, 2687-2689.

102. Hiroyuki, N., Ikemoto, T., Nakatsugawa, H. Cosmetics containing hydrogenated chlorogenic acids as antioxidants. Patent US20140179747 A1, 2000.

103. Buchanan, M. S.; Carroll, A. R.; Edser, A.; Parisot, J.; Addepalli, R.; Quinn, R. J. Tyrosine kinase inhibitors from the rainforest tree polyscias murrayi. *Phytochemistry* **2005,** *66*, 481-485.

104. Shakya, R.; Navarre, D. A. Rapid screening of ascorbic acid, glycoalkaloids, and phenolics in potato using high-performance liquid chromatography. *Journal of Agricultural and Food Chemistry* **2006**, *54*, 5253-5260.

105. Segu, V. B. G.; Li, G.; Metz, S. A. Use of a soluble tetrazolium compound to assay metabolic activation of intact β cells. *Metabolism: Clinical and Experimental* **1998,** *47*, 824-830.

106. Stockert, J. C.; Blázquez-Castro, A.; Cañete, M.; Horobin, R. W.; Villanueva, A. MTT assay for cell viability: Intracellular localization of the formazan product is in lipid droplets. *Acta Histochemica* **2012,** *114*, 785-796.

107. Iles, K. E.; Dickinson, D. A.; Watanabe, N.; Iwamoto, T.; Forman, H. J. AP-1 activation through endogenous H2O2 generation by alveolar macrophages. *Free Radical Biology and Medicine* **2002,** *32*, 1304-1313.

108. Luo, W.; Semenza, G. L. Emerging roles of PKM2 in cell metabolism and cancer progression. *Trends in Endocrinology & Metabolism* **2012,** *23*, 560-566.

109. Iqbal, M. A.; Gupta, V.; Gopinath, P.; Mazurek, S.; Bamezai, R. N. K. Pyruvate kinase M2 and cancer: an updated assessment. *FEBS Letters* **2014,** *588,* 2685-2692.

110. Shirai, T.; Nazarewicz, R. R.; Wallis, B. B.; Yanes, R. E.; Watanabe, R.; Hilhorst, M.; Goronzy, J. J.; Weyand, C. M.; Giacomini, J. C.; Assimes, T. L.; Tian, L.; Harrison, D. G. The glycolytic enzyme PKM2 bridges metabolic and inflammatory dysfunction in coronary artery disease. *Journal of Experimental Medicine* **2016,** *213,* 337-354.

111. Vaughan, R. A.; Garcia-Smith, R.; Dorsey, J.; Griffith, J. K.; Bisoffi, M.; Trujillo, K. A. Tumor necrosis factor alpha induces Warburg-like metabolism and is reversed by anti-inflammatory curcumin in breast epithelial cells. *International Journal of Cancer* **2013,** *133,* 2504-2510.

112. Semenza, G. Hydroxylation of HIF-1: oxygen sensing at the molecular level. *Physiology (Bethesda)* **2004,** *19,* 176-182.

113. Jantsch, J. Toll-like receptor activation and hypoxia use distinct signaling pathways to stabilize hypoxia-inducible factor 1α (HIF1A) and result in differential HIF1A-dependent gene expression. *Journal of Leukocyte Biology* **2011,** *90,* 551-562.

114. Blouin, C. C. Hypoxic gene activation by lipopolysaccharide in macrophages: Implication of hypoxia-inducible factor 1 alpha. *Blood* **2004,** *103,* 1124-1130.

115. Kaelin, Jr. Oxygen sensing by metazoans: The central role of the HIF hydroxylase pathway. *Molecular Cell* **2008,** *30,* 393-402.

116. Bonello, S.; Zahringer, C.; Rachida S. BelAiba, R.; Djordjevic, T.; Hess, J.; Michiels, C.; Kietzmann, T.; Gorlach, A. Reactive oxygen species activate the HIF-1

promoter via a functional NFB site. *Arteriosclerosis Thrombosis and Vascular Biology.* **2007,** *27*, 755-761.

117. Roman, J. Transcriptional regulation of the human interleukin 1beta gene by fibronectin: role of protein kinase C and activator protein 1 (AP-1). *Cytokine* **2000,** *12*, 1581-96.

118. Freemerman, A. J. Metabolic reprogramming of macrophages: Glucose transporter 1 (GLUT1)-mediated glucose metabolism drives a proinflammatory phenotype. *Journal of Biological Chemistry* **2014,** *289*, 7884-7896.

119. Bulua, A. C.; Simon, A.; Maddipati, R.; Pelletier, M.; Park, H.; Kim, K.-Y.; Sack, M. N.; Kastner, D. L.; Siegel, R. M. Mitochondrial reactive oxygen species promote production of proinflammatory cytokines and are elevated in TNFR1-associated periodic syndrome (TRAPS). *The Journal of Experimental Medicine* **2011,** *208*, 519-533.

120. Anastasiou, D.; Yu, Y.; Israelsen, W. J.; Jiang, J.-K.; Boxer, M. B.; Hong, B. S.; Tempel, W.; Dimov, S.; Shen, M.; Jha, A.; Yang, H.; Mattaini, K. R.; Metallo, C. M.; Fiske, B. P.; Courtney, K. D.; Malstrom, S.; Khan, T. M.; Kung, C.; Skoumbourdis, A. P.; Veith, H.; Southall, N.; Walsh, M. J.; Brimacombe, K. R.; Leister, W.; Lunt, S. Y.; Johnson, Z. R.; Yen, K. E.; Kunii, K.; Davidson, S. M.; Christofk, H. R.; Austin, C. P.; Inglese, J.; Harris, M. H.; Asara, J. M.; Stephanopoulos, G.; Salituro, F. G.; Jin, S.; Dang, L.; Auld, D. S.; Park, H.-W.; Cantley, L. C.; Thomas, C. J.; Vander Heiden, M. G. Pyruvate kinase M2 activators promote tetramer formation and suppress tumorigenesis. *Nature Chemical Biology* **2012,** *8*, 839-847.

121. Lopes-Virella, M. F.; Huang, Y.; Samuvel, D. J.; Sundararaj, K. P.; Nareika, A. Lactate boosts TLR4 signaling and NF-κB pathway-mediated gene transcription in macrophages via monocarboxylate transporters and MD-2 up-regulation. *Journal of Immunology* **2009,** *182,* 2476-2484.

122. Miguel, M. G. Anthocyanins: Antioxidant and/or anti-inflammatory activities. *Journal of Applied Pharmaceutical Science* **2011,** *1*, 07-15.

123. Miyoshi, N.; Takabayashi, S.; Osawa, T.; Nakamura, Y. Benzyl isothiocyanate inhibits excessive superoxide generation in inflammatory leukocytes: implication for prevention against inflammation-related carcinogenesis. *Carcinogenesis* **2004,** *25*, 567-575.

124. Lee, Y. M.; Seon, M. R.; Cho, H. J.; Kim, J.-S.; Park, J. H. Y. Benzyl isothiocyanate exhibits anti-inflammatory effects in murine macrophages and in mouse skin. *Journal of Molecular Medicine* **2009,** *87,* 1251-1261.

125. Benjamin, J. L.; Paul, J. H. Identification of the cellular targets of bioactive small organic molecules using affinity reagents. *Chemical Society Reviews* **2008,** *37,* 1347-1360.

126. Colegate, S. M.; Molyneux, R. J. In *Bioactive natural products : detection, isolation, and structural determination,* second edition; Colegate S. M.; Molyneux R. J., Eds.; CRC Press: Boca Raton, 2008.

127. Samuel, H.; Lim, T. K. In *Edible medicinal and non-medicinal plants: Fruits*: Springer: New York, 2012; Vol. 1.

128. Mezadri, T. Antioxidant compounds and antioxidant activity in acerola (Malpighia emarginata DC.) fruits and derivatives. *Journal of Food Composition and Analysis* **2008,** *21,* 282-290.

129. Ana Lúcia A, V. Phenolic compounds in acerola fruit (Malpighia punicifolia, L.). *Journal of the Brazilian Chemical Society* **2004,** *15,* 664.

130. Mezadri, T. Carotenoid pigments in acerola fruits (Malpighia emarginata DC.) and derived products. *European Food Research and Technology* **2005,** *220,* 63-69.

131. Hanamura, T.; Mayama, C.; Aoki, H.; Hirayama, Y.; Shimizu, M. Antihyperglycemic effect of polyphenols from acerola (Malpighia emarginata DC.) fruit. *Bioscience, Biotechnology, and Biochemistry* **2006**, *70,* 1813-1820

132. Wakabayashi, H. Inhibition of LPS-stimulated NO production in mouse macrophage-like cells by Barbados cherry, a fruit of Malpighia emarginata DC. *Anticancer Research* **2003,** *23*, 3237-41.

133. Motohashi, N.; Wakabayashi, H.; Kurihara, T.; Fukushima, H.; Yamada, T.; Kawase, M.; Sohara, Y.; Tani, S.; Shirataki, Y.; Sakagami, H. Biological activity of Barbados cherry (Acerola fruits, fruit of Malpighia emarginata DC) extracts and fractions. *Phytotherapy Research* **2004**, *18,* 212-223.

134. Aguilar-Guadarrama, A. B.; Rios, M. Y. Terpenos y flavonoides glicosídicos de Tetrapterys heterophylla (Griseb.) W.R. Anderson (Malpighiaceae). *Revista Cubana Planta Medica* **2007,** *12*.

135. Huang, T. C. A stable reagent for the liebermann-burchard reaction: Application to rapid serum cholesterol determination. *Analytical Chemistry* **1961,** *33,* 1405-1407.

136. Noratto, G. Identifying peach and plum polyphenols with chemopreventive potential against estrogen-independent breast cancer cells. *Journal of Agricultural and Food Chemistry* **2009,** *57,* 5219-5226.

137. Begum, A. S.; Sahai, M.; Fujimoto, Y.; Asai, T.; Schneider, K.; Nicholson, G.; Suessmuth, R., A new kaempferol diglycoside from Datura suaveolens Humb. & Bonpl. ex. Willd. *Natural Product Reserch* **2006,** *20,* 1231-1236.

138. Kuroda, M.; Mimaki, Y.; Ori, K.; Sakagami, H.; Sashida, Y. Steroidal glycosides from the bulbs of ornithogalum thyrsoides. *Journal of Natural Products* **2004,** *67,* 1690-1696.

139. Murakami, A. Glyceroglycolipids from citrus hystrix, a traditional herb in Thailand, potently inhibit the tumor-promoting activity of 12-O-tetradecanoylphorbol 13-acetate in mouse skin. *Journal of Agricultural and Food Chemistry* **1995,** *43,* 2779-2783.

140. Flacher, V. Mannoside glycolipid conjugates display anti-inflammatory activity by inhibition of toll-like receptor-4 mediated cell activation. *ACS Chemical Biology* **2015,** *10,* 2697-2705.

141. Reshef, V. New acylated sulfoglycolipids and digalactolipids and related known glycolipids from cyanobacteria with a potential to inhibit the reverse transcriptase of HIV-1. *Journal of Natural Products* **1997,** *60,* 1251-1260.

142. Ha, D. T.; Trung, T. N.; Phuong, T. T.; Yim, N.; Chen, Q. C.; Bae, K. The selected flavonol glycoside derived from Sophorae Flos improves glucose uptake and

inhibits adipocyte differentiation via activation AMPK in 3T3-L1 cells. *Bioorganic & Medicinal Chemistry Letters* **2010,** *20*, 6076-6081.

143. Ginestra, G.; Parker, M. L.; Bennett, R. N.; Robertson, J.; Mandalari, G.; Narbad, A.; Lo Curto, R. B.; Bisignano, G.; Faulds, C. B.; Waldron, K. W. Anatomical, chemical, and biochemical characterization of cladodes from prickly pear [Opuntia ficus-indica (L.) Mill.]. *Journal of Agricultural and Food Chemistry* **2009,** *57*, 10323-10330.

144. Guevara-Figueroa, T.; Jiménez-Islas, H.; Reyes-Escogido, M. L.; Mortensen, A. G.; Laursen, B. B.; Lin, L.-W.; De León-Rodríguez, A.; Fomsgaard, I. S.; Barba de la Rosa, A. P. Proximate composition, phenolic acids, and flavonoids characterization of commercial and wild nopal (*Opuntia* spp.). *Journal of Food Composition and Analysis* **2010,** *23*, 525-532.

145. Sánchez-Rabaneda, F.; Jauregui, O.; Lamuela-Raventós, R. M.; Bastida, J.; Viladomat, F.; Codina, C. Identification of phenolic compounds in artichoke waste by high-performance liquid chromatography–tandem mass spectrometry. *Journal of Chromatography A* **2003,** *1008*, 57-72.

146. Abad-García, B.; Garmón-Lobato, S.; Berrueta, L. A.; Gallo, B.; Vicente, F. On line characterization of 58 phenolic compounds in *Citrus* fruit juices from Spanish cultivars by high-performance liquid chromatography with photodiode-array detection coupled to electrospray ionization triple quadrupole mass spectrometry. *Talanta* **2012,** *99*, 213-224.

147. Truchado, P.; Ferreres, F.; Tomas-Barberan, F. A. Liquid chromatography–tandem mass spectrometry reveals the widespread occurrence of flavonoid glycosides in honey, and their potential as floral origin markers. *Journal of Chromatography A* **2009,** *1216*, 7241-7248.

148. Smith, W. L.; DeWitt, D. L.; Garavito, R. M. Cyclooxygenases: Structural, cellular, and molecular biology. *Annual Review of Biochemistry* **2000,** *69*, 145-182.

149. Vane, J. R.; Bakhle, Y. S.; Botting, R. M. Cyclooxygenases 1 and 2. *Annual Review of Pharmacology and Toxicology* **1998,** *38*, 97-120.

150. Kurumbail, R. G. Structural basis for selective inhibition of cyclooxygenase-2 by anti- inflammatory agents. *Nature* **1996,** *384*, 644-648.

151. Herschman, H. R. Prostaglandin synthase 2. *Biochimica et Biophysica Acta. Lipids and Lipid Metabolism* **1996,** *1299*, 125-140.

152. Ricciotti, E. Prostaglandins and Inflammation. *Arteriosclerosis, Thrombosis, and Vascular Biology* **2011,** *31*, 986-1000.

153. Wang, D.; Dubois, R. N. The role of COX-2 in intestinal inflammation and colorectal cancer. *Oncogene* **2010,** *29*, 781-788.

154. Kalinski, P. Regulation of immune responses by prostaglandin E-2. *The Journal of Immunology* **2012,** *188*, 21-28.

155. Herrera Salgado, Y. Myo-inositol-derived glycolipids with anti-inflammatory activity from Solanum lanceolatum. *Journal of Natural Products* **2005,** *68*, 1031-1038.

156. Ringbom, T., COX-2 inhibitory effects of naturally occurring and modified fatty acids. *Journal of Natural Products* **2001,** *64*, 745-749.

157. Berg, J. M.; Tymoczko, J. L.; Stryer, L. In *Biochemistry,* seventh edition; W.H. Freeman and Company: New York, 2012.

158. Singh, S.; Pandey, V. P.; Naaz, H.; Singh, P.; Dwivedi, U. N. Structural modeling and simulation studies of human cyclooxygenase (COX) isozymes with selected terpenes: Implications in drug designing and development. *Computers in Biology and Medicine* **2013,** *43*, 744-750.

159. Romero, J. Synthesis, anti-inflammatory activity and modeling studies of cycloartane-type terpenes derivatives isolated from Parthenium argentatum. *Bioorganic & Medicinal Chemistry* **2014,** *22*, 6893-6898.

APPENDIX

Appendix A HPLC-MS chromatogram of the total acerola leaf extract at 365 nm.

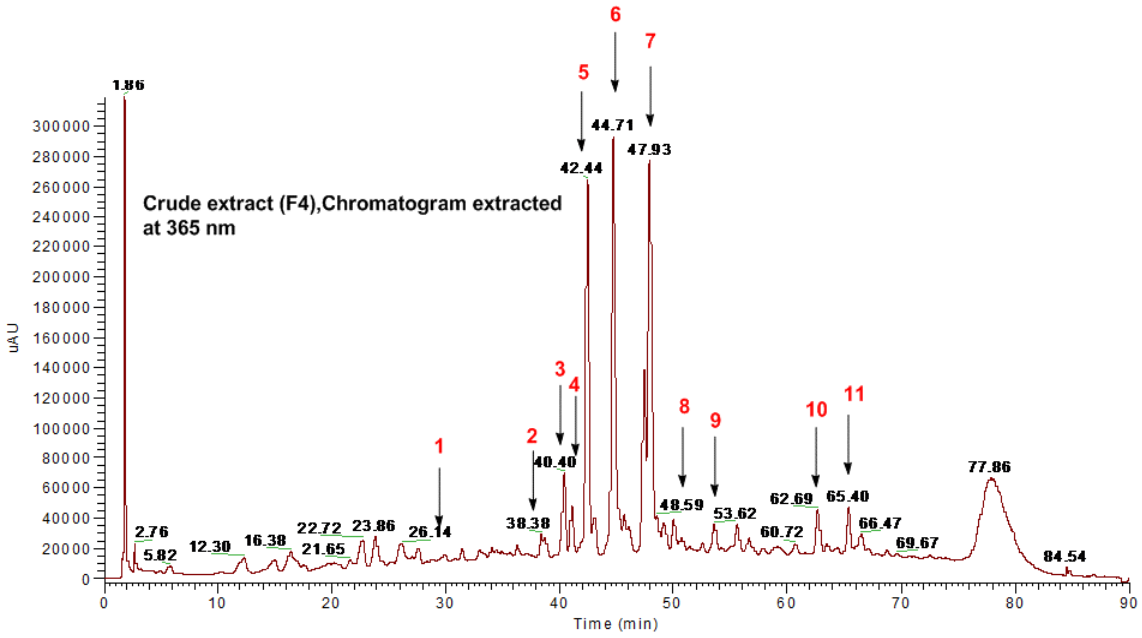

Appendix B Identified components from the Acerola leaves extract (crude extract F4)

Peak no	Retention time	UV	MS [M-H]-	MS^2	Identification
1	29.3	253, 328, 352	755	755, 609, 301	Quercetin 3-O-rhamnosyl-(1→2)-[rhamnosyl-(1→6)]-glucoside
2	38.3	242, 271, 382	593	447, 441, 301	Quercetin 3-O-dirhamnoside
3	40.4	242, 265, 299, 353	609	301	Rutin
4	40.8	242, 266, 307, 348	463	301, 151	Quercetin 3-*O*-glucoside
5	42.4	242, 266, 345	711	579, 463, 396, 329, 287	Identified by NMR [Kaempferol derivative]
6	44.7	242, 266, 347	579	447, 287	kaempferol 3-[β-D-xylofuranosyl-(1→6)-β-D-galactopyranoside]
7	47.9	242, 266, 345	579	447, 287	kaempferol 3-[β-D-xylofuranosyl-(1→6)-β-D-galactopyranoside] (isomer)
8	48.5	253, 328, 354	725	725, 579, 287	Kaempferol 3-*O*-robinobioside-7-*O*-arabinofuranoside
9	53.6	230, 242, 270, 312	451	451, 386, 329, 303, 287, 256, 245, 228	Kaempferol 3-*O*-glucoside
10	62.6	253, 328, 354	739	739, 579, 287	Kaempferol 3-*O*-(rhamnosyl-glucoside)-7-*O*-rhamnoside
11	65.4	230, 242, 270, 315	769	769, 317, 609	Isorhamnetin 3-*O*-rhamnoside-7-*O*-(rhamnosyl-hexoside)

Appendix C GCMS of F4 extract

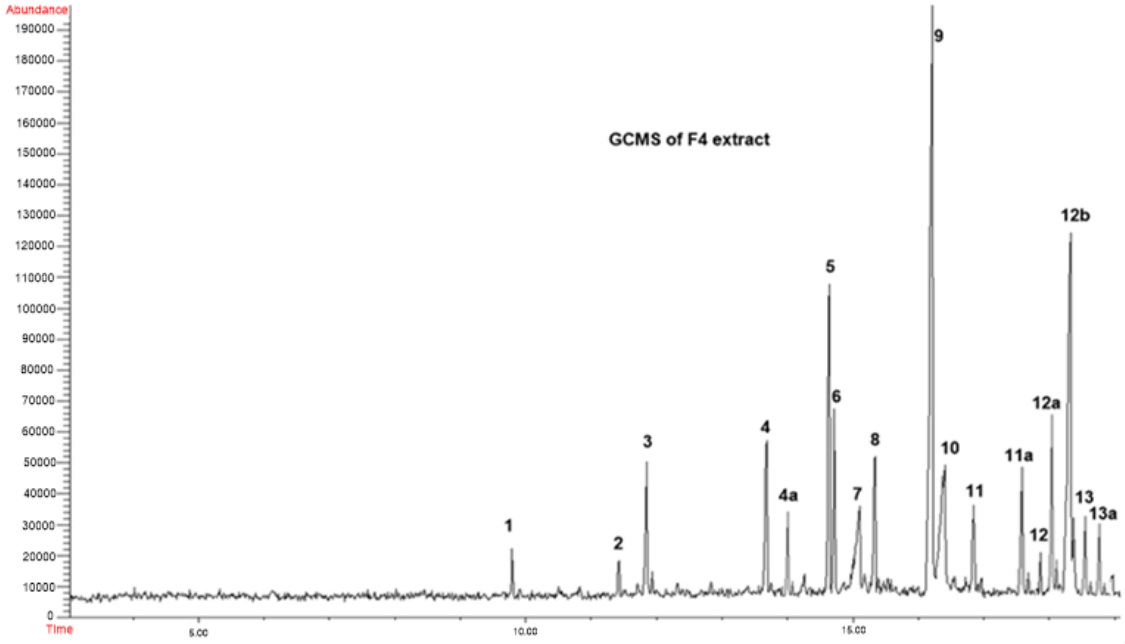

Appendix D GC-MS of F4 extract

Peak no	Retention time	MW	Identification	Type of compound
1	9.793	196	5-tetradecene	Alkene
2	11.416	322	Cyclopropane Nonanoic acid, [2-butyl-]	Lipid
3	11.844	336	Cyclotetracosane	Cycloalkane
4	13.664	280	5-Eicosene	Alkene
5	14.629	292	Androstane-3,17-diol[3β-5α	Diterpene
6	14.717	334	1,2-Benzene dicarboxylic acid, butyl-7-ol	Phenolic acid
7	15.090	256	Hexadecanoic acid	Lipid
8	15.331	270	1-octadecanol	Alcohol
9	16.186	296	Phytol	Diterpene alcohol
10	16.373	108	1,4 cyclo-octadiene	Cyclo alkene
11	16.855	224	Cyclohexane 1,2-dimethyl-3-pentyl-4-propyl	Substituted cycloalkane
11a	16.890	541	-	Tritepene
12	16.844	336	cyclotracosane	Cyclo alkane
12a	16.177	533	-	Triterpene
12b	18.305	530	-	Tritepene
13	18.303	278	Dibutyl phthalate	Aromatic alkane
13a	18.151	543	-	Triterpene

Appendix E HPLC-MS chromatograms of acerola leaf extract (F4) and fractions (F1, F2, and F3) at 365 nm.

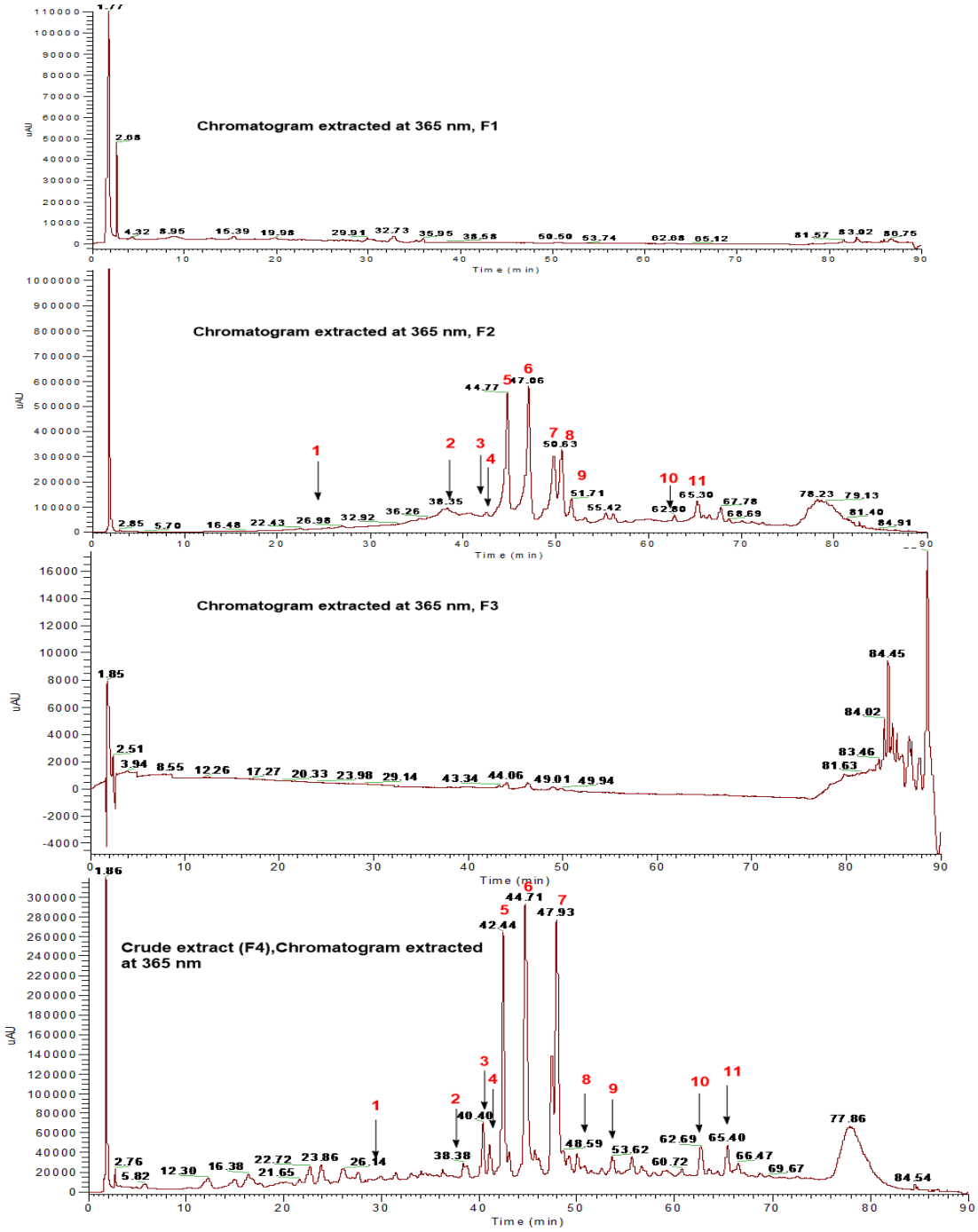

Appendix F ^{1}H NMR of crude fraction F2B Acetone-d_6